UNIVERSITY OF OKLAHOMA

GRADUATE COLLEGE

INVESTIGATION OF PLUGGING IN ORIFICE, SLOT, AND PORE-THROAT BY FINE PARTICLES

A DISSERTATION

SUBMITTED TO THE GRADUATE FACULTY

in partial fulfillment of the requirements for the

Degree of

DOCTOR OF PHILOSOPHY

By

TUNG VU TRAN
Norman, Oklahoma
2010

INVESTIGATION OF PLUGGING IN ORIFICE, SLOT, AND PORE-THROAT BY FINE PARTICLES

A DISSERTATION APPROVED FOR THE
MEWBOURNE SCHOOL OF PETROLEUM AND GEOLOGICAL ENGINEERING

BY

Dr. Faruk Civan, Chair

Dr. Chandra S. Rai

Dr. Subhash Shah

Dr. Roy Knapp

Dr. Richard Mallinson

Acknowledgements

I would like to express my deepest appreciation to Dr. Faruk Civan for his unlimited support and guidance throughout the course of this work. He has been an amazing advisor.

I would like to thank my committee members Dr. Chandra Rai, Dr. Subhash Shah, Dr. Roy Knapp and Dr. Richard Mallinson for their helpful comments and suggestions. I would like to thank my research group colleagues and friends. A special acknowledgement is due to Dr. Ian Robb of the Halliburton Services Company for many useful discussions, guidance and his collaboration and providing the materials used in this work. Thank you to Mike Shaw and Brad Todd for their helpful discussions and suggestions on the experimental set-up.

I would like to acknowledge Dr. Chandra Rai and the IC^3 staffs for providing me an opportunity to conduct several important measurements in their facility.

I would like to thank Dr. Roy Knapp for his time and effort with the writing correction of this dissertation. His encouragement, guidance, and advice are truly appreciated.

I would like to acknowledge PetroVietnam and the Mewbourne School of Petroleum and Geological Engineering for their financial supports during my study at the University of Oklahoma.

The Mathematica^{TM} 7.0 computer program provided by Vinh Nguyen for application of the Civan and Nguyen (2005) deep-bed filtration model is appreciated.

Finally, I would like to thank my parents, my brother Toan Tran, my cousin Nghia Vu for their support and encouragement during the course of this study. I would like to thank my wife Phuong Le for her companionship and understanding. This work is dedicated to my two beautiful daughters Phuong Nhi and Tue Nhi. They are my aspirations.

Table of Contents

List of Tables

List of Figures

Abstract

The conditions favorable for plugging of perforations, fractures, slots, and pore-throats during petroleum reservoir production were investigated and useful correlations were developed for prediction of such conditions.

First, conditions leading to plugging of perforations, fractures, or slots in wells and pore-throats in porous formations were studied experimentally. Accurate correlations were developed for the effects of orifice- or slot-to-particle-size ratio on flowing fluid conditions and plugging time that lead to particle bridging. It was demonstrated that the critical orifice- or slot-to-particle-size ratio vs. particle-volume-fraction Reynolds number could be correlated satisfactorily using an exponential function and the dimensionless plugging time vs. reciprocal-particle-volume-fraction yields a power-law-type correlation. Such empirical correlations can be used to determine and avoid the conditions which induce perforation, fracture, slot and pore plugging by migrating particles in petroleum reservoirs. The dimensionless correlations developed here can also be used as a screening tool to choose the best lost circulation material (LCM) candidates.

Second, the measured permeability reduction obtained from laboratory tests by injecting particulate drilling fluid in a representative core sample was used to determine empirical parameters used in models of particle migration and deposition in porous media. This study provided a concept to evaluate drilling fluids in term of their formation damage potential. Experimental and numerical work was carried out to investigate formation damage induced by particles suspended in the drilling fluid. The study applied

the Nuclear Magnetic Resonance (NMR) technology to provide insight into damage mechanisms along the formation. The formation permeability reduction was less while injecting treated drilling mud that contained polymer additives. It was observed that suspended small particles penetrated further along the length of the core whereas bigger particles and non-treated drilling mud tended to form external filter cake at the core inlet face.

Finally, the core flood test results were used to validate and compare two current deep-bed filtration models. Simulations were run for two sets of data, and the adjustable parameters were determined to match with the experimental results. The Wojtanowicz et al. (1987) diagnostic method and Civan (2007) predictive model were applied to core flooding experiments to describe damage mechanisms and to estimate reductions in porosity and permeability.

1. Chapter 1: Introduction

Flowing suspended-particles can cause many problems during various operations in the oil and gas industry. Typical examples are encountered during many phases of reservoir development such as drilling, completion, production, stimulation, water-flooding, and even primary enhanced recovery. The over-all objective of the present study is to determine the effects of various factors that contribute to plugging of perforations, slot, and pore-throats by suspended particles under specific conditions and the processes that take place at the micro-scale. This chapter reviews the various phenomena involving damage caused by particle-suspensions.

1.1 Plugging caused by solid particles in petroleum production operations

Formation damage is undesirable in oil and gas industry. Formation damage occurring during drilling, completion, production, simulation, water-flooding, and enhanced oil recovery (EOR) is reviewed in the following sections.

1.1.1. Drilling operation

There are two primary damage mechanisms to consider in drilling such as drill solid invasion and drilling-mud filtrate loss to the formation. With pressure maintained above the formation pressure, the drilling mud invades the formation due to the positive differential pressure. Suspended particles and drilling mud can cause damage to the formation as the following:

- Plugging and bridging by weighting material such as bentonite clay or barite (barium sulfate),
- Subsequent plugging by drill cuttings,
- Lost circulation material (LCM) entering the formation void pore spaces or natural fractures.

1.1.2. Completion operation

Damage during completion probably does not occur as often as in other operations. However, the cementing and perforating program must be designed carefully to avoid the following formation damage possibilities:

- High losses of high-pH cement filtrate, which can disturb clays and induce fines migration (Cunningham and Smith, 1968).
- Invasion and plugging by cement solids.
- Loss of whole cement to the formation.
- Perforating plugging caused by injecting dirty fluid at high velocity.
- Compaction or crushing of the formation within a thin rim around the perforation.

1.1.3. Production operation

A sudden decline in production is the strongest indicator of formation damage. In many cases, damage is caused by fine migration, inorganic scale deposition, and organic solid deposition (e.g. paraffin and asphaltenes).

Mobile fines in produced fluids can form bridges and accumulate at pore throats, and reduce matrix permeability (Muecke, 1979). Deposition of inorganic scale usually associates with a breakthrough of water production. Common inorganic scales are calcium carbonate, calcium sulfate, barium sulfate, and iron carbonate (Krueger, 1986). At appropriate temperatures, paraffin and asphaltenes in production fluids deposit and cause formation plugging and alter the rock wettability. Identification of organic deposits is very important in an acid treatment candidate well, because this damage is not acid removable.

1.1.4. Stimulation operation

The most common method to treat a damaged formation is acid stimulation. Although the objective of acid stimulation is to remove damage and improve well productivity, acid treatments can easily cause damage, rather than remove or bypass damage successfully. Damage can occur during acidizing and fracturing in both sandstones and carbonates.

During acid treatments, injection of solids into the formation can occur if dirty fluids are used or acid is pumped through dirty or rusty tubing. The use of acid additives which are incompatible with the formation may also induce damage, sometimes irreversibly. Therefore, fluid-compatibility testing, proper planning, and additive selection are necessary to prevent these damage problems.

Hydraulic fracturing is one effective way to improve the well productivity. However, it can also cause significant damage by inducing the following damage mechanisms:

- Fines generation and migration,
- Plugging in the proppant pack.

1.2 Objectives of the Study

The specific objectives of the study on the conditions leading to plugging of the pore-throat, perforation, or fracture during drilling and completion operations are presented as follows:

Experimental approaches:

- Investigate the conditions that lead to plugging and develop accurate correlations for the effect of the particle size on the plugging time and the pore-throat-to-particle-size ratio leading to particles bridging as a function of particle Reynolds number.
- Investigate the effect of pore/perforation opening geometry on the plugging ability and time for particulate flow.
- Investigate the plugging condition for slots by particles of different size, shape, and concentration; and develop empirical correlations on the basis of relevant

dimensionless numbers which determine the effect of the geometry of the fracture opening and particle size distribution on the plugging conditions.

- Study the permeability and porosity variation in core flow tests to determine the different damage mechanisms involved in consolidated cores.
- Apply laser diffraction particle size analysis (LDPSDA) and nuclear magnetic resonance (NMR) techniques to study the particle deposition/invasion inside the core samples.

Data analysis approaches

- Develop empirical correlations for condition and time leading to plugging of orifice, slot, and pore-throat by suspended particles.
- Develop quantitative methods and correlations to estimate the plugging time.
- Apply diagnostic method to determine different formation damage mechanisms occurring during the core flood tests.
- Apply mathematical models to predict the damage caused by particles inside the core plugs.
- Characterize the formation damage of deep bed filtration from core injection and
- Numerical simulation to gain insight into the damage of the core sample caused by particulate invasion.

1.3 Description of materials presented in various chapters

Chapter 2 presents a literature study and an overview of the conditions leading to plugging in orifice, slot, and pore-throat of porous formations caused by particulate processes. A brief review of the mathematical models applied here for formation plugging data analysis is also presented.

Chapter 3 presents a detailed look into the effect of the relative size between the migrating particles and flow constrictions (pore-throat, fracture, and perforation). The main condition determining the plugging time and particle size compared to the pore-throat size as a function of the particle-volume-fraction Reynolds number for relatively monodisperse particles and mixtures is studied. Useful correlations for time and condition of plugging of perforations by migrating suspended particles are developed. The effects of particle size, concentration, flow conditions, and fracture-opening aspect ratio on bridge formation are studied. The correlations developed can be used to alleviate the field problems affecting the flow efficiency and productivity of wells completed in petroleum reservoirs.

Chapter 4 studies the plugging of slots by suspended particles (this can be applied for natural fracture and slotted liner). Empirical correlations are developed on the basis of the relevant dimensionless numbers which determine the effect of the aspect ratio (length-to-width ratio) of the slot and particle size distribution on plugging conditions. Plugging capabilities and fluid loss through slots and fractures are found to depend on the particle shape, size, composition, particle concentration, flow conditions, and fluid properties.

Chapter 5 describes experimental apparatus, experimental procedures, results and data analysis for formation core plugging, thin section formation plugging, and sectional core plugging tests.

Chapter 6 summarizes conclusions and recommendations for future work.

2. Chapter 2: Literature Review

This chapter is a review of literature on the plugging of perforations, fractures, and pore-throats of porous media by suspended particles.

2.1. Perforation and pore plugging by particles

In petroleum engineering, perforation and pore plugging by particles has attracted much attention. Oil productivity decline is often caused by fines migration and formation clogging (Civan 2000, 2007; Bertness, 1953; Krueger et al. 1967; Nowark and Krueger, 1951). Sudden change in fluid chemistry can trigger fines mobilization, consequent placement into suspension and retention at pore throats that reduces the permeability of the matrix material.

Pore throat plugging can occur by size exclusion or jamming of fine particles that migrate and are deposited during fluid flow. This type of deposition and entrapment plays a critical role in the design of filters in structures like dams and retaining walls. This type of plugging has been studied using both experiments and models. Most studies concerning the clogging, plugging, and formation damage mechanisms use micron-size particles. A wide range of parameters that affect fines migration in porous media were analyzed by researchers, such as the effect of the mean particle size, standard deviation of particle size distribution, clay concentration, rate of release coefficient, starting pressure, tramping length, network connectivity, and the role of pH and ionic concentration.

Many parameters affecting fines migration in porous media have been analyzed in numerous studies, such as the mean particle size, standard deviation of particle size

distribution, clay concentration, rate of release coefficient, starting pressure, tramping length, network connectivity, and the role of *pH* and ionic concentration (Cerda, 1988; Gaida et al., 1985; Khilar and Fogler, 1998; Muecke, 1979). However, there are only a few reported studies relevant to particle bridging phenomenon of large pores and perforations. Haynes and Gray (1974) studied particle transport efficiency of suspensions through sand particles packed over a perforated casing. They proposed that a low-viscosity fluid would minimize the channeling and reduce particle transport efficiency because of less drag applied on particles. Fresh water and low viscosity brine were used to carry the particles into the perforations. They found that the particle transport efficiency improved with increasing flow rate and decreased with the particle size and concentration.

Muecke (1979) studied the effects of single- and multi- phase fluid flow and wettability on fine-particle movement. Conditions leading to bridging were evaluated in terms of particle size and concentration. A monolayer of d = 200μm Pyrex glass chips between two flat 6x8x0.5 in dimension glass plates were used to confine the sand. Calcium Carbonate ($CaCO_3$) particles were injected into a large confined sand pack. Conclusions were based on the qualitative observations. Fine particles were carried by the wetting fluid in the multi-phase fluid system. Bridging of fines at pore throats was observed to depend on the size and concentration of mobilized fines, and the velocity of the flowing fluid.

The effect of flow rate and pressure on the release and entrapment of fines were evaluated by Gruesbeck and Collins (1982a). Both oil and water were tested as carrier

fluids. Columns packed with sand of diameters between 200-840μm were used and dispersions of $CaCO_3$ particles were used as fines. They investigated cases involving both dirty injection-fluid-clean pack and clean injection-fluid-dirty pack systems. The results showed that the critical velocity required for plugging was inversely proportional to fluid viscosity. Flow reversals caused bridge destabilization and hence temporary permeability increase.

Valdes and Santamarina (2006) studied the interplay between various particle-level forces, the relative size between particles and pore throat, and the spatial variability of the velocity field. They found that radial clogging evolves into a self-stabilizing ring pattern when the pore-to-particle size radio is below the critical size ratio. A similar device was used for their flushing studies. They observed "finger-type" flow localization near the discharge point when particles are much smaller than pore throats.

Bouhroum and Civan (1995) concluded that the existing gravel-pack design was based on the geometrical retention criteria, and neglected the hydrodynamics and clogging effects. The commonly known geometrical retention criterion is the 1/3-rule, for which the pore throat-to-particle diameter ratio is equal to 3. However, the data of Gruesbeck and Collins (1982b) indicated that bridging could occur over a range of diameter ratios depending on the particle volume fraction of the flowing suspension of particles and not necessarily at a fixed value of 3 as inferred by the 1/3-rule. Civan (2000) effectively correlated their experimental data using the power- and exponential-law functions.

Iscan and Civan (2006) presented a criterion for effective plugging based on experimental determination and analysis of the critical conditions that lead to plugging. The graphs of the perforation or pore size to particle size ratio versus the particle-volume-fraction Reynolds number according to Civan (2000) were shown to determine the conditions that lead to perforation and pore-plugging. The experimental data obtained using three different water-based drilling fluids and several reported experimental data were analyzed and correlated by means of the power- and exponential-law expressions. Both approaches adequately described the conditions leading to perforation and pore plugging.

2.2. Plugging of fractures and slot-liners by suspended particles

The basic problems associated with lost circulation in drilling for oil, plugging mechanism, and prevention measures were reviewed in detail by Messenger (1981). Several lost-circulation materials (LCM) were investigated and techniques were presented with case histories that involved granular, fibrous materials, bentonite, cement, barite, and barite in diesel oil. Messenger claimed that if the above materials were applied correctly, they would cure any loss zone that could be cured. The plugging mechanisms were divided into two types: plugging horizontal zones and induced vertical fractures. For porous sands and gravel, Messenger recommended bridging agents combined with fibers. Bridging agents can be used effectively for natural fractures up to ¼ inch wide, and a granular agent approximately the width of the fracture size should be used for the blend. Cement slurries can be used for natural horizontal fractures from ¼ in. to 1 ft wide.

Soft/hard and soft plugs were effective for natural horizontal fractures of this size. In induced vertical fractures, bridging agents were recommended to permanently seal fractures. Plugging induced vertical fractures using Portland cements and soft plugs was also discussed. In general, Messenger recommended considering the plugging mechanism when choosing the functionally correct LCM and technique for a particular application.

The use of specialized water-base drilling fluid selection has become common practice in the last decades (Bleier, R. 1990). Fluids based on clear brine and added chemical such as calcium carbonate, sodium chlorite, potassium chlorite as a bridging agent have been proven and widely accepted in the field (Burton and Hodge, 1999).

Gentzis et al. (2009) studied mud systems and additives used in coalbed methane drilling. They suggested that appropriate drilling fluid properties would be effective to seal the coal cleats and minor fractures and could easily be removed during production. The drilling fluid should not cause any formation damage while drilling. They used laboratory tests conducted with large-diameter cores but not under in-situ confining stress conditions, to screen various mud formulations and determine their effectiveness during simulated drilling and production conditions. They concluded that a small pressure was sufficient to remove filter cake during simulated production and the drilling mud did not cause permanent permeability damage. However, they reported that coal fines generated during simulated drilling of a coal seam with brine severely damaged the cleats and reduced the wellbore permeability by 87.5%. The selected mud fluids, with addition of two specific trade name fluid loss additives to a non-ionic polymer system, were then successfully used in drilling 1400 m and 953 m of horizontal well sections. These two

mud fluids were found to be effective in building a thin filter cake on the coal surface in a short time. The results showed no borehole instability problems during drilling and low mud losses in both cases.

Loeppke et al. (1990) investigated LCMs used in sealing fractured formations for geothermal applications. They focused on high-temperature, fracture-dominated loss zones rather than the matrix loss zones which are more typical of oil and gas drilling operations. Single- and two-particle bridging phenomena were studied. Different particle sizes, shapes, and types were used to determine the potential for plugging bit nozzles in field LCM applications. Plugging performance plots were presented for several commercial LCMs that might be used in severe, fracture-dominated, under-pressured loss zones. They reported that the particle size and shape affected the maximum allowable pressure differential across the plug. The bridges are stable only if the size of particles has certain dimensions relative to fracture width. However, only a few particles are actually involved in any given bridge and particle concentration does not significantly affect the pressure capability of any given plug. Particles that are not in the effective range do not contribute to forming a bridge; they will act as filter material once the bridge is formed by large particles. They developed a plugging performance plot of concentration versus a pluggable slot / particle-size ratio for LCM comparison. The experimental data showed that higher concentration (as high as 20 lb/bbl) of granular particles would provide higher pluggable slot / particle-size ratio. For concentrations above 20 lb/bbl, pluggable slot / particle-size ratio did not increase significantly. Their data on the plugging performance curve of thermoset rubber appears to follow the exponential function used in Tran et al. (2009).

Ali et al. (1994) presented an approach for industrial development and successful use of an LCM blend that could effectively seal the fracture and prevent lost circulation in depleted unconsolidated sandstone reservoirs. Different blends of particles with different sizes and types were mixed. They reviewed six case histories of using fresh water/bentonite/LCM mud system for side-track wells to show the sealing effectiveness of the LCM blend. The authors determined that the LCM blend not only effectively prevented lost circulation but also eliminated the need for intermediate drilling-casing strings, and substantially reduced the well cost.

Jiao and Sharma (1996) studied fractured formations from a different point of view. Their study focused on investigating mud additives that not only reduced the loss of mud fluids but also minimized the formation damage to existing natural fracture systems. They tested two types of additives, long, slender fibers and granular additives. Their study revealed that the granular additives such as calcium carbonate ($CaCO_3$) were not very effective. They suggested the use of sized fibers as additives for drilling muds and showed that fibrous additives plugged across the fracture face and trapped the bentonite particles to form an effective mud cake.

2.3. Plugging the porous formation by suspended particles

The occurrence of a change in permeability of the near-wellbore formation is most frequently related to the effects of the invasion of mud filtrate and solid particles. Drilling fluids contain a large quantity of solids that consist of organophilic clays and barite. During drilling, fine particles, which range in size from larger to slightly smaller

than the pore openings of the rock, build up on the wellbore to form a low permeability filter cake. Particles which are much smaller than the pore openings flow into the formation along with the mud filtrate. These particles eventually form internal bridges at pore restrictions between interconnecting mineral grains. Most of the external filter cake will be removed during the drilling operation due to the movement of drill bit or mud circulation, but most internal cakes are very difficult to remove and create a skin effect around the wellbore that results in a significant formation pressure drop. The type of formation damage depends upon the characteristics of the mud filtrate and particles.

Core tests have been done in the past to investigate the formation damage during water injection (Barkman and Davidson, 1972). The experiments were designed to flow contaminated water into a core at constant pressure. The cumulative volume throughput was plotted versus square root of time. From this plot, the "water-quality ratio", the ratio of the weight of solids in water to the filter cake permeability, was determined.

Sharma and Yortsos (1987a) proposed a mathematical model for the processes of fines migration and fines injection in a porous medium. The model was formulated for the general class of problems that involve the transport of stable particulate suspensions in porous media. Their goal was to study the local mechanisms of particle release and capture and to quantitatively incorporate these effects into population balance equations. They found that particle capture or entrainment occurred by surface deposition or release when the particles being filtered had sizes much smaller than the pore throats. Smaller particles were more easily deposited onto or removed from the solid surface, while low ionic strength caused particle deposition or removal to be retarded, for the constant surface boundary condition. In many cases, these rates are controlled by mass transfer,

thus by the network fluid velocity distribution. The population balance equation therefore contained the various rates of deposition and release and also included the terms that reflected the relative size of particles and pore throats. Sharma and Yortsos (1987b) continued this work and found the solution of the population balances for particular cases of both fines migration and fines injection. They considered the dynamics of the process immediately after the onset of fines migration for single-size particles. They studied the formation damage zones for different functions and coefficient from the population balance equation. The rate of growth of filter cake and permeability of filter bed were developed in terms of particle and pore sizes.

Jiao and Sharma (1996) studied fluid loss and damage to pre-existing fractures that a drilled well intersects. They used Berea core samples and created fracture surface that was similar to fresh fracture surfaces in rocks. They presented results of fracture permeability impairment and fluid loss without bridging additives and showed that drilling mud could cause severe permeability damage to the fracture system. Effects of fibrous additives and granular additives were also studied. They recommended the use of fibrous additives when drilling through naturally fractured reservoirs.

Massei et al. (2002) used short-pulse injection to study the transport and deposition kinetics of suspended particles in a highly permeable column of gravel. They found that the solid phase transport kinetics could present unexpected changes that depended on the flow rate, with a reversal of the residence times for the two mobile phases (tracer and particles). The resident time for the particulate material depends on three parameters: the size of the pores, the size of the particles and the flow rate.

Bedrikovetsky et al. (2002) presented a three-point pressure method, which used pressure data at an intermediate point of the core and the pressure measurements at core inlet and outlet, for deep bed filtration. They tested the flow of water with particles in porous media and obtained the values of filtration and formation damage coefficients for flow of solid and liquid particle dispersions in a number of different cores. Effects of particle type and porous media wettability on permeability decline were also examined.

Krueger et al. (1967) studied the validity of oil flow cleanup (back-flush), and flow reversals (for bridge stabilization) to restore permeability of water sensitive core damage. Back-flush is a field treatment applied to wells, in which solvents, crude oil or surfactants are injected into well in the direction opposite to production flow. The experiments were done in water damaged Miocene and Pliocene oil cores and Berea cores. Mud damaged Berea cores were subjected to oil flow cleanup at low and high "draw down" pressures. It was concluded that low rate clean-up is better than high rate clean-up in Miocene and Pliocene producing zones. Oil back flush simulation reduced the well-bore damage caused by silt migration. The production rate declined gradually as the solid content increased in the produced oil.

Iscan et al. (2007) performed several experiments on permeability changes caused by drilling fluid invasion and flow reversal. The damage caused by two different drilling fluids was measured experimentally as a function of filtration pressure and was analyzed using a simulator developed by Civan and Nguyen (2005) for describing the fines migration and retention in porous media. They found that the damage ratio increased with longer circulation periods. The water-based polymer XL mud was less damaging than

conventional bentonite mud. The average non-plugging and plugging deposition rates were higher than the average non-plugging and plugging clean-up rate.

Cerda (1988) studied the mobilization of quartz fines in sandpacks. The roles of pH and ionic concentration in permeability declines were studied. Fisher silica sand (base ~180μm and fines~ 1μm) was packed in 1.2 cm diameter and 5 cm long acrylic cells and flooded with electrolytes of varying pH. The experiments were done with rectangular microcell: packed bed thickness ~ 0.15 cm ($5.9x10^{-2}$ in.) for visualization. Cerda concluded that mobilization depended on very high fluid velocity within a narrow range of ionic concentration for large particles. In microcells, fines deposition at low pH was independent of ionic concentration. At high pH, deposition was dependent on ionic concentration. Fines were deposited around stagnation points, where hydrodynamic forces where maximized.

The role of pH and ionic concentration changes in permeability were examined by Kia et al. (1987) and Vaidya and Fogler (1990). They all reported that high calcium concentration renders no mobilization. Because the Ca^{2+} ions provide a better coverage of the surfaces than Na^{+} ions do, the surface potentials are reduced, and thus, the double layer repulsive force is reduced. Vaidya and Fogler (1990) used a constant displacement pump to saturate and flow brine of selected ionic concentration and pH values for natural Berea sandstone cores. Pressure gauges were placed along 2 feet length of Hassler core holder to monitor permeability declines. They found that conditions of high pH and low ionic concentration are needed to mobilized fines. Salinity decrease by itself caused no mobilization. When Ca^{2+} is present, no permeability decrease occured, even when pH was higher than 12. Gradual reduction in salinity did not change pH significantly and less

mobilization was observed. Khilar et al. (1983) reported that permeability decreases rapidly as salinity decreases and pH increases. Fines mobilization depends on salt type due to different cation-exchange capabilities for different salts. If the percentage of calcium in solution is above 15%, fines release is prevented.

McDowell and Boyer (1992) investigated mobilization by evaluating re-entrainment of particles as the result of changes in water chemistry. NaCl, $NaCl^+$ particles (polystyrene latex microspheres) and pure water were injected through a Monterrey No. 80 sand column and head loss was monitored by manometer. They established the critical salt concentration – salt concentration below which particles are mobilized.

Sharma et al. (1992) tried a different approach. They measured the critical hydrodynamic force required to detach glass and polystyrene particles from a glass substrate. For equipment, they used fluid reservoir, displacement pump, vacuum pump, particle syringe and optical microscope. The flow cell was constructed by placing glass particles between two ~4x8 cm microscope slides placed 200 ± 10 μm apart. A centrifuge experiment was conducted on a similar flow cell. Under the experimental conditions gravitational forces are negligible for spherical glass and polystyrene particles with $d \leq 10$ μm. For d>40μm particles, gravity becomes important for particle detachment. The critical hydrodynamic force decreases, as pH and elastic modulus increase. The critical hydrodynamic force increases, as the ionic strength increases,.

Wennberg et al. (1995) studied the mobilization, migration and clogging of fines in porous media models. In their studies, the micro-scale clogging process was identified

in time and space. Conceptual modeling was used to examine the process of mobilization to induce permeability changes that cause rearrangement of the pore velocity field. Clogging appeared self-stabilizing in the macro-scale; however, it was nonlinear at the micro-scale. The problem of mobilization at local sites that induced permeability decreases, and consequent mobilization in adjacent sites due to more rapid flow that avoids the already clogged regions, was presented. This process was dependent on the typical distance a particle traveled through the matrix.

Maroudas and Eisenklam (1965) studied the process of particle deposition in model porous media and established key factors for partial and complete pore blocking. A two-dimensional network of interconnecting channels of a regular staggered-square pattern was used in their studies. The critical velocity (u_c), which is the fluid velocity that causes no deposition (flushing) increased slightly with particle size. The blocking velocity (u_b), which is maximum applied fluid velocity that can be reached before complete blocking ends, increased greatly with particle size.

Baghdikian et al. (1987) evaluated the effect of pH, ionic concentration, clay type, and concentration of injected fines on permeability reduction through studies of deposition. They also analyzed clay dispersion and flocculation effects on permeability damage. In their research, Kaolinite and Bentonite suspensions were injected into 63 mm ID, 322 mm 40/170 Ottawa sand packs of porosity 0.375, and permeability of 8 darcies (average pore size: 18 μm). A peristaltic pump was used with an accumulator to damp pulses. The permeability was determined from pressure drop across the sand pack. Once bridges were formed, they acted as increasingly effective traps for flowing particles. Therefore, the particle sizes and concentrations required for consequent bridging changed

with time. The bridging potential was enhanced by the ability of clay particles to flocculate. In this case, the bridge strength was dependent on the strength of the flocculates. The porosity was unchanged during permeability decline and indicated size exclusion as the retention mechanism. Permeability decreased rapidly as salinity decreased and pH increased. Fines concentration affected deposition. For low ionic concentrations and equal clay concentrations, bentonite was more detrimental than kaolinite, owing to the bridge formation and flocculation abilities of bentonite.

After a permeability reduction, a brief flow reversal followed by continued production at the initial rate results in the re-establishment of the original permeability, followed by continuation of the original slow decline (Gruesbeck and Collins, 1982a). This suggests use of a brief flow reversal in a well as a test for potential problems with fines. However, flow reversal effects only occur at flow rates that exceed the critical velocity required for particle entrainment. New bridges that form in the opposite direction render this method only partially effective for repairing permeability damage (Krueger et al., 1967).

Formation damage due to fines migration was studied by Gruber and Adair (1995). They used 1.5 in.-diameter and 2.0-in.-long core plugs and determined the threshold pressure and permeability to oil by chemical gel and resin mud. It was noted that no flow occurred until the threshold pressure was reached, 30kPa (4.35psi). They found that the determination of threshold pressures where the flow starts is important.

Argiller et al. (1999) analyzed the formation damage potential of water-based drilling fluids. They conducted experiments with three water-based formulations. It was

found that static filtration was mainly governed by external mud cakes. They also stated that formation damage caused by water-based fluids can be avoided by optimizing the fluid loss reducer and particle size distribution

Bailey et al. (1999) studied the particle invasion from drilling fluids. The particulate invasion was found to be one of the primary mechanisms of formation damage caused by drilling fluids. Particles are forced into the formation generally during the earlier stages of the filter cake growth. The experiments were done with KCl polymer fluid and different grades of barite and carbonate weighing agents. They found that fine particles penetrated deeply into the formation and could not be easily removed by back-flushing. Larger particles were observed to deposit near the surface of the injection point. The permeability reduction was greatest in single-phase brine conditions.

Ding et al. (2004) studied near wellbore damage and natural clean-up of horizontal wells. Near wellbore properties were altered by drilling fluid, fluid-fluid interaction, and fluid-filtrate invasion during overbalanced drilling operations. The degree of formation damage was affected by many properties, and operating conditions. The permeability reduction factor was correlated with flow rate. A rapid fluid loss, indicating as a spurt loss, when the drilling bit contacts the reservoir, was observed. A deeper particle invasion of the internal filter cake decreased the flow efficiency while preventing the filtrate invasion. Serious loss of production occurred with damaging and non-optimized drilling fluids. The formation damage was more severe with a water-based mud than an oil-based mud.

Parn-anurak and Engler (2005) developed a model to simulate invasion of water-based drilling fluid into hydrocarbon bearing formations. The model was based on mass balance of the introduced solid particles into the formation. The reduction of permeability was analyzed in the damaged zone in terms of water phase saturations and skin concept along the radial direction. The average permeability was approximated along the radius of the skin zone. They numerically solved the convection-dispersion equation to characterize filtrate invasion behavior and concluded that their model can be used to simulate the radial flow of water-based filtrate.

Pandya et al. (1998) studied the migration of latex particle in glass bead packs. They observed that there was a critical particle concentration beyond which the packs were completely plugged. The critical concentration increased as particle size decreased. Reddi et al. (2000) reported similar results for cases of kaolin migrating through sandpacks. They said that the permeability reduction rate increased as particle concentration increased. They also reported that there were critical amounts of clogging beyond which the pore velocities were high enough to transport other fines through the remaining pore space without additional plugging or deposition.

2.4. Formation plugging by particles data analysis approaches

Ohen and Civan (1993) developed a model to account for fines migration and clay swelling during fluid flow through porous media. An optimal parameter identification algorithm was utilized to determine the best estimates of the system parameters using experimental data. The ionic concentration and *pH* effects on fines release and deposition

were not considered. The rates of particle deposition and entrainment were assumed to be governed only by the hydrodynamics.

Chang and Civan (1991) developed a model of formation damage caused by physical and chemical interactions between the reservoir fluids and formations. This model included chemical reactions involving dissolution/precipitation and ion exchange. The precipitates were considered mobile and mixed with other fine particles to contribute to pore throat plugging. The size distribution of both precipitates and clay fines were accounted for with bimodal distribution functions. The model parameters were determined through an optimization method by fitting with experimental data. This model showed good agreement with experimental results. It has a broad applicability in diagnosis, evaluation, and simulation of formation damage during drilling, production, and enhanced oil recovery (EOR) processes. It can also be used to predict the performance of acidizing and other chemical flooding processes.

Size exclusion during particle suspension transport in porous media was studied by Santos and Bedrikovetsky (2004). They derived a population balance model for stable particulate suspensions in porous media. Particle flow reduction due to restriction of large particles to move through small pores was studied. They concluded that populations of particles with different sizes filter independently. The capture rate for each population was a function of the particle radius. The smaller the particles the deeper they penetrate. They also proposed an average model that included three systems of equations for different size of particles.

Wojtanowicz et al. (1987) developed a theory to describe pore blocking mechanisms caused by foreign particle invasion. The simple approach used straight-line plots to identify the dominated damage mechanism to replace the complex statistical interactions between populations of particles and populations of pores presented by Yortsos and Sharma (1986).

Nguyen and Civan (2005) modeled the fine particle invasion and clean-up processes using a set of equations that describe the particle concentration and fractional deposition of particles with permeability. The porous medium is assumed to include plugging and non-plugging pathways. This is a pore-scale model. No fracture or wormhole existence was considered. Darcy flow conditions exist. The fluids are assumed to be incompressible and Newtonian. A transient-state one-dimensional-space solution along the core plug is calculated. The model showed that pore throat plugging induced an internal cake formation at a rate proportional to the volumetric particle flux and pore volume.

3. Chapter 3: Investigation of Plugging in Orifice by Suspended Particles

3.1. Introduction

Plugging of perforations in wells and pores of porous formations can occur during water flooding, drilling, perforation, and workover. Particles migrating at sufficiently high concentrations with an unfavorable particle-to-hole size ratio may form bridges that narrow the perforations and pore throats, reducing the flow rate through reservoirs. This reduces the productivity of the oil and gas wells. Hence, the operational conditions must be adjusted to avoid plugging of pores and perforations by suspended particles.

The mechanism of pore throat plugging in porous formations is of interest in geotechnical engineering and the petroleum industry. Pore throat plugging can occur by size exclusion or jamming of fine particles during fluid flow (Figure 3.1). Migration and entrapment of fine particles during flow in petroleum reservoirs can lead to clogging and decreased oil productivity. The pore throats control the rate of flow through the interconnected-pore space inducing a gate or valve effect (Chang and Civan, 1991).

A wide range of parameters affecting fines migration in porous media have been analyzed in numerous studies. These include the mean particle size, standard deviation of particle size distribution, clay concentration, rate of release coefficient, starting pressure, tramping length, network connectivity, and the role of *pH* and ionic concentration (Muecke, 1979; Gaida et al., 1985; Cerda, 1988; Khilar and Fogler, 1998). However,

there are only a few reported studies of particle bridging phenomena of large pores and perforations. Haynes and Gray (1974) studied the particle transport efficiency of suspensions through sand particles packed over a perforated casing. They proposed that a low-viscosity fluid would minimize channeling and reduce the transport efficiency because of less drag applied to particles. Fresh water and low viscosity brine were used to carry the particles into the perforations. They found that particle transport efficiency improved with increasing flow rate and decreased with particle size and concentration.

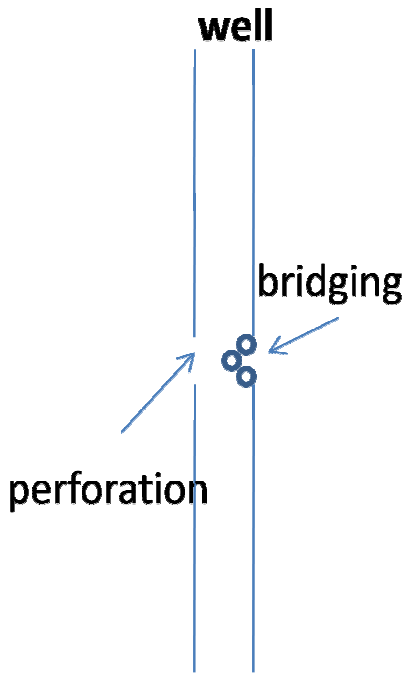

Figure 3.1: Example of particle bridging at a perforation

The following experimental study investigated the main condition that determine the plugging time for particle size compared to the pore-throat size as a function of the particle-volume-fraction Reynolds number for relatively monodisperse particles and

mixtures. The experimental data were analyzed to develop correlations for time and condition of plugging of perforations by migrating suspended particles. The correlations can be used to avoid field problems that affect flow efficiency and productivity of wells completed in petroleum reservoirs.

3.2. Experimental System and Procedure

The equipment, materials, and procedure utilized in this investigation are described in the following.

3.2.1. Equipment

The experimental equipment (Figure 3.2) used in the studies consisted of three major parts: (1) the fluid driving system that was a 2000 psig nitrogen tank equipped with a pressure regulator, (2) the transparent-plastic test cell equipped with different sizes of orifices, $D_{T,}$ and (3) a data acquisition system used to record the fluid weight and pressure in the test cell. The experiments were conducted at ambient room conditions. The equipment used in this experimental study are described as follows.

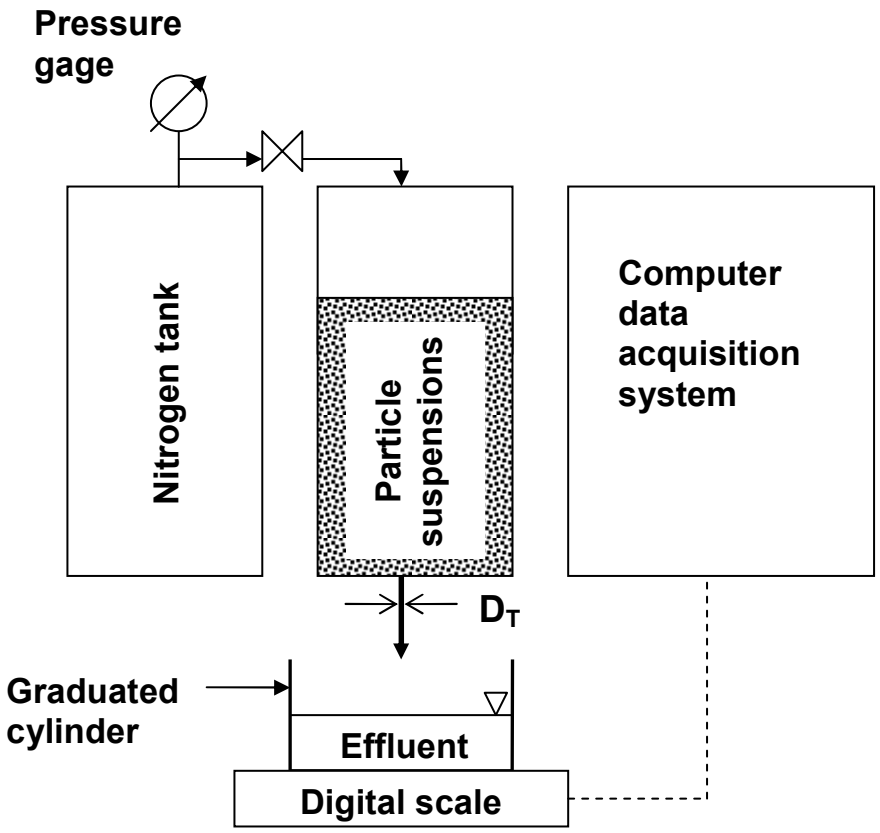

Figure 3.2: Experimental Apparatus

The commercial 82 cubic feet NI 200 Nitrogen tank was equipped with a double gauge regulator which can supply up to 2000 psig pressure to the system (Figure 3.3). The gas specification is 99.99% purity.

Figure 3.3: NI 2000 Nitrogen tank equipped with a double gauge regulator

A Honeywell ST3000 Smart Pressure transducer, Series 900 (Figure 3.4) was used to read the pressure applied to the top of the testing cell. The absolute pressure limit was 3000 psig in the temperature range from -40 to 110 ^{o}C. The transducer was calibrated using a dead-weight tester with an interval of 50 psig.

Figure 3.4: NI ST3000 Pressure transducer

A plastic 500 cm^3 capacity cylindrical test cell, with a pressure limit of 200 psi at 100 ^oF, was used. This test cell was equipped with interchangeable plastic disk at the bottom (Figure 3.5).

Figure 3.5: A 500 cm^3 cylindrical test cell

An Ohaus Explorer digital balance (Figure 3.6) was used to measure the effluent weight during the experiments. The weight capacity of the balance was 4,100 grams. The balance was connected to the computer using the standard RS232 communication port. The weight of the effluent was recorded as a function of time in the computer using the Balance Talks^{TM} software provided by Ohaus

.

Figure 3.6: Ohaus Explorer digital balance

The Data Acquisition System used for this study was the NI SC 2345 series signal conditioning box from National Instruments (Figure 3.7). The DAQ system has 16 analog inputs, 8 digital I/O lines, and 2 unconditioned counter/time I/O lines. The box was connected to the computer's serial data port. Labview 8.0 software was used to process

acquired data and timing information and display the results in engineering units on a graph.

Figure 3.7: DAQ system model NI SC 2345

A vacuum pump (Figure 3.8) was used to remove air trapped in the test fluids prior to experimental runs. The vacuum pump used for in this work was a Welch Duo-Seal Vacuum Pump Model 1400 from Sargent-Welch Scientific Company in Illinois. The pump had 1/3 horse power and operated at 580RPM.

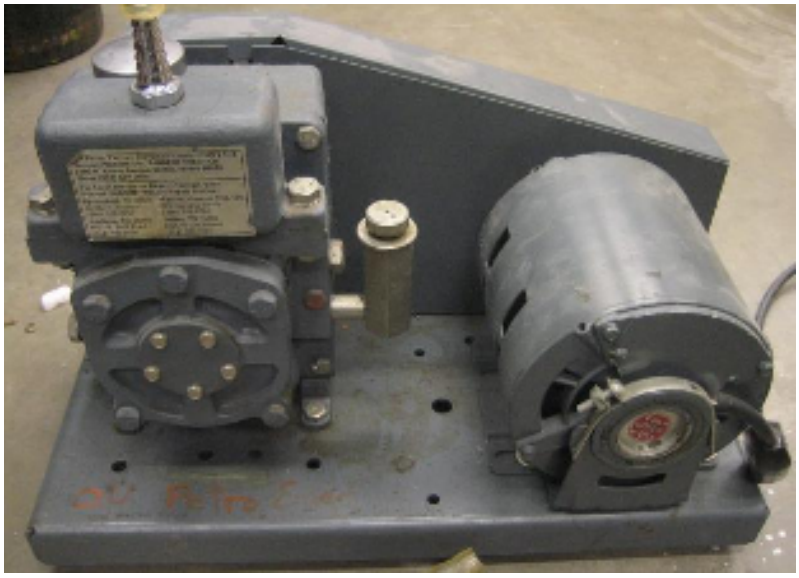

Figure 3.8: Welch Vacuum Pump

3.2.2. Materials

The fluids used in orifice plugging studies were brine and Geovis XT fluid (from C.P. Kelco Inc). The compositions and properties of the fluids are listed in Table 3-1. The particles used in the brine fluid system were spherical nylon particles with a density of 1.13 g/cm^3 and diameters of 0.16, 0.24, 0.32, and 0.48 cm. The particles used in the Geovis XT fluid system were 20/40 mesh, 30/50 mesh, and 30/70 mesh ceramic proppants with a density of 2.72 g/cm^3 (from Carbo Ceramics). The orifice diameters used in the experiments were 0.16, 0.20, 0.24, 0.32, 0.46, and 0.64 cm. The apparent viscosity of the Geovis XT fluids measured at 75^{o}F ranged from 15 to 100 cP (at shear rate of 511 s^{-1}) and was sufficient to maintain a stable suspension of proppant in the system. This was done by dissolving different weights of Geovis XT powder in 250 cm^3

of water. Mixing for more than 2 hours resulted in a well-mixed stable viscous fluid. Vacuum was then applied to the fluid for another hour to remove the trapped air from the solution. A fluid viscosity of 31 cP was chosen to ensure that the fluid effectively suspended the particles and flowed easily under the test conditions chosen. For the brine and nylon particle system, sodium chloride (NaCl) was added to the system so the density of brine equaled the density of the nylon particles. This avoided particle settling or buoyancy affects.

Table 3-1: Fluids and properties

Fluids	Additives	Composition	Density, g/cm^3
Saline Water	Water + Salt Viscosity = 1.1 cP	Water = 50 ml NaCl = 1.76 g	1.13
Geovis XT Fluid	Water + Geovis XT Viscosity = 31.0 cP at 511 s^{-1} shear rate	Water = 250 ml Geovis XT = 2.50 g	1.05

3.2.3. Procedure

The experiments were conducted at different flow rates, orifice-to-particle size ratios, fluid viscosities, and particle concentrations for each material. The effect of each

parameter on the plugging condition was evaluated. The particle concentration was varied from 0.03 g/cm^3 to 1.92 g/cm^3 of fluid, and corresponded to 0.01 to 0.40 volume fractions. The dimensionless Particle-Volume-Fraction Reynolds number (defined on page 42) varied from 0.1 to 950, so flow was laminar in terms of the pipe flow Reynolds number criteria. The orifice diameter was varied from 0.16 to 0.64 cm by installing plastic plates with different hole-sizes at the bottom of the test cell (Figure 3.9).

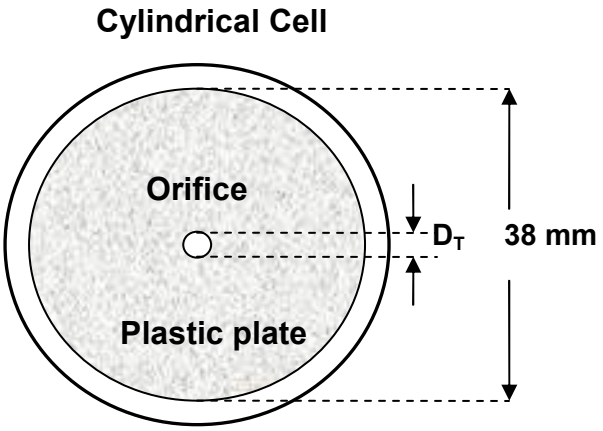

Figure 3.9: Bottom of the testing tube

The experimental procedure was as follows:

1. Particles were mixed thoroughly with fluid to the desired concentration.
2. Vacuum was applied to remove entrapped air bubbles before placing the particle-suspension into the test cell.
3. The flow rate was controlled by setting the pressure from the nitrogen tank.
4. The fluid (particle suspension) sample was poured into the test cell.

5. The nitrogen tank valve was opened with the bottom valve closed until the pressure in the cell stabilized.
6. Began flow by opening the bottom valve.
7. Collected the effluent and recorded weight as a function of time.

The plugging time for the hole was established for a specific orifice size to particle size ratio and particle concentration. Each test was repeated ten times to check reproducibility. The weight of sample transported through a orifice was collected and measured in a graduated cone at one second intervals. The weight of the collected samples was plotted versus time to determine the plugging time for each case. The plugging time was defined as the moment when the slope of the cumulative weight of effluent vs. time curve reduced significantly.

3.3. Data Analysis

The experimental data were analyzed to determine the plugging conditions and time, and the effect of coarse-fine particle mixtures.

3.3.1. Plugging Conditions

The probability of bridging increases as the particle concentration of migrating particles increase. Figure 3.10 shows the three different situations that might occur at the orifice/pore throat depending on the particle concentration.

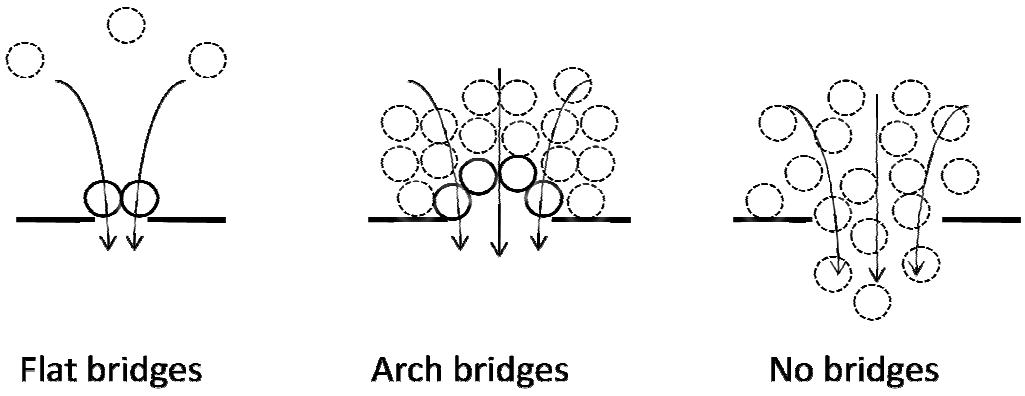

Figure 3.10: The probability of bridging depends on the concentration of particles (after Valdes and Santamarina, 2006)

Typical results determining whether plugging happened during various tests are shown in Figure 3.11. A change in slope indicates plugging. Figure 3.11a) shows the measurement data for monodisperse nylon particle (0.24 cm in diameter) flowing through a 0.64 cm diameter circular hole. The measured weight of the collected sample is plotted against time for the flow of the suspension. From the plot, it was observed that the slope did not change for the two largest solid volume fractions until the particle volume fraction increase to 0.16. The plugging was then noted and confirmed by visual observation through the transparent plastic testing cell.

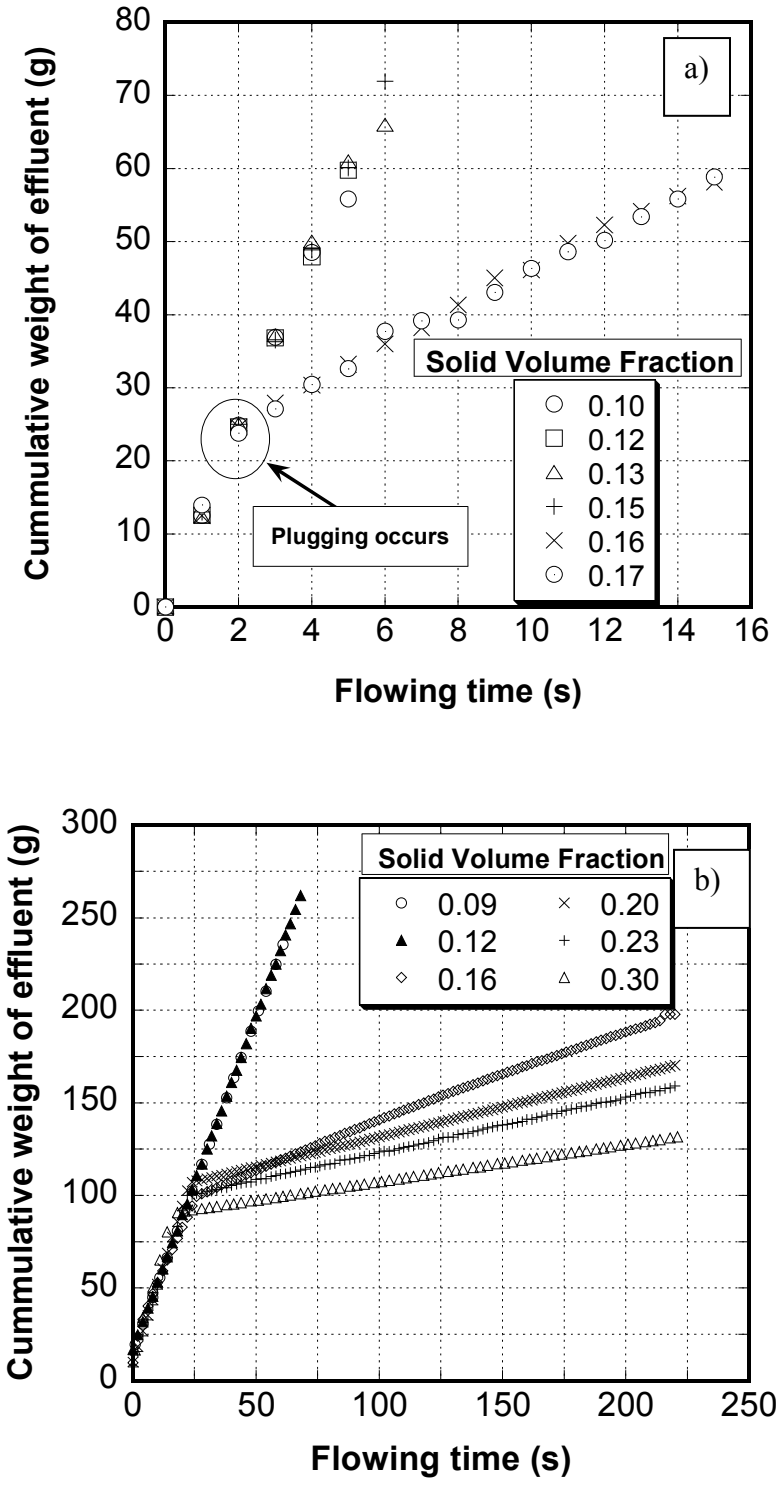

Figure 3.11: Typical results of measured weight versus time for a) nylon particle flow ($\beta = 2.67$), b) 20/40 mesh Carbo proppant flow ($\beta = 3.00$)

The maximum particle concentration that could be transported through an orifice without plugging was approximately 0.12 by volume for 20/40 mesh Carbo proppant flow test (Figure 3.11b). When the solid volume fraction was increased to 0.16, there was a decline in the slope after 24 seconds, indicating that the orifice was plugged.

This study reported experiments elucidating the effect of velocity, particle concentration, and ratio of orifice size to particle size on the plugging mechanism. The experimental data were correlated using two dimensionless variables reported by Civan (2000, 2007) to determine the condition that resulted in plugging the orifice. The first dimensionless variable was the orifice-to-particle diameter ratio:

$$\beta = D_T/D_p \text{----------(3.1)}$$

The second dimensionless group of variables, referred to as the Particle-Volume-Fraction Reynolds number was:

$$Re_p = \rho_p \sigma_p v D_p/\mu \text{----------(3.2)}$$

where ρ_p is the particle density, σ_p is the particle volume fraction, v is velocity of the particles (assumed to be the same as the suspension velocity, neglecting any slip effect), μ is the fluid viscosity, D_T is the average pore diameter, and D_p is the volume average particle diameter defined as:

$$\left(D_p\right)_{avg} = \frac{\sum_{i=1}^{n} \sigma_i \left(D_p\right)_i}{\sum_{i=1}^{n} \sigma_i} \text{----------(3.3)}$$

where σ_i is the volume fraction of particle *i*, and $(D_p)_i$ is the diameter of particle *i*.

The occurrence of plugging/bridging at certain fluid-particle conditions was determined by the following power-law and exponential-law equations, given by Civan (2000, 2007):

$$\beta = A_1 \,\mathrm{Re}_p^{\,B_1} + C_1 \qquad (3.4)$$

and

$$\beta = A_2 \left(1 - \exp\left(-B_2 \,\mathrm{Re}_p\right)\right) + C_2 \qquad (3.5)$$

The empirical parameters A_1, B_1, C_1, A_2, B_2, and C_2 were determined from regression of the experimental data using the linearized forms of equation (3.2) and (3.3).

$$\log\left[\frac{\beta - C_1}{A_1}\right] = B_1 \log\left(\mathrm{Re}_p\right) \qquad (3.6)$$

and

$$\ln\left[1 - \frac{\beta - C_2}{A_2}\right] = -B_2 \,\mathrm{Re}_p \qquad (3.7)$$

These fitting parameters were estimated by trial and error until the coefficient of determination for the data set converged to 1. The best values of the empirical parameters *A*, *B*, and *C* for the present experimental data were determined as shown in Table 3-2. Equation (3.4) and (3.5) imply that the lower-limit value of β is equal to *C* for $Re_p = 0$ for both power-law and exponential law models; and β attains an upper-limit value of

infinity and (A_2+C_2) as Re_p approaches infinity for power and exponential models, respectively. The upper limit of β in the power-law model does have an actual physical meaning for plugging/bridging situation since there is a physical upper limit β beyond which no plugging/bridging will occur for all Re_p. Therefore the model chosen to correlate the data here was the exponential-law model. The correlation for the power-law equation was also developed for nylon particle experiments (Appendix C), given by Civan (2000, 2007), but it was found to be less accurate than the exponential-law.

Table 3-2: Best-estimate parameter values

Exponential function equation (3.5) with enforcing $C = 1$

Fluid	A	B	C	R^2
Brine	1.77	0.011	1.00	0.91
Geovis XT (all data points)	3.34	0.69	1.00	0.98
Geovis XT (under constant flow rate condition)	3.49	0.67	1.00	0.99
Geovis XT (under constant particle volume fraction condition)	2.70	1.13	1.00	1.00

Exponential function equation (3.5) without enforcing $C = 1$

Fluid	A	B	C	R^2
Brine	1.58	0.0062	1.35	0.95
Geovis XT (all data points)	3.27	0.47	1.39	0.99
Geovis XT (under constant flow rate condition)	3.77	0.27	1.70	1.00
Geovis XT (under constant particle volume fraction condition)	2.68	1.09	1.03	1.00

The physical limit on the coefficient C in equation (3.4) and (3.5) is unity. However, Iscan and Civan (2006) concluded that the value of C might be greater than 1.0 because other factors such as fluid viscosity, surface forces, and inertial retardation, might prevent a single particle from moving through a pore throat even if the particle size is smaller than the pore throat size. Correlations of this study were developed for plugging conditions with and without enforcing the limiting value of C = 1.0. The fit coefficients are presented in Table 3-2. The results showed that higher regression coefficients were achieved when C was determined for best fit of the experimental data instead of setting its value as C = 1.0 (Figure 3.12 and 3.13).

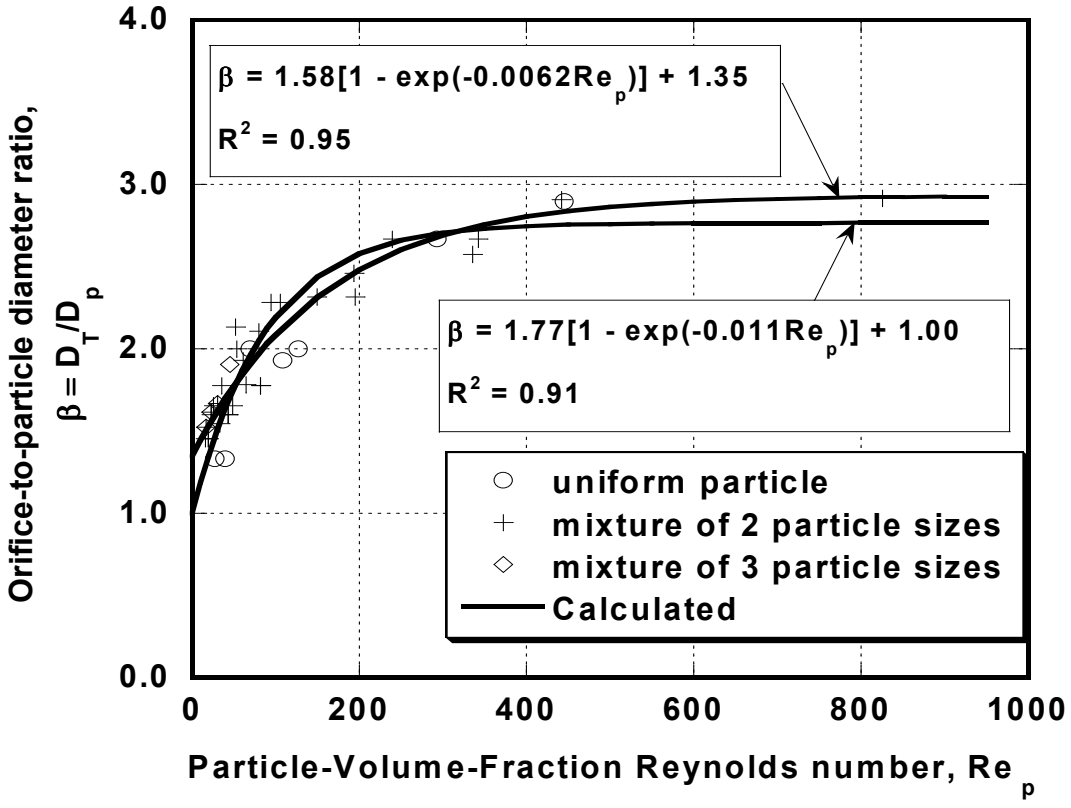

Figure 3.12: Exponential law model for mixture of nylon particles in brine under constant flow rate of 8.00 cm^3/s

Figure 3.12 shows the exponential correlation fits using both models for nylon particles (diameter of 0.16, 0.32, and 0.48 cm) in brine. The test was repeated with relatively monodisperse particles, mixtures of two and three different diameter particles of various ratios (1:3, 1:1, 3:1- of big-small particles, 1:1:4, 1:2:4, 4:1:1, 4:2:1) to explore a wide range of plugging conditions. Nylon particles were mixed with brine of equal density, $\rho_f = \rho_p$, to create a stable suspension.

The region below a curve indicates the plugging conditions while the region above it is the non-plugging. The exponential model works well for these experimental data with high regression coefficients of $R^2 = 0.91$ for $C = 1$ and $R^2 = 0.95$ for $C \neq 1$. This model is concentration sensitive for low β ($1 < \beta < 1.5$) as a small change in particle concentration will shift the position from non-plugging to the plugging region. Bridging inside a orifice occurs even at low particle concentration as the pore throat to particle diameter ratio approaches 1. For $\beta > 2$, the critical concentration for bridging increased dramatically because the probability of the particles approaching the orifice "*simultaneously*" to form a bridge was small at such concentrations. However, when $\beta > 3$, no plugging occurs over the range of $0 < Re_p < 1000$ even at a particle concentration of 1.92 g (0.40 volume fraction), as seen in the region above the curve in Figure 3.12.

Similar results were observed for the Carbo proppant in Geovis XT fluid. The exponential-law model works well to determine the fitting parameters of the plugging conditions. The regression coefficients R^2 were 0.98 for $C = 1$ and 0.99 for $C \neq 1$. Figure 3.13 is for determination of particle bridging conditions.

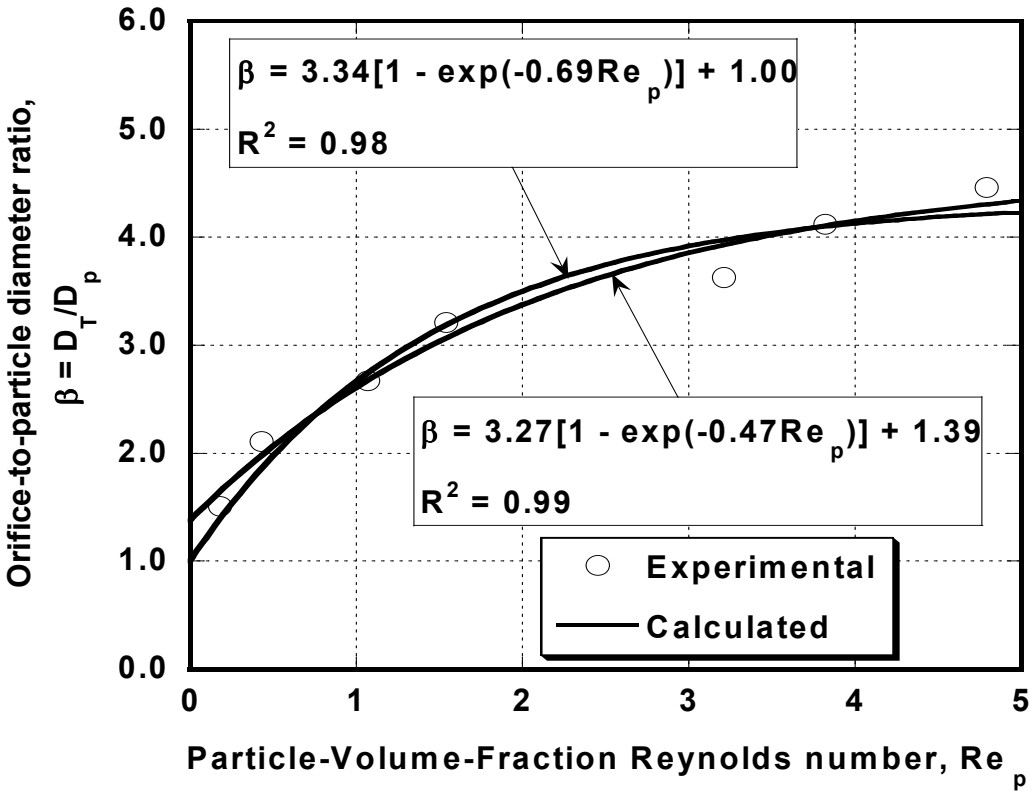

Figure 3.13: Exponential law model for mixture of Carbo proppants in Geovis XT fluid for all data points

A stable bridge was observed for $1 < \beta < 5$ with Carbo proppants and no bridge was formed for $\beta > 5.0$ over the range of $0 < Re_p < 5$, even at high particle concentrations. Field engineers are more interested in operation conditions under constant flow rate or constant particle volume fraction of the flowing fluid. Figures 3.14 and 3.15 show the bridging condition curves under constant flow rate and constant particle volume fraction, respectively.

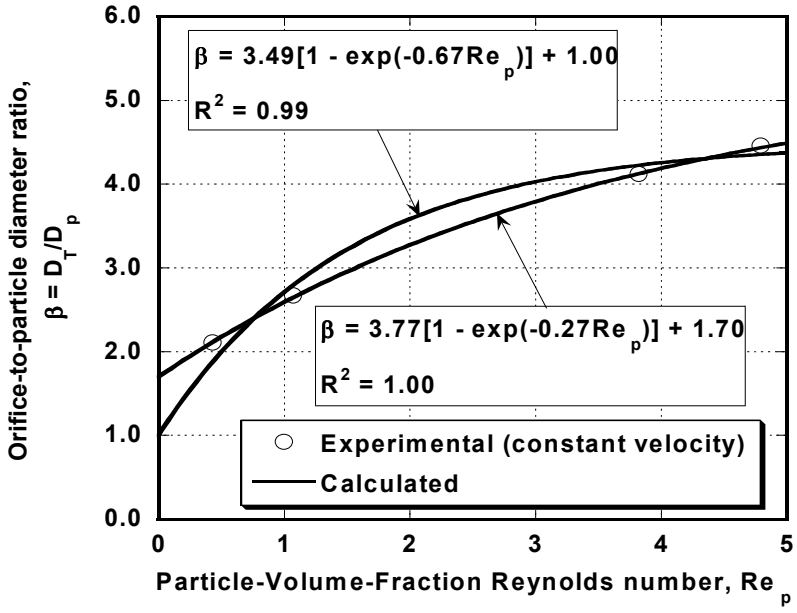

Figure 3.14: Exponential law model for mixture of Carbo proppants in Geovis XT fluid under constant flow rate of 4.25 cm^3/s

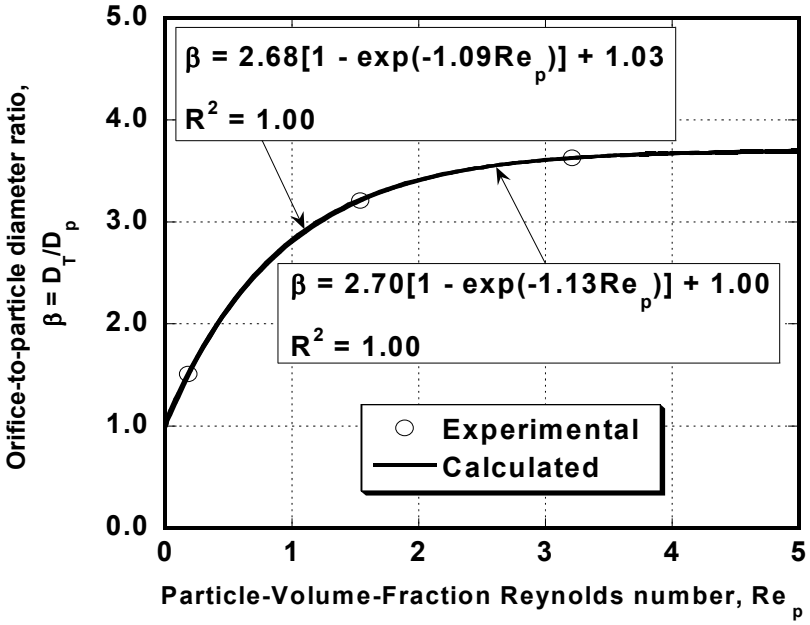

Figure 3.15: Exponential law model for mixture of Carbo proppants in Geovis XT fluid under constant particle volume fraction of 0.07

3.3.2. Plugging Time

Orifice and pore-throat plugging do not happen instantaneously as indicated by the experimental data presented in Figure 3.11. There is some retardation effect that delayed the jamming process. The plugging time primarily depends on the probability of more than one particle arriving at the orifice or pore throat at the same time. The plugging time gets shorter as the particle concentration increases. This is confirmed in Figure 3.16 that shows the cumulative weight of effluent versus time for nine different particle concentrations. The change of slope of the straight lines indicates the plugging time for each run. The experimental data presented in Figure 3.16 were obtained using 31 cP Geovis XT fluid and Carbo proppant with diameter of 0.07 cm. The pore throat-to-particle diameter ratio was 2.5. The tests were run at a constant flow rate of 8.25 cm^3/s. It can be seen from Figure 3.16 that the plugging time depends on the particle concentration. Complete plugging occurred faster for higher particle concentration fluids (7s for particle volume fraction of 0.305); and it took longer to plug the pore throat for lower particle concentration (17 s for particle volume fraction of 0.065). No plugging was observed for concentrations no greater than 0.055 by volume fraction. Hence, the critical volume fraction for plugging was determined to be 0.055.

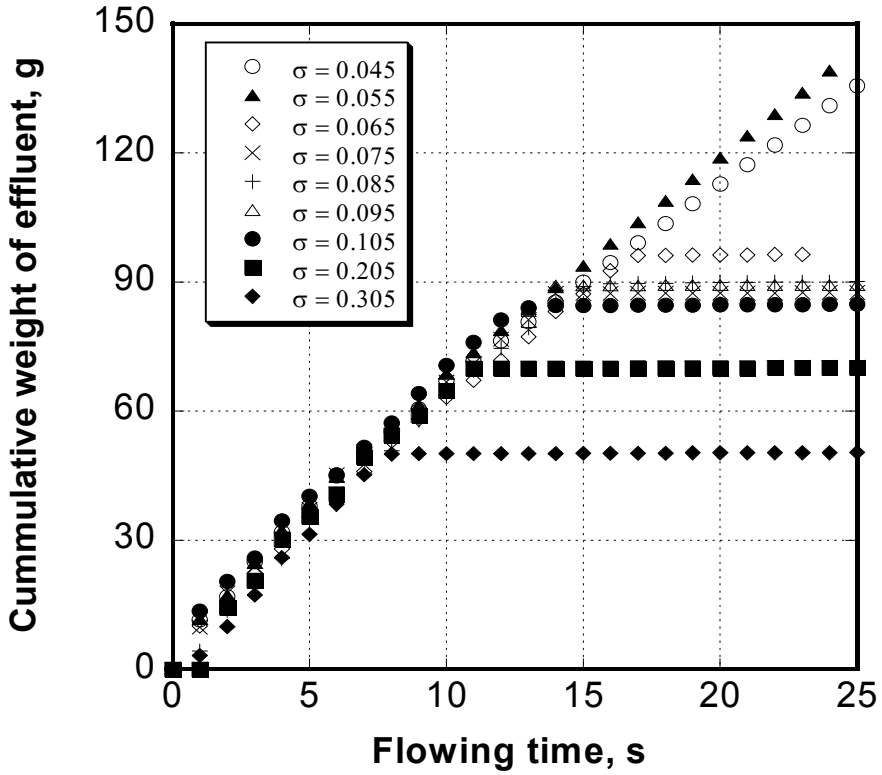

Figure 3.16: Effect of particle concentration on plugging time (β = 2.5, μ = 31 cP, q = 8.25 cm^3/s)

The plugging times are shown in Figure 3.17 for various particle volume fractions under the same flow condition.

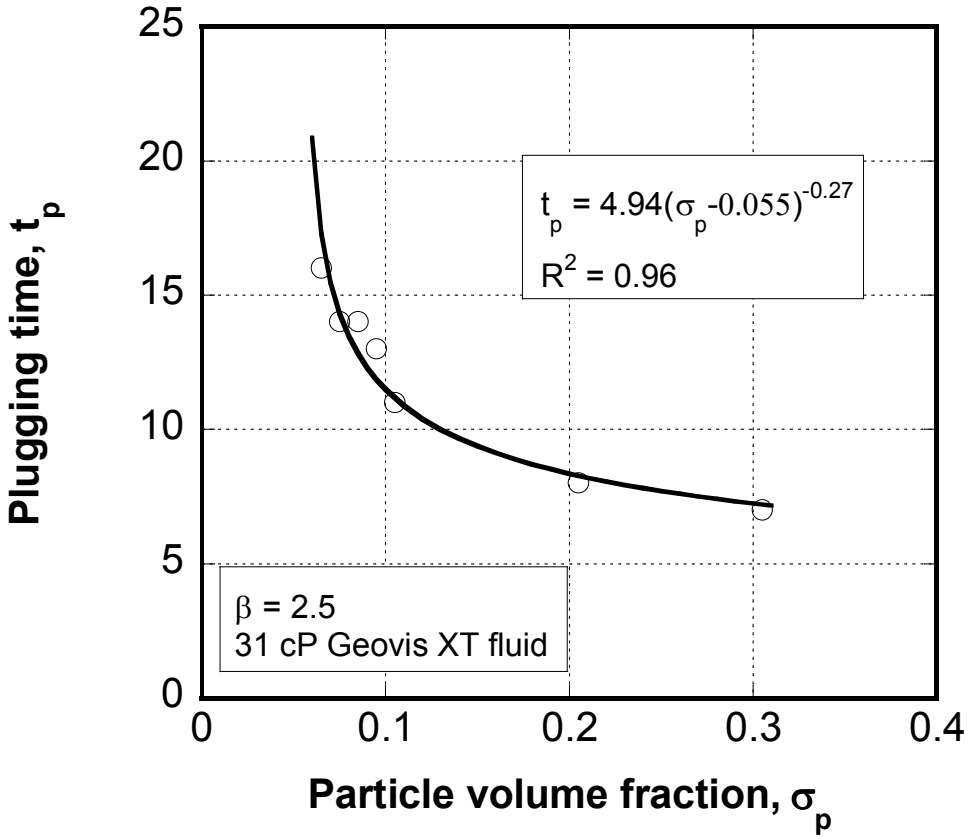

Figure 3.17: Plugging time vs. particle volume fraction under condition of constant flow rate of 8.25 cm^3/s

As demonstrated in Figure 3.17, the plugging time t_p can be correlated successfully by a power law function of the reciprocal-particle volume fraction σ_p above its critical value:

$$t_p = a\left(\sigma_p - \sigma_{pcr}\right)^{-b} \text{----------(3.8)}$$

where a and b are the model fitting parameters, σ_{pcr} is the critical particle volume fraction for the plugging to occur ($\sigma_{pcr} = 0.055$ for this case). Figure 3.18 is the log-log plot of t_p vs. $(\sigma_p - \sigma_{pcr})$. The straight-line was obtained where parameters b was the slope and $log(a)$ was the intercept.

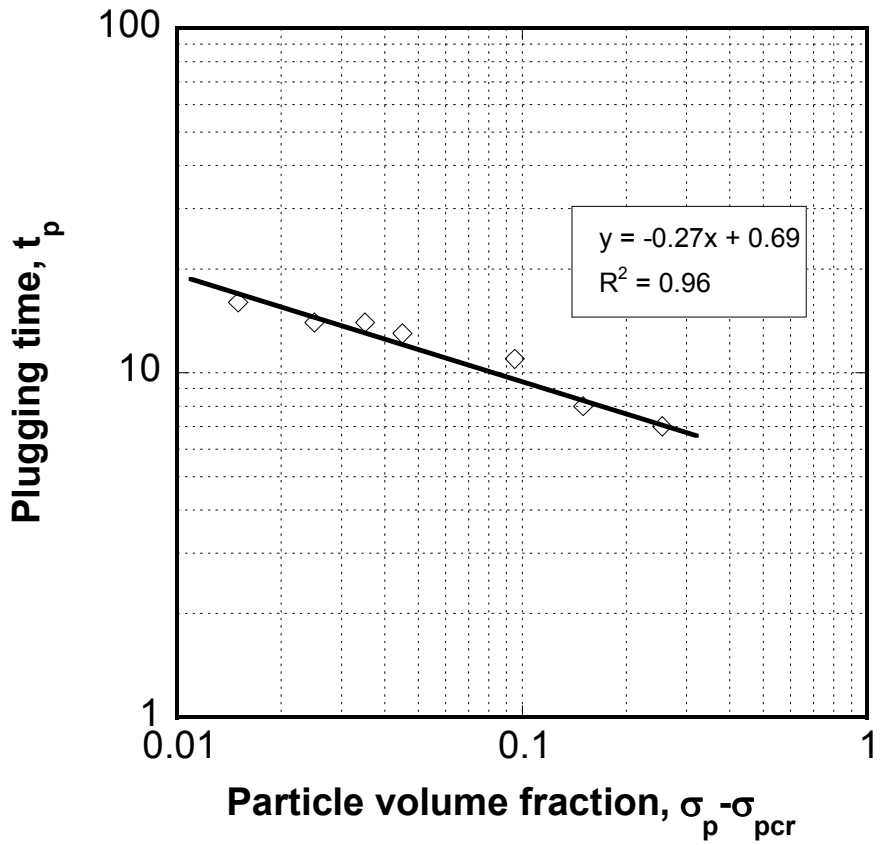

Figure 3.18: Log-log plot of t_p vs. ($\sigma_p - \sigma_{pcr}$)

Figure 3.19 is the plugging time comparison for different orifice-to-particle diameter ratios. As expected, plugging occurred faster for smaller β, and it took longer to plug the pore throat for a larger β. Empirical parameters for the exponential function for the plugging time are presented in Table 3-3.

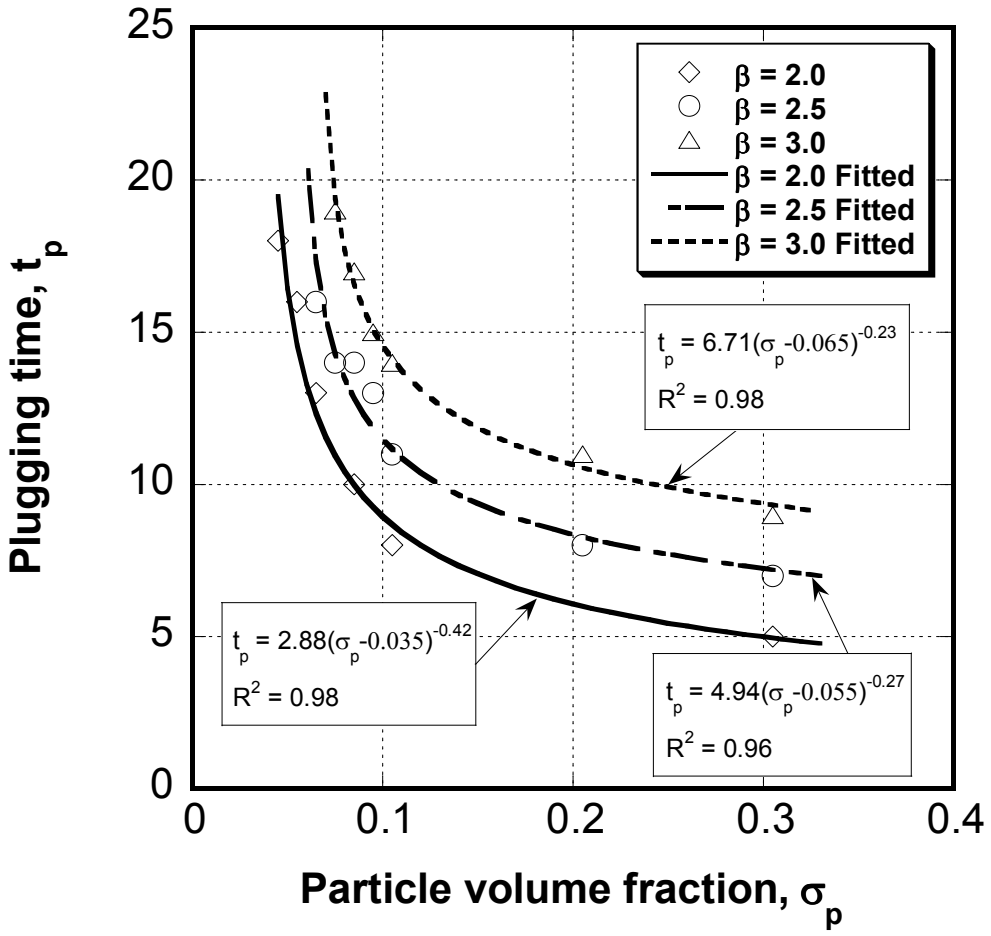

Figure 3.19: Plugging time vs. Particle volume fraction for different orifice-to-particle diameter ratio

Table 3-3: Best-estimate parameter values for equation (3.8)

Power law function equation (3.8)

β	a	b	R^2
2.0	2.88	0.42	0.98
2.5	4.94	0.27	0.96
3.0	6.71	0.23	0.98

3.3.3. Coarse/fine Particle Mixtures

A mixture of coarse and fine particles was prepared to investigate the effect of particle size distribution on the plugging time. The two particle sizes used had diameters of 0.02 and 0.07 cm and the orifice diameter was 0.20 cm. The fine particles did not have significant impact on plugging time in the mixture.

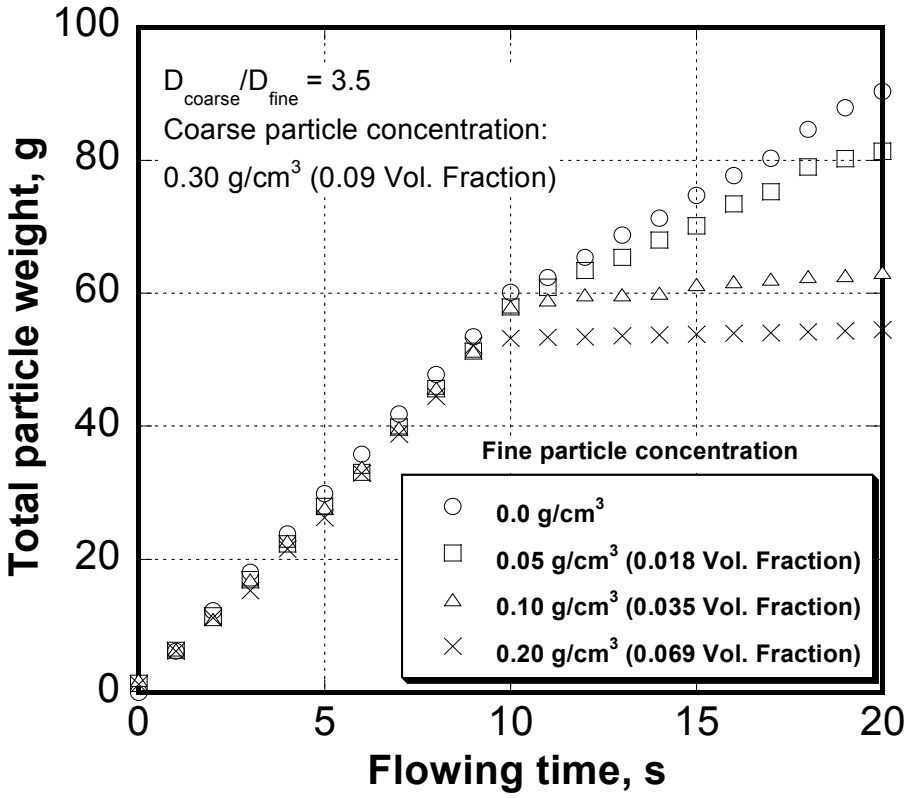

Figure 3.20: Effect of fine particle on plugging time in the mixture

As shown in the Figure 3.20, the plugging time for different fine particle concentrations did not change significantly compared to the plugging time for the monodisperse coarse particle (0.0 g/cm^3 of fine particle). After plugging occurred (about 9 to 10 seconds), the slope was smaller as fine particles were added into the mixture. Once the bridge was formed by coarse particles, it acted as increasingly effective traps for the flowing particles. The fine particles continued depositing at the bridge and acted as a membrane, retarding fluid from flowing.

3.3.4. Effect of the flow field on the plugging condition

The case of laminar flow in a pipe toward an orifice (e.g. pore throat) was considered. In the far field of the orifice, stream lines are straight and parallel. As flow progresses toward the orifice (near field), the flow streamlines curve and begin to converge. The local suspended particle concentration at the near field will increase and result in a higher probability of bridging.

In this experiment, the flow field disruption was created by altering the angle of the funnel-like opening hole at the bottom of the testing cell (Figure 3.21).

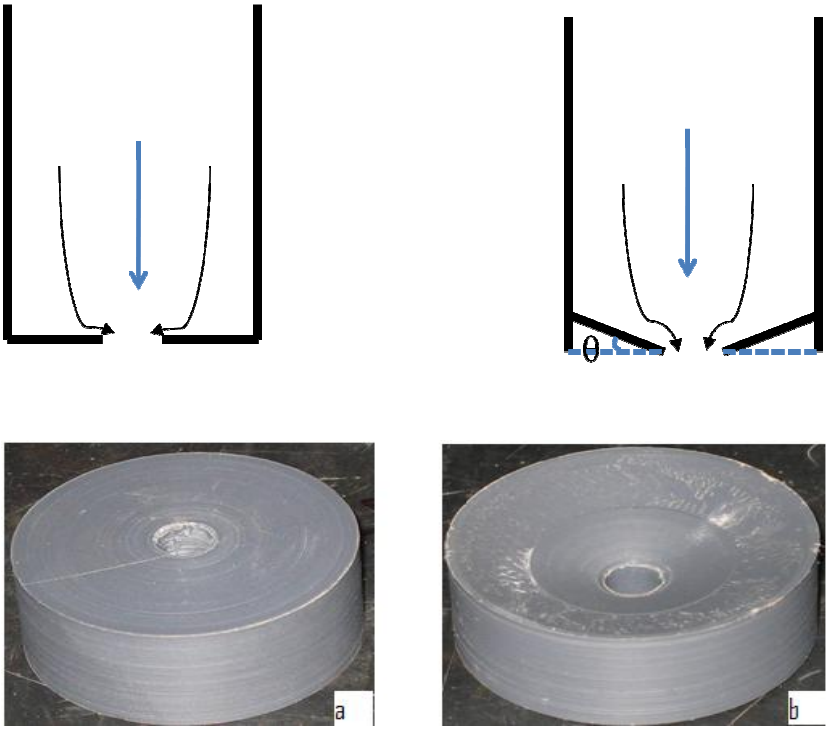

Figure 3.21: Geometry of the investigated pore throat: a) θ = 0^o and b) θ > 0^o

The objectives of this study were to determine plugging conditions for different angle θ and correlate plugging time as a function of θ.

Nylon particles were used for this set of experiments at different diameters: 0.48 - 0.40 - 0.31 cm. Materials used in the experiments are presented in Table 3-4.

In this study, it was observed that there was no bridging for Reynolds number less than 10, even though the orifice-throat-to-particle diameter was varied. Thus, there might be a critical Reynolds number below which bridging did not occur for a particular fluid suspension.

Table 3-4: Materials used for the flow disruption tests

Fluids/Particles	Additives	Composition	Density, g/cm^3	Angle θ, degree
Saline Water/ Nylon particles	Water + Salt Viscosity = 1.1 cP	Water = 500 cm^3 NaCl = 17.6 g	1.13	0 15 30 45
Pore throat diameter = 0.64 - 0.80 cm Particle diameters = 0.48 - 0.40 - 0.31 cm				

Because the fluid used in this set of experiments was brine, the viscosity and retardation effects could be assumed to be insignificant. Hence, the coefficient *C* in equation (3.5) could be assumed to be unity. The critical Reynolds number term was added to equation (3.5) as another fitting parameter as described in equation (3.9):

$$\beta = A\left\{1 - \exp\left(-B\left(\mathrm{Re}_p - \mathrm{Re}_{pc}\right)\right)\right\} + 1 \quad \text{----------(3.9)}$$

Figure 3.22 shows curve fitting using equation (3.9) for different angles, θ. As observed, bridging occurred at higher β for lower angle θ at the same flow condition (same Re_p). The empirical parameters for equation (3.9) are presented in Table 3-5. The critical Reynolds numbers (Re_{pc}) were found to decrease as the angle θ increased.

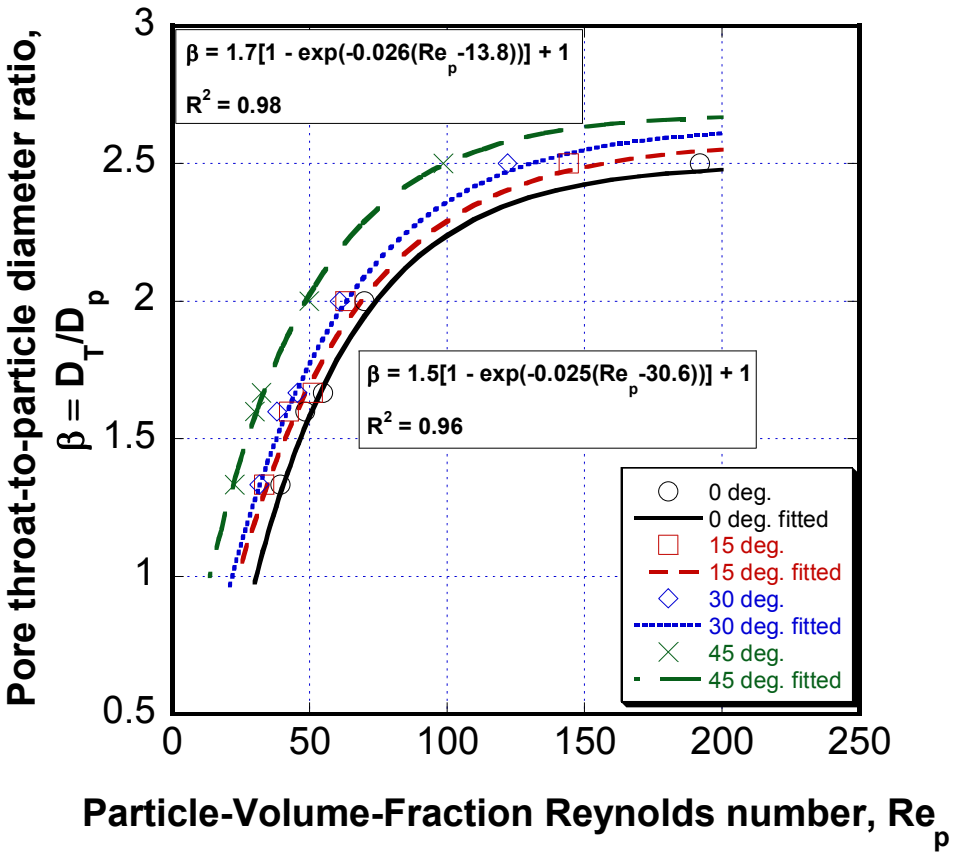

Figure 3.22: Exponential model for nylon particle plugging at different θ

Table 3-5: Empirical parameters for equation (3.9)

θ, degree	A	B	Re_{pc}	R^2
0	1.50	0.025	30.6	0.96
15	1.58	0.022	24.0	0.97
30	1.64	0.023	21.9	0.93
45	1.68	0.026	13.8	0.98

The parameters of equation (3.9) were correlated with respect to angle θ as shown in Figure 3.23 and 3.24.

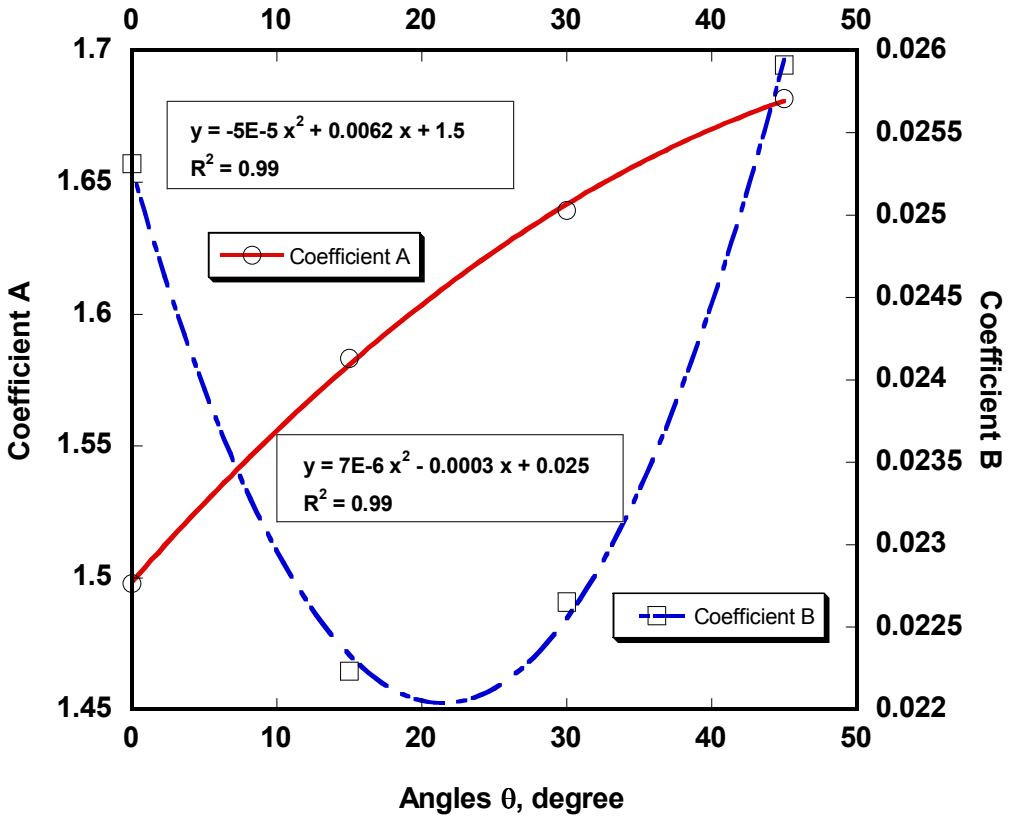

Figure 3.23: Coefficients *A* and *B* for equation (3.6)

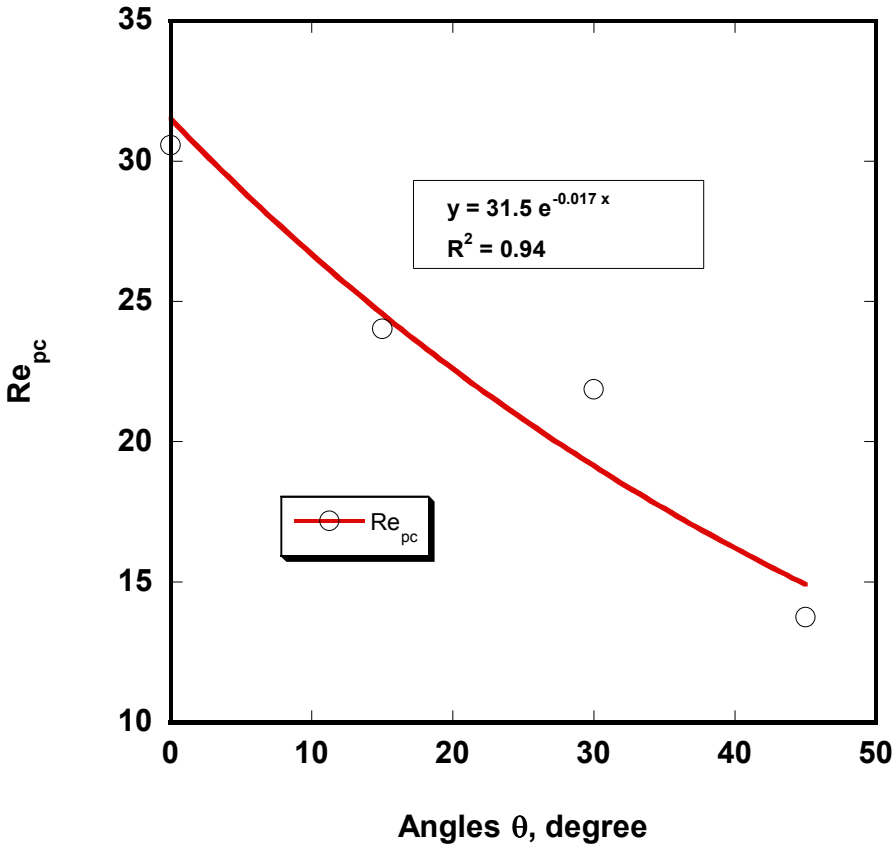

Figure 3.24: Coefficients Re_{pc} for equation (3.9)

The above correlations can be used to generate plugging curves for different θ angles. These allow predicting plugging/non-plugging conditions at pore throats. Figure 3.25 represents the simulated plugging curves for θ = 0, 15, 30, 45, and 60 degree.

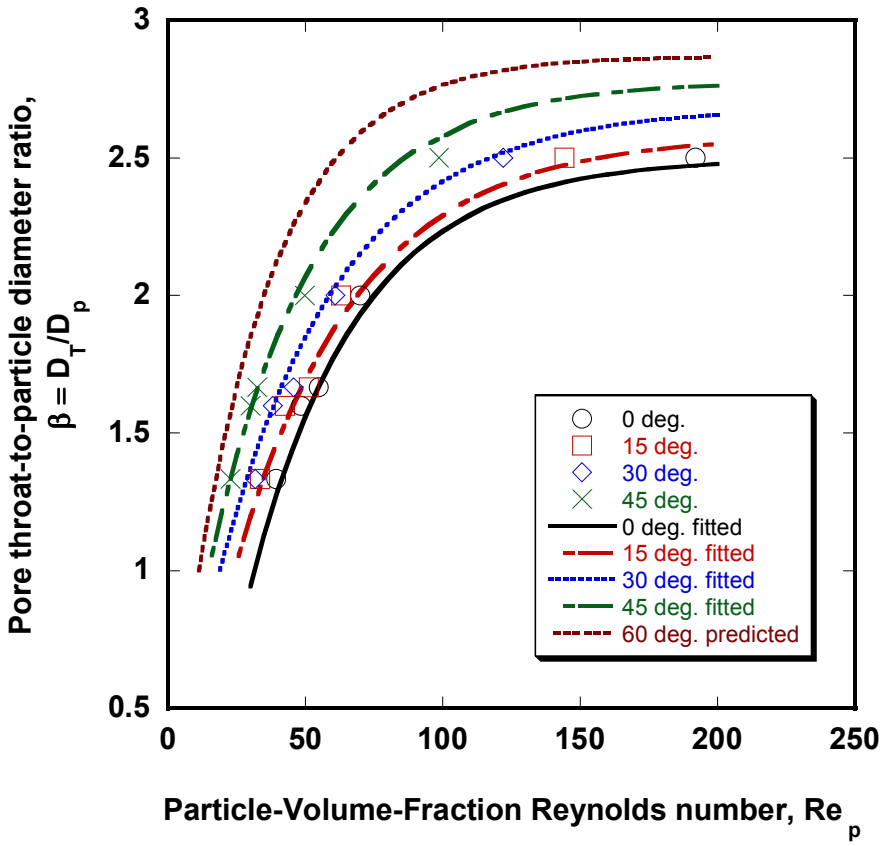

Figure 3.25: Generated plugging condition curves for different θ angles

3.4. Conclusions

On the basis of the studies conducted here, the following conclusions may be made:

1. The empirical correlations developed in this study can be used in determine orifice plugging conditions during flow of spherical particle suspensions. Conditions that cause pore plugging by migrating particles can be avoided in the field.

2. It is obvious that the 1/3-rule strictly applies only under limited conditions of volume fraction of solids and flow rates and is not adequate for general applications. To prevent plugging, the ratio of orifice diameter to average particle diameter versus Particle-Volume-Fraction Reynolds number (Re_p) should be in the region above the correlated curve using the exponential-law expression.
3. The use of the dimensionless Particle-Volume-Fraction Reynolds number (Re_p) proved convenient because it represented the essential fluid characteristics to provide a criterion for determining the conditions that lead to plugging. The effects of temperature and pressure are implicitly included through the physical properties involved the Particle-Volume-Fraction Reynolds number (Re_p).
4. The plugging time varied with the volume of particles contained within the suspension of particles. When plugging conditions exist, the higher the particle volume fraction, the shorter the plugging time. The plugging time vs. reciprocal-particle-volume-fraction yields a power law-type correlation. This correlation helps estimation of time required for the plugging to occur.
5. There is an existence of a critical Reynolds number below which the bridging does not occur. The angle θ at the opening hole does have an effect on the condition leading to plugging of the suspensions i.e. plugging occurs more easily for higher θ.
6. The conclusion of Iscan and Civan (2006) that the lower-limit value of the critical pore-to-particle diameter ratio below which plugging occurs may exceed the physical limit of 1.0 was reconfirmed. Further study is recommended to investigate how relevant factors affect this condition.

4. Chapter 4: Investigation of Plugging in Slot by Suspended Particles

4.1. Introduction

Naturally fractured formations and slotted-liner completions often undergo plugging phenomenon caused by particulate matter under certain fluid and flow conditions. This plugging causes loss of well performance during oil and gas production from hydrocarbon reservoirs. The reduction in productivity results when particles migrating at high concentrations form bridges across the fractures or slots and reduce permeability of naturally-fractured porous formations or slotted liner completions. In spite of the practical importance, few studies have been reported in the literature concerning the plugging of rectangular openings like fractured formations and slotted liners.

This chapter is an extension of the Chapter 3 studies to provide correlations that can be used to determine operational conditions that avoid plugging of non-spherical openings in slotted liners and natural fractures by spherical particles. The experiments were conducted to gain insight into bridge formation dependence on particle size, concentration, flow conditions, and fracture-opening aspect ratio (which will be discussed in a later section). This work also investigated the role of slot (or fracture opening) length, which had not been previously reported. Although the present tests were run at ambient conditions, the effects of temperature and pressure on correlations are implicitly included through fluid density and viscosity.

4.2. Experimental System and Procedure

The experimental setup and procedure were similar to those used in the orifice plugging study in Chapter 3.

4.2.1. Equipment

The experimental apparatus was similar to one in Chapter 3. The setup contained a 1.5-in ID 2-ft long transparent-plastic test cell. An interchangeable simulated slot was placed at the bottom of the cell as shown in Figure 4.1. A prescribed 500 cm^3 volume of fluid with suspended particles was loaded in the test cell and forced through the slot using the 2,000-psig nitrogen tank. A pressure regulator was used to adjust the flow rate. The weight of the effluent from the slot was measured and recorded using the computer data acquisition system.

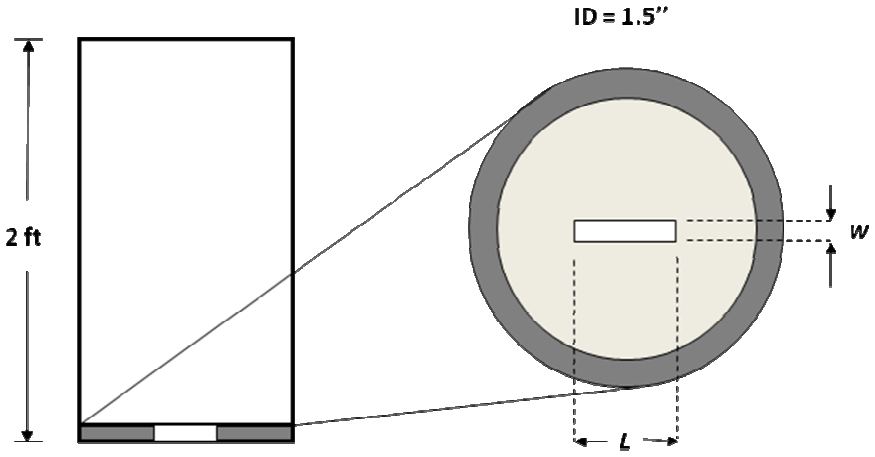

Figure 4.1: Schematic of the test cell

4.2.2. Materials

Diutan powder (from C.P. Kelco, Inc.) was used to increase the viscosity of the carrier fluid. A commercial blender was used to prepare the fluid. The Geovis XT powder was mixed into 500 cm^3 of water for 30 minutes to make sure the powder was fully dissolved. After the fluid was prepared, it was centrifuged and vacuumed to remove any air bubbles. The apparent viscosity was then measured at ambient temperature 75^oF with a Fann 35 controlled strain rate apparatus at a shear rate of 511 s^{-1}. Several concentrations of Diutan were studied. The one chosen was 1.86% by weight and had a viscosity of 65 cP. This concentration avoided particle settling and buoyancy effects during the test. Detailed properties of the fluid are presented in Table 4-1.

Table 4-1: Fluid properties

Fluids	Additives	Composition	Density, g/cm^3
Diutan Fluid	Water + Diutan Viscosity = 65 cP at 511 s^{-1} shear rate	Water = 500 cm^3 Diutan = 9.30 g	1.02

The particles used in the experiments were glass beads and ceramic proppants from Carbo Ceramics, Inc. with densities of 2.54 g/cm^3 and 2.72 g/cm^3, respectively. The particles were carefully sieved using sieves number 14, 18, 20, 25, and 30 to get several

different uniform particle sizes. Table 4-2 summarizes the properties of the particles that were used in the experiments.

Table 4-2: Solid particle properties

Particle Type	Density, g/cm^3	Shape	Diameter, cm
Ceramic Proppant	2.54	Sphere	0.06; 0.07; 0.08; 0.10; 0.14
Synthetic Glass Bead	2.72	Sphere	0.10; 0.12; 0.15; 0.20; 0.25

The slot dimensions used in this study were combinations of widths w = 0.16 and 0.32 cm, and lengths L = 0.64, 1.28, and 2.56 cm.

4.2.3. Procedure

The particles were thoroughly mixed into the fluid at the desired concentration and vacuum was applied to remove air bubbles before putting the particle-suspension into the test cell. The flow rate was adjusted using pressure applied from the nitrogen tank. After placing the particle suspension into the test cell, the nitrogen tank valve was opened while keeping the bottom valve closed until the pressure in the cell stabilized. Fluid flow was then initiated by opening the bottom valve. The plugging response was determined for the specific slot size to the particle size ratio and particle concentration. Each test was repeated ten times to check reproducibility. The sample weight transported through a slot was collected and measured in a graduated cylinder at 1-second intervals. This was plotted versus time to determine the plugging time for each case. The plugging time was

defined as the moment when the slope of the cumulative fluid weight vs. time curve decreased significantly.

4.3. Data Analysis

In this section, the plugging conditions and plugging time are analyzed and correlated using relevant parameters.

4.3.1. Plugging Conditions

The flow of the particle dispersions through the various slot geometries was measured similar to the experiments of Chapter 3. Typical results are shown in Figure 4.2. The change in slope indicates the onset of plugging. The highest particle concentration that could be transported through the slot without plugging was 0.25 by volume fraction in this particular case. A plug formed when the particle concentration increased to 0.28.

Variables in the test included fluid properties, flow rate, slot size, fracture opening geometry, particle size, and particle concentration in the fluid. Experimental data were correlated using two dimensionless groups modified after Civan (2000, 2007). The first dimensionless group was slot width-to particle diameter ratio $\beta = w/D_p$. The second dimensionless group was the Particle-Volume-Fraction Reynolds number $Re_p = \rho_p \sigma_p v D_p/\mu$, where ρ_p is the particle density, σ_p is the particle volume fraction, v is velocity of the particles (assumed to be the same as the suspension velocity, neglecting

any slip effect), μ is the fluid viscosity, w is the slot width, and D_p is the volumetrically-weighted average particle diameter defined as in equation (3.3).

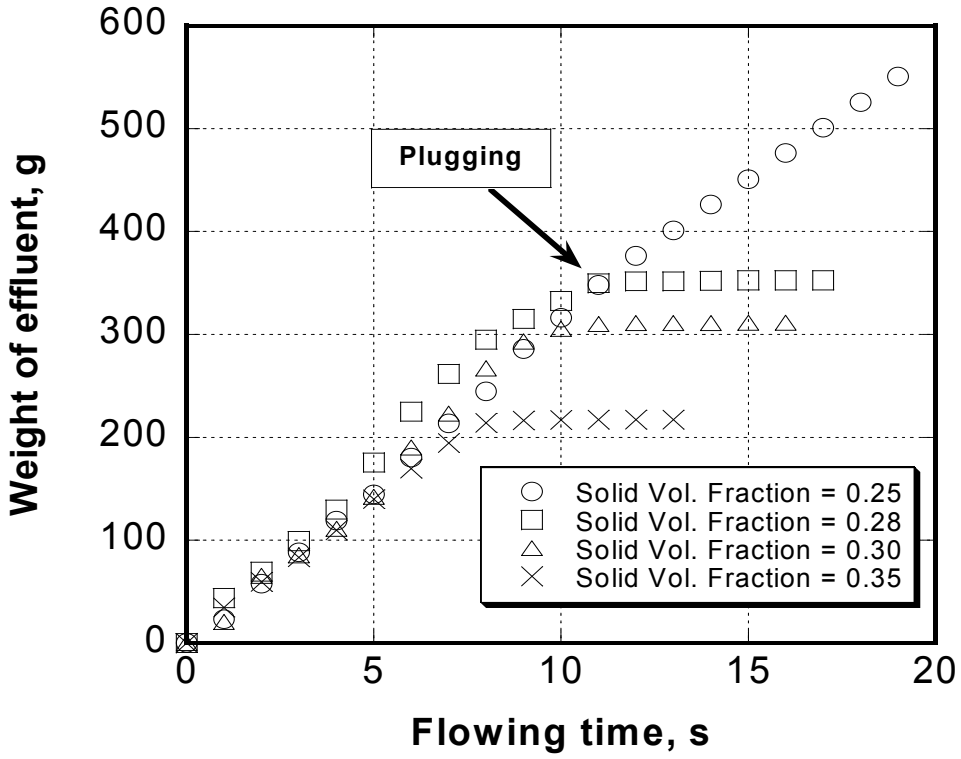

Figure 4.2: Typical result of the measured weight vs. time for Ceramic proppant (particle diameter ~ 0.10 cm) with Diutan fluid flowing through a rectangular slot (w = 0.16 cm, L = 0.64 cm)

Figure 4.3 shows the correlations for plugging of Ceramic proppants (particle diameters of 0.06, 0.07, 0.08, 0.10, and 0.14 cm) suspended in 65 cP Diutan fluid under a constant flow rate of 4.50 cm^3/s. The test was repeated with dispersions of various sizes

of proppant to develop a wide range of plugging conditions. Three different slots were used. The width was constant at w = 0.16 cm, but different lengths L = 0.64 cm, 1.28 cm, and 2.56 cm were used. The exponential model worked well for all three sets of data. The fitting parameters for β are presented in Table 4.3. Similar to the orifice plugging experiments, the model was particle-concentration-sensitive at low β. It was observed that for $\beta > 3$, no plugging occurred during the experiment even at high particle concentration (over 0.40 of solid volume fraction). In addition, results showed that the plug formed at higher particle concentration in longer slots (longer L) but not shorter lengths. In other words, the plugging condition not only depends on slot width/particle size, and the particle concentration, but is also influenced by the slot length. The greater the length of the slot the more difficult it is to plug a rectangular opening. This was expected from the reduced crowding near the ends of the slot. The maximum β under which plugging can occur are approximately 3, 2.5, and 1.9 for the slot lengths of 0.64, 1.28, and 2.56 cm, respectively. Hence, another dimensionless variable, the aspect ratio of slot, was used to include the effect of slot dimensions in the equation through described in the modified slot size-to-particle size ratio.

$$\beta' = \gamma / D_p \quad \text{----------(4.1)}$$

where β' is the modified slot size-to-particle size ratio, γ is the shape factor of the fracture.

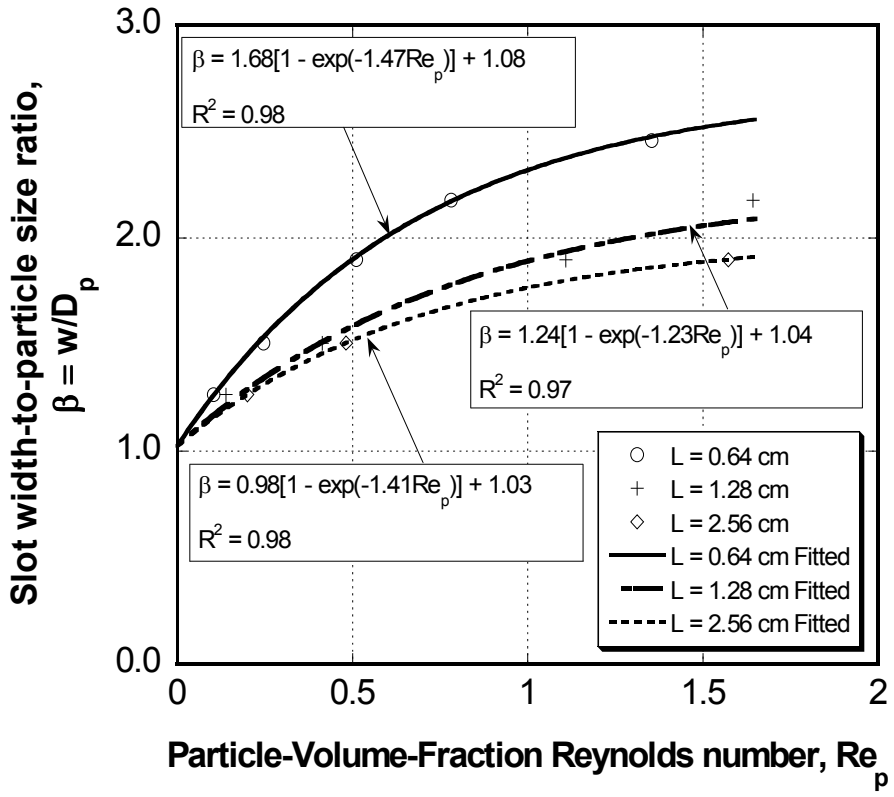

Figure 4.3: Exponential law model for various sizes of Ceramic proppant suspensions under constant flow rate of 4.50 cm^3/s (w = 0.16 cm)

The shape factor defined as $\gamma \equiv \frac{wL}{w+L}$ is the harmonic average of the slot width and length. All three sets of data used in Figure 4.3 were combined to develop a single correlation that included all three cases. Figure 4.4 shows the particle plugging conditions using the slot shape factor-to-particle size ratio β'. The regression coefficient was R^2 = 0.97 for the exponential model. A stable plug was observed for $0.795 < \beta' < 2.0$. No plug was formed for $\beta' > 2.0$ over the range of $0 < Re_p < 2.0$ even at particle concentrations as

high as 0.55 volume faction. The top-line of Table 4-4 lists the coefficient values for *A*, *B*, and *C* for equation (3.5) using *β'* for the ceramic proppant suspensions.

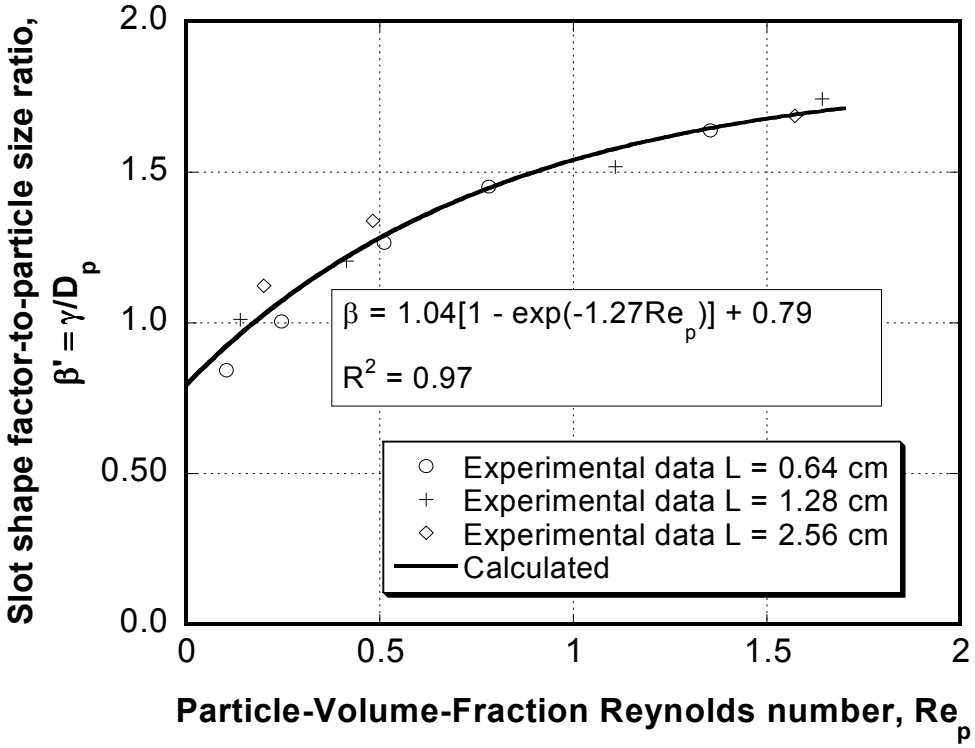

Figure 4.4: Experimental and calculated results from exponential model for Ceramic proppant suspensions using shape factor equation (w = 0.16 cm)

Similar results were obtained using glass beads suspended in Diutan fluid. Suspensions of glass beads with diameters of 0.10, 0.12, 0.15, 0.2, and 0.25 cm were used. Three different slots were used. The tests used the same slot lengths as the ceramic proppant tests. The width was constant at w = 0.32 cm. Figures 4.5 and 4.6 show the

exponential correlations obtained using the dimensionless variables β and β'. The regression coefficient for the exponential model using the modified β' is found to be R^2 = 0.98. No plug was formed for $\beta' > 2.0$ in these experiments.

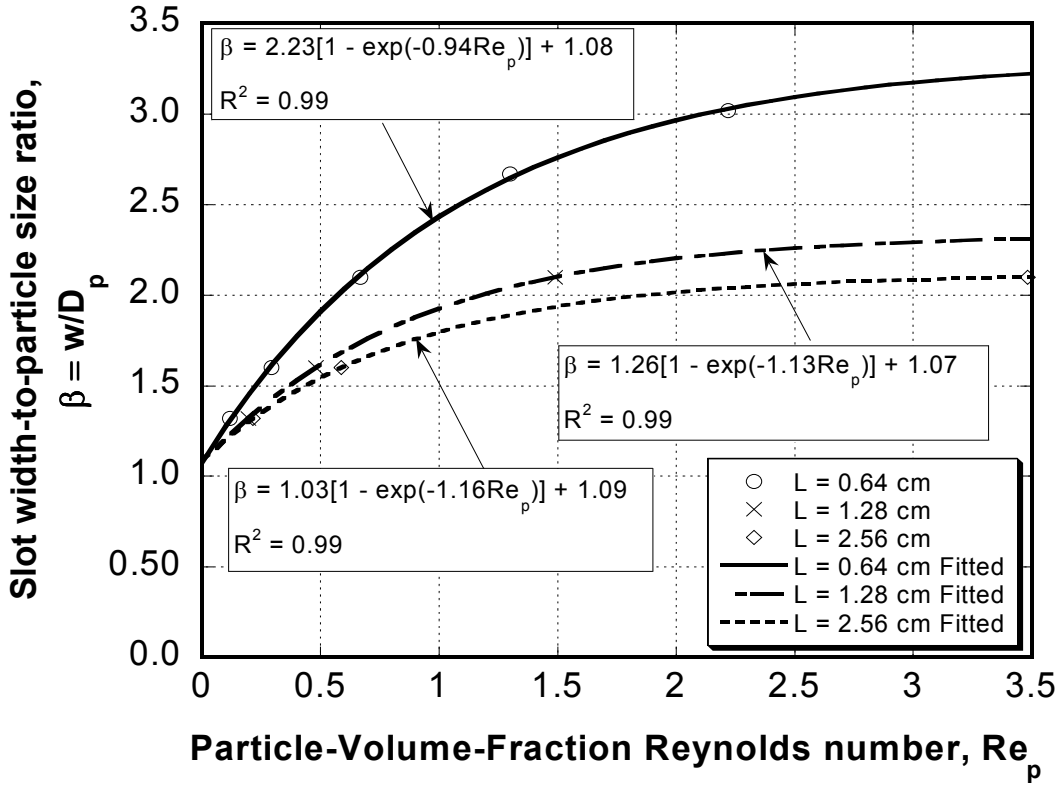

Figure 4.5: Exponential law model for glass-bead suspensions under constant flow rate of 4.50 cm^3/s (w = 0.32 cm)

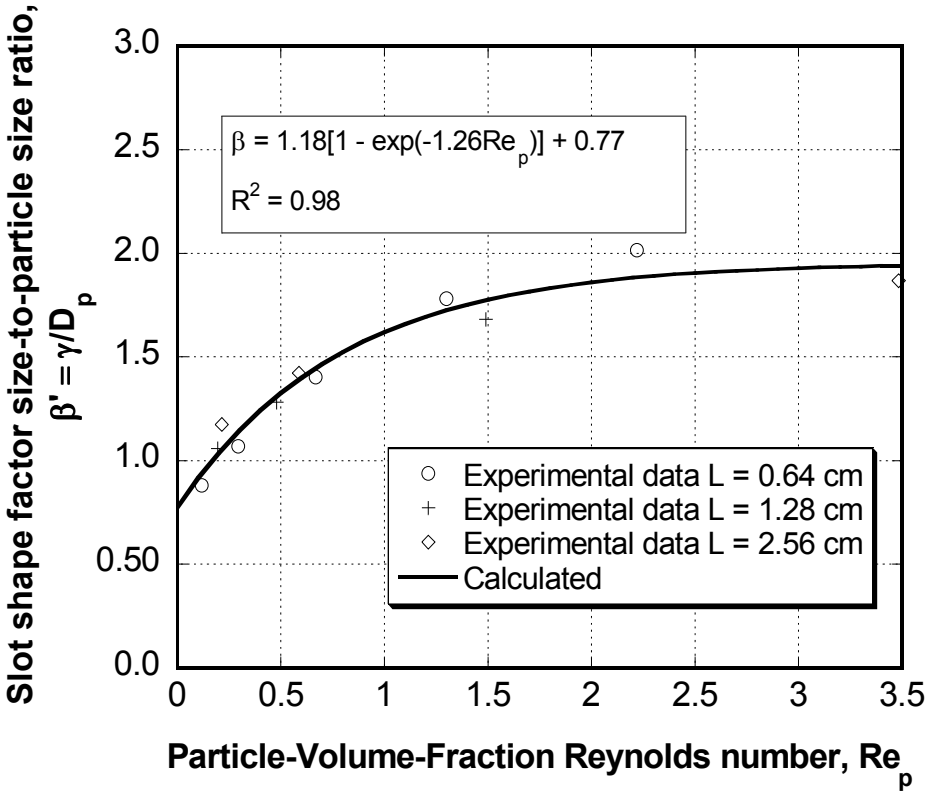

Figure 4.6: Experimental and calculated results from exponential model for glass-bead suspensions using shape factor equation (w = 0.32 cm)

The plugging performance curves presented in Figures 4.3 and 4.5 show that as fracture opening length, L, increased the curves approached each other. In other words, there exists a critical length, L, beyond which the plugging condition becomes independent of the fracture opening length. If we define β_{max} as the width-to particle diameter ratio as Re_p approaches infinity, then β_{max} equals to 2.75, 2.29, and 2.02 for Ceramic proppant cases with w = 0.16 cm; L = 0.64, 1.28, and 2.56 cm, respectively. Figure 4.7 shows a plot of fracture opening length, L versus β_{max} for the ceramic proppant

experiments. As fracture opening length, L, increases, β_{max} reaches asymptote when $L > 4$ cm (or L/w ratio > 25). This shows that the plugging condition of flow through a rectangular slot is influenced by the slot length. However when the slot length-to-width ratio is sufficiently high, plugging is independent of the slot length. This can be explained by the following algebraic expression as L goes to ∞, γ reaches w, which is independent of L.

$$\lim_{L\to\infty}\gamma = \lim_{L\to\infty}\frac{wL}{w+L} = \lim_{L\to\infty}\frac{w}{w/L+1} = w \quad \text{---------- (4.2)}$$

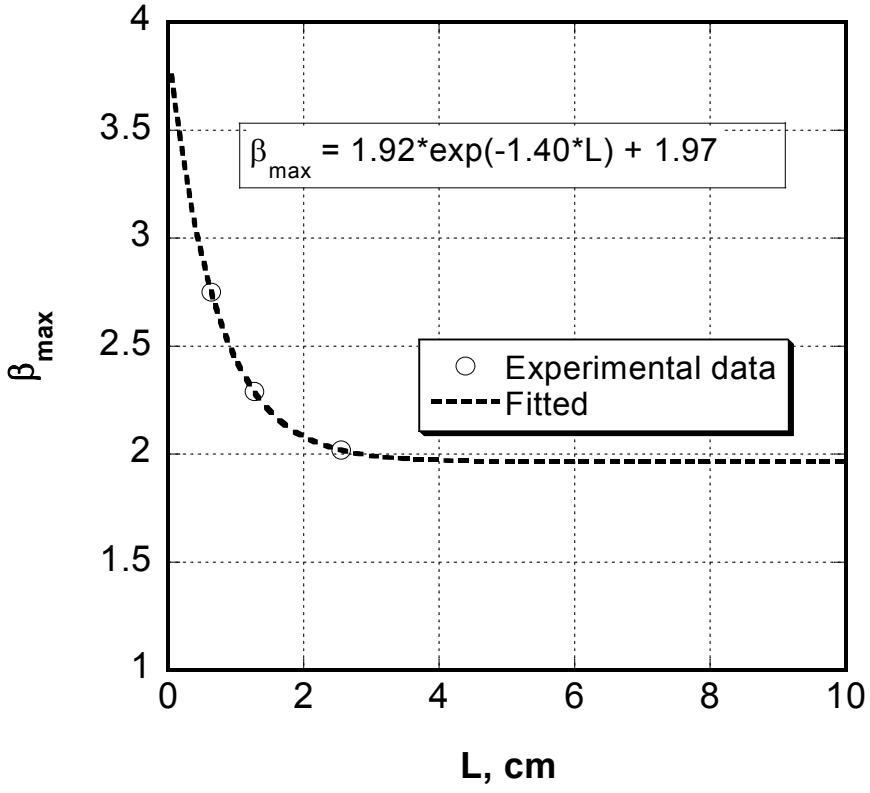

Figure 4.7: Effect of fracture opening length, L on β_{max} (w = 0.16 cm)

A summary of the correlations for plugging/bridging using the exponential-law equation given by Civan (2000, 2007), were developed as presented in equation (3.5). The A, B, and C coefficients of the fit parameters are shown in Table 4-3 and Table 4-4.

Table 4-3: Best-estimate parameter values for equation (3.5) using β

Case	A	B	C	R^2
w = 0.16 cm; L = 0.64 cm	1.68	1.47	1.07	0.98
w = 0.16 cm; L = 1.28 cm	1.24	1.23	1.04	0.97
w = 0.16 cm; L = 2.56 cm	0.98	1.41	1.03	0.98
w = 0.32 cm; L = 0.64 cm	2.23	0.94	1.08	0.99
w = 0.32 cm; L = 1.28 cm	1.26	1.13	1.07	0.98
w = 0.32 cm; L = 2.56 cm	1.03	1.16	1.09	0.99

Table 4-4: Best-estimate parameter values for equation (3.5) using β'

Case	A	B	C	R^2
Ceramic Proppant	1.04	1.27	0.79	0.97
Synthetic Glass Beads	1.18	1.26	0.78	0.98

4.3.2. Plugging Time

In the orifice plugging condition reported in the previous chapter, the plugging time was correlated as function of particle volume fraction using a power law equation:

$$t_p = a\sigma_p^{-b}$$ ---------- (4.3)

where t_p is the time elapsed until bridge formation, σ_p is the particle volume fraction, and a, b are the empirical parameters.

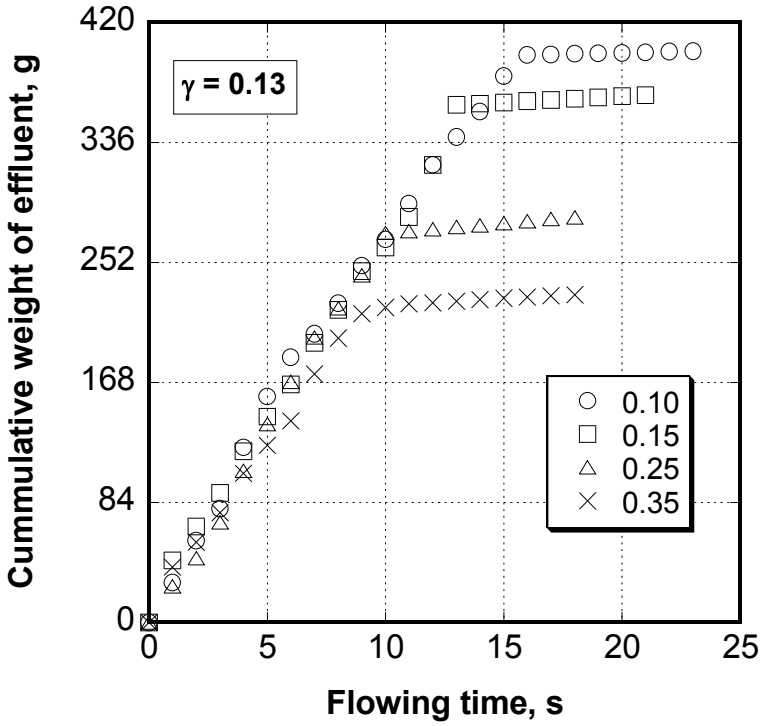

Figure 4.8: Plugging time variations as a function of particle volume fraction (γ = 0.13)

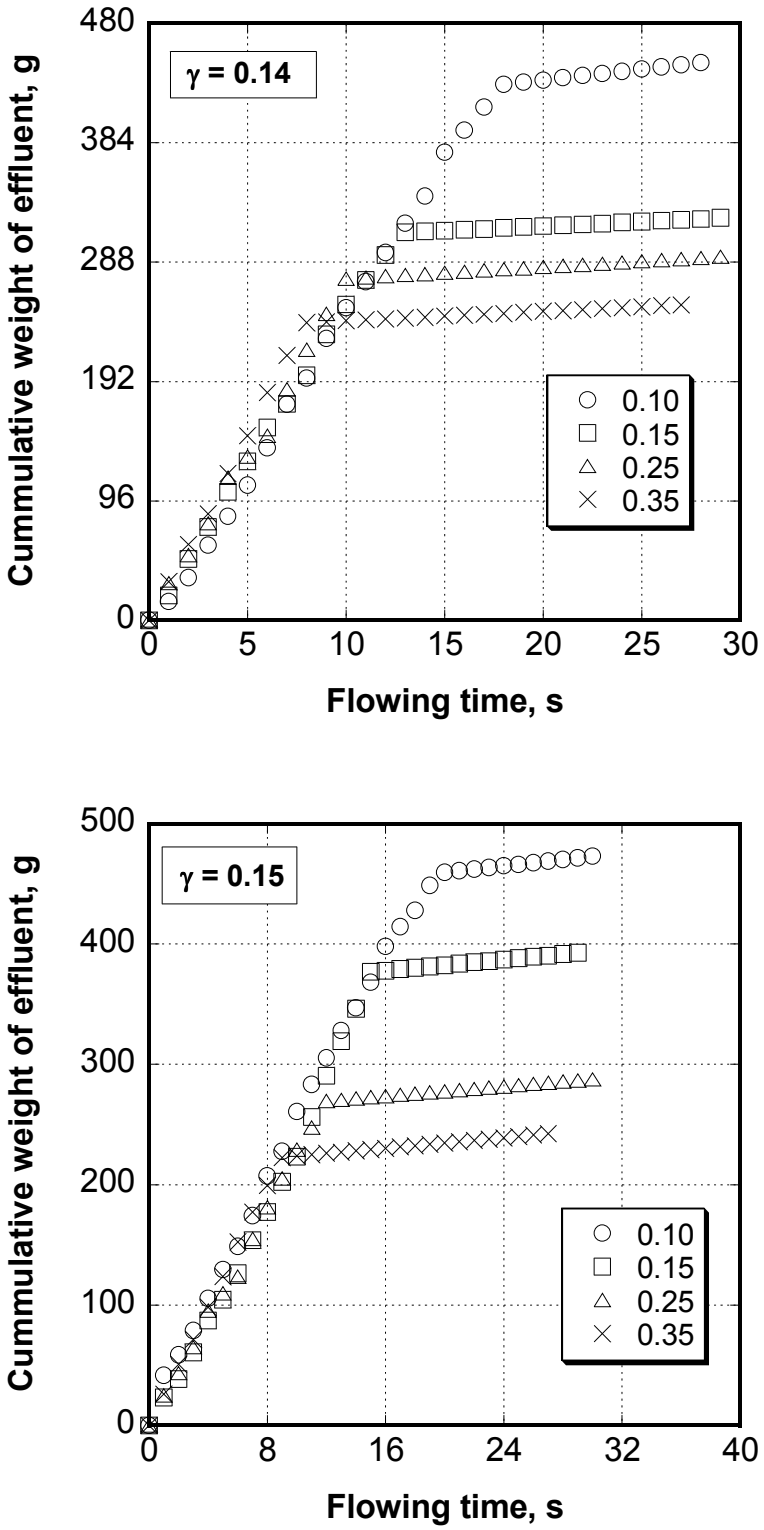

Figure 4.9: Plugging time variations as a function of particle volume fraction (γ = 0.14 and γ = 0.15)

Several concentrations of ceramic proppant mixtures were tested for plugging time. Proppant mixtures of 0.07 cm diameter particle size were flowed through different slot geometries (γ = 0.13, 0.14, and 0.15). Figures 4.8 and 4.9 show the plugging times for different ceramic proppant concentrations. The shape factors were 0.13, 0.14, and 0.15 for the tests. For γ = 0.13, the plugging time varied from 16 seconds to 8 seconds as the concentration of the solid increased from 0.10 to 0.35 volume fraction.

The plugging time was plotted against the particle volume fraction for three different shape factors (Figure 4.10). It was shown that higher β' resulted in longer plugging time. The fit parameters are presented in Table 4-5.

Table 4-5: Best-estimate parameter values for equation (4.3)

Case	*a*	*b*	R^2
β' = 1.83	4.59	0.55	0.9
β' = 2.03	4.36	0.62	0.98
β' = 2.15	4.89	0.61	0.98

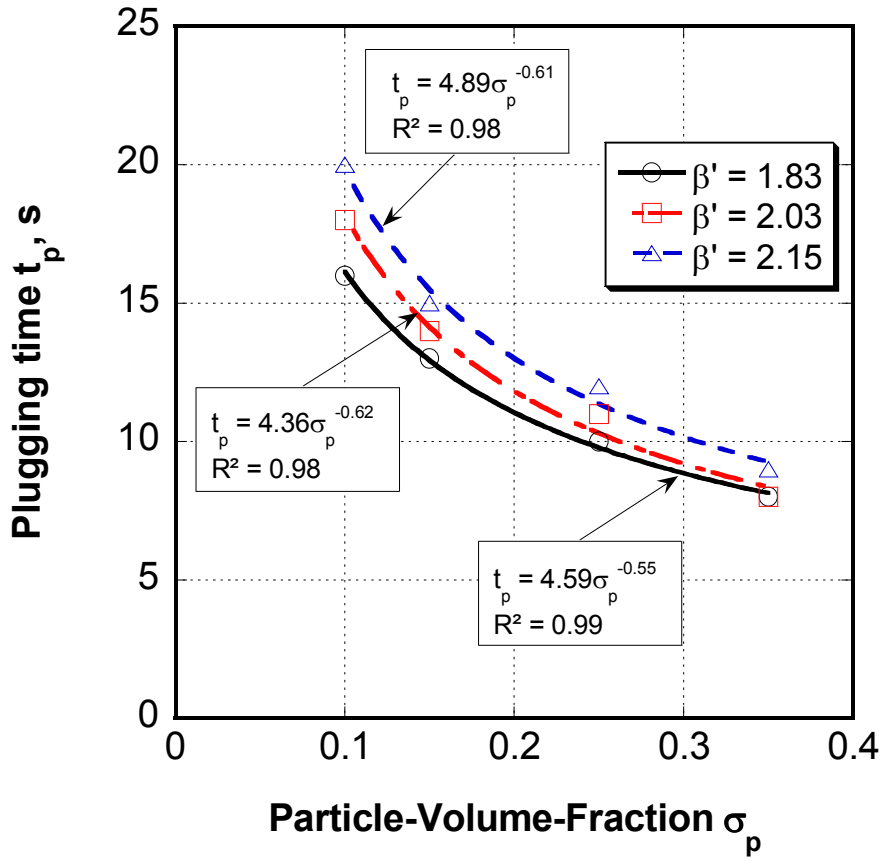

Figure 4.10: Effect of Ceramic proppant concentration on the plugging time under condition of constant flow rate

4.4. Conclusions

1. This study confirmed that plugging in naturally fractured formations and slotted liners by suspended particles can be described successfully under various conditions using two dimensionless groups, the slot width-to-particle diameter ratio and Particle-Volume-Fraction Reynolds number.

2. In addition to the variables of slot width, particle size, and particle concentration, the study showed that slot length also affects plugging.
3. The plugging time is affected by the slot shape factor-to-particle size ratio, β', and particle concentration. When plugging conditions exist, higher β' results longer plugging time and higher particle concentration results shorter plugging time.
4. Because the relative ratio between the slot shape factor/ particle size was conveniently defined, the results can be applied to different sizes of the same materials as long as the particle shapes and their relative size ratios are similar.

5. Chapter 5: Investigation of Plugging in Pore-throat by Suspended Particles

5.1 Introduction

Fluid flow through a porous network is often accompanied by migration of fine particles. These are small particles that are present in porous media. During the flow of a permeating liquid through a porous network, fine particles attached to pore surfaces are released or detached under certain sets of conditions. When the fine particles are released, they will migrate with the permeating liquid until they get captured, retained and deposited at another location in the porous medium or flushed out of the system. The consequences of the migration of fine particles can be either beneficial or adverse depending on the applications. Core test evaluation can provide some insight into flow-induced fines migration. Therefore, both induction and prevention techniques are desired from studies of migration of fine particles in porous media.

Applications concerning the consequences of the migration of fine particles are found in different fields; including petroleum, geotechnical, environmental and hydraulic engineering. In petroleum engineering, a widely recognized consequence of migration of fines in sandstone oil reservoirs is known as water sensitivity of sandstone. It occurs from oil field operations such as drilling, work-over, acidization, steam and water flooding and enhanced oil recovery. It can also occur when the water from the natural spring or water aquifer permeates into the oil formation zone as well as in-situ operations such as solution mining, and hydraulic fracturing, etc.

In geotechnical engineering, the consequences of the migration of fine particles are desired in the study of soil erosion. The fine particles in this case are clayey fines released by colloidal and hydrodynamic forces generated by the seepage flow of water. They are carried away with the seepage stream and cause soil erosion.

From the environmental aspect, the migration of fine particles in ground soil can cause soil and ground water pollution. The fine particles themselves can be pollutants such as organic waste particulates or micro-organisms. They can detach from one site, move with the flow and become contaminants in another site and thus spread pollutants. This process can happen through the accidental release of materials on the surface or through direct introduction of contaminants into the subsurface and by the presence of micro-organism.

In chemical engineering, unconsolidated porous media are used in operations and processes such as deep bed filtration and washing of filter cakes. In designing these operations, consideration is given to present the occurrence of entrapment or plugging of the bed. For the regeneration of bed filters, a complete washout of the captured particles is required.

The particulate processes in porous media are categorized into two groups by Civan (2007) as being internal processes and external processes. Internal processes include pore surface processes (deposition, removal), pore throat processes (plugging, unplugging), and pore volume processes (internal filter cake formation, internal filter cake depletion, migration, generation and consumption, and interface transport or

exchange). The external processes include external filter cake formation, external filter cake removal and fine particle invasion.

The size, shape and other characteristics of the pore structure and the fine particles are essential in studying the release and migration of fine particles in porous media. Characterization of the fines and the porous media is required to obtain this knowledge. For the migration of particles, the size of fines, size of pore constrictions, surface charge of fines and porous surface, and the interactions between the permeating liquid and the porous media are more relevant and often taken into consideration.

Formation damage in petroleum-bearing formation is frequently caused by migration and deposition of fine particles such as iron debris produced by oxidation and corrosion of surface equipment, fine sand and clay particles during water-flooding and mud fines during overbalanced drilling. As these particles are transported along the tortuous pathways of the porous formation, they can be captured and deposited within the porous matrix. Consequently, the formation porosity and permeability is reduced. Several damage mechanisms caused by particles were carefully reviewed by Civan (2007). In this chapter the focus is on the deposition and blocking caused by foreign particle invasion at pore-throats.

The philosophy behind the approach of this chapter was to investigate various formation damage mechanisms developed for a single-phase fluid system based on laboratory core tests.

5.2 Core Studies

This section presents various experimental studies conducted for determining plugging conditions and times of core samples.

5.2.1 Core Measurements

The objectives of the experimental work were to examine the effects the plugging conditions and time on permeability impairment as a function of the particle size, concentration, pore size distributions, and fluid properties in core samples.

5.2.1.1 Flow Test

5.2.1.1.1 Experimental System and Procedures

Experimental System:

The experimental apparatus included five main components (shown in Figure 5.1): (1) an electrical pump (Ruska), (2) an accumulator which contained fluid with suspended particles, (3) a Hassler-sleeve core holder, (4) back pressure regulator, and (5) a computer based data acquisition system.

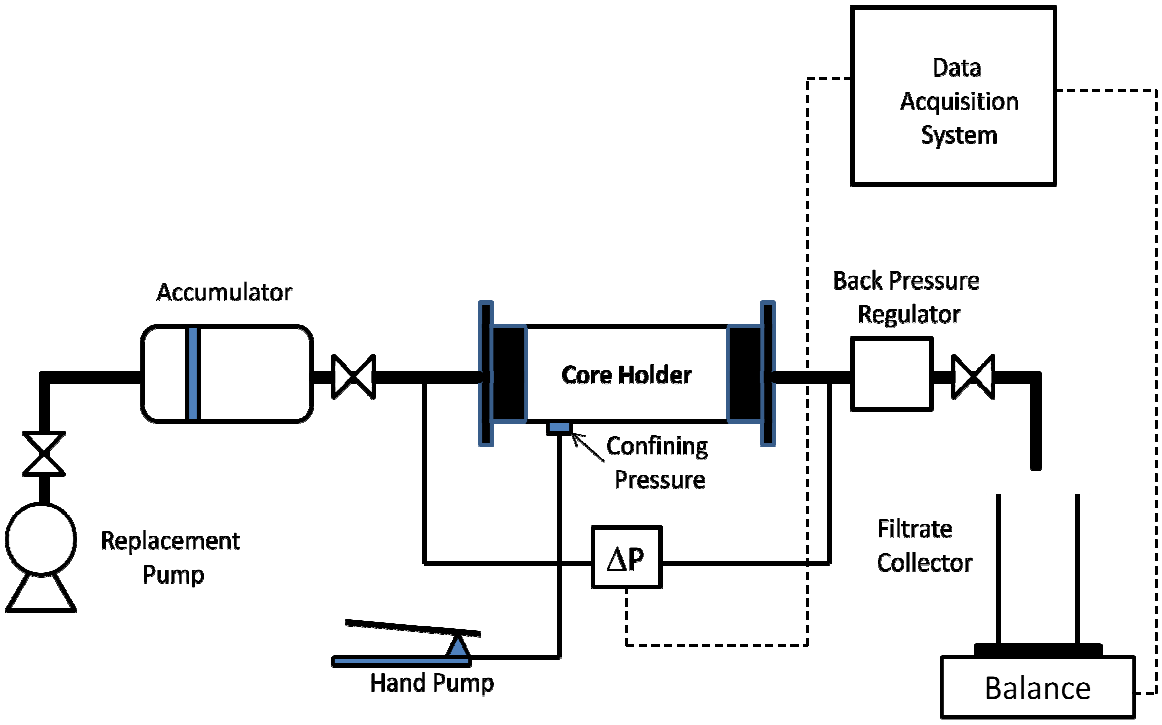

Figure 5.1: Core plugging experimental apparatus

The positive displacement Ruska pump was used to inject fluid with suspended particles in the testing core at a constant flow rate. The pump has one 500 cm^3 cylinder, which is able to pump at rates varying from 2.57 to 576 cm^3/hour under pressures up to 1,000 psig. The pump was driven by a 3/4 horse power - 1/60/115/230 Volt - 1725 RPM motor with a quick change transmission. It was mounted on a cart with casters (Figure 5.2). The pump was equipped with a pressure gauge rated 0-2000 psi.

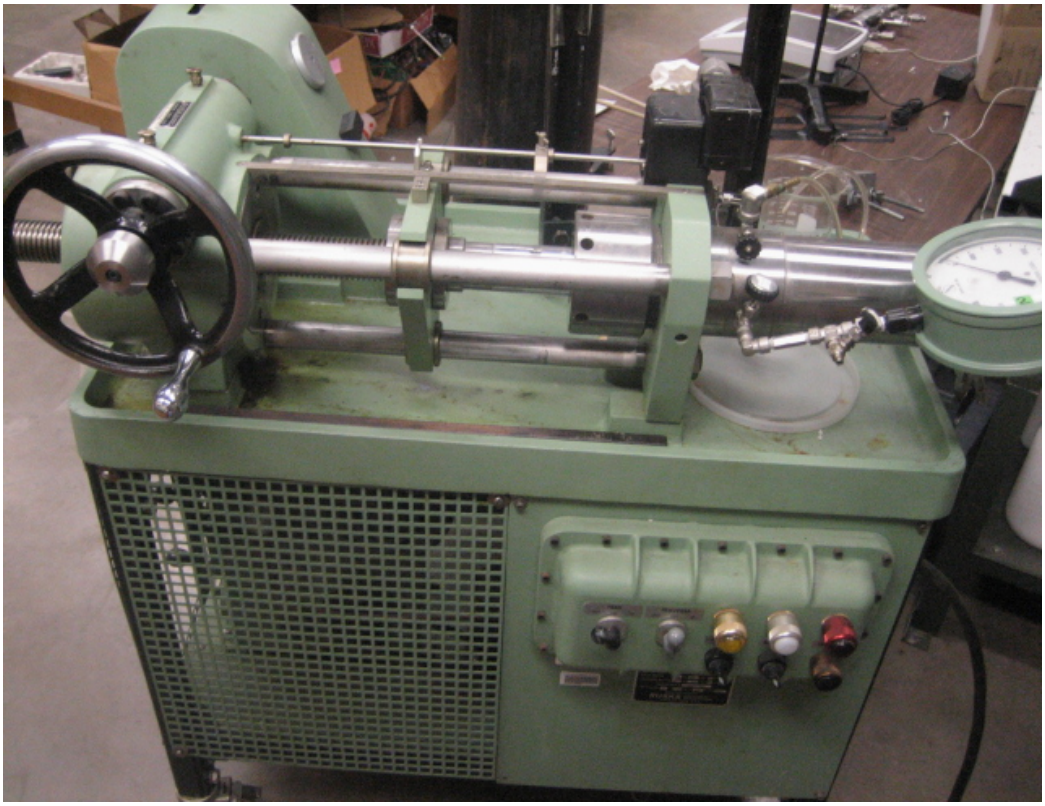

Figure 5.2: A Positive Displacement Ruska pump available at Production Laboratory, Room D103 Sarkeys Energy Center

A 500 cm^3 high-pressure-floating-piston fluid transfer accumulator provided by Phillips 66 Company, with a pressure limit of 5,000 psi at 300 ^oF, was used for fluid displacement. The accumulator construction material was 316 Stainless Steel. The accumulator was connected to the Ruska pump. Mineral oil from the pump cylinder was pumped into the accumulator at constant flow rate to push the test fluid into the core holder. Figure 5.3 is a photo of the accumulator.

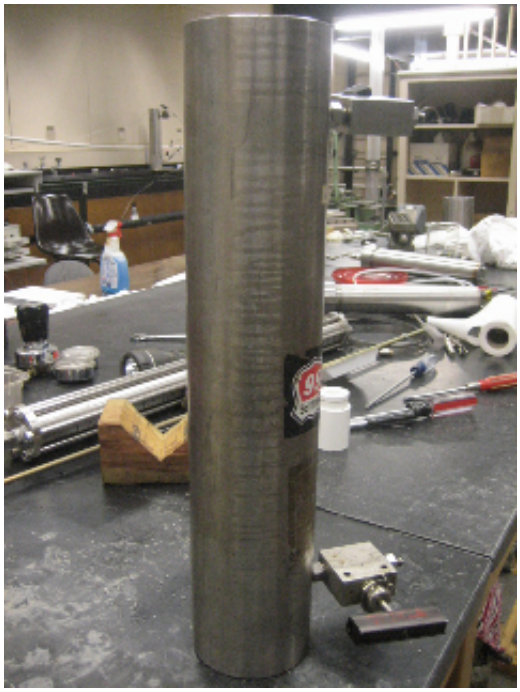

Figure 5.3: A High-Pressure-Floating-Piston Fluid Accumulator

The TEMCO back pressure regulator was set to 500 psig and the flow rate was held constant at 90.3 cm^3/hour.

A Hassler core holder was used to hold 1 inch diameter consolidated cores. The length of the cores used in the experiments was 2.0 inches. There was a port in the middle of the core holder section to apply confining overburden pressure. The core holder was designed so fluid entered directly into one end and was produced from the other under pressure. The velocity of flow was adjusted using the gears of the Ruska pump.

A differential pressure transducer was used to measure the pressure differences between the inlet and outlet. The data was recorded using the data acquisition system. Figure 5.4 is a picture of the Hassler core holder.

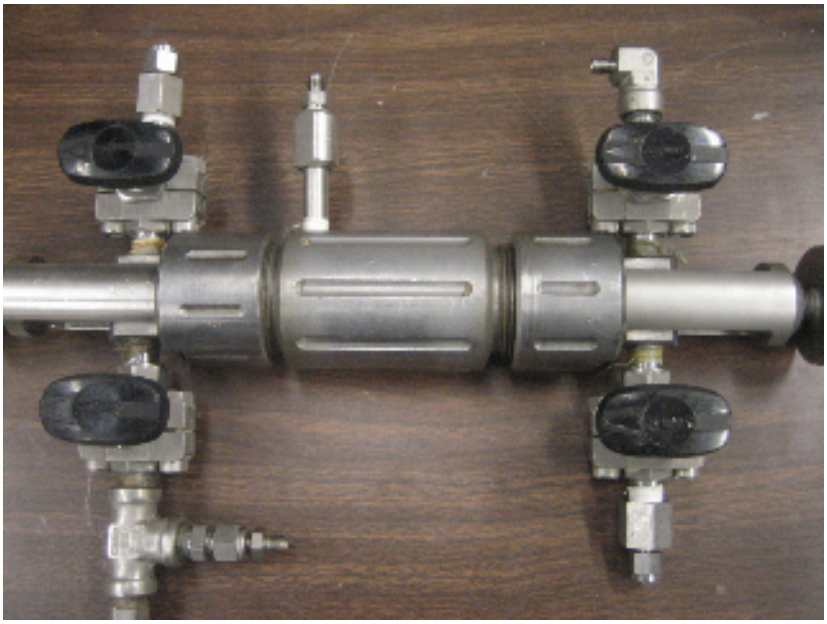

Figure 5.4: Hassler Core Holder

Procedures:

Prior to a core flood test, the equipment was completely cleaned. The 16 Berea cores were obtained from Berea Sandstone Petroleum Cores, Inc. An average permeability of 316 mD and porosity of 0.27 for the core samples were measured and reported by the company.

Water-based drilling muds were prepared by mixing water and bentonite with additives at desired concentrations. The fluid samples were aged for 48 hours. Fluid viscosities were measured with a Chann 35 viscometer. Vacuum was used on the test fluid to make sure there were no trapped air bubbles.

The Berea core samples used were 2.0 inch long and 1.0 inch in diameter. Prior to injection, the cores were saturated with 3% KCl brine. Three different water base drilling muds were prepared to study the effect of particle concentration and drilling mud properties on permeability impairment. A fluid loss-reducing polymer, Geovis XT, was used in the test fluid to increase viscosity. Table 5-1 is a list of suspensions' properties for the experiments.

Table 5-1: Properties of suspensions

	Composition	Density	Viscosity
Fluid-1	500 ml water + 15 g bentonite	1.03 g/cm^3	7 cP
Fluid-2	500 ml water + 30 g bentonite	1.06 g/cm^3	12 cP
Fluid-3	500 ml water + 30 g bentonite + 1 g Geovis XT	1.06 g/cm^3	29 cP

The cores were placed in the core holder under a 1000 psi confining pressure. The pump rate was constant at 90.3 cm^3/hour. The back pressure regulator was set to 500 psig. Operating conditions were at ambient temperature (70 ^{o}F). Pressure drops across the core were measured using the differential pressure transducer. Data were recorded every 15 minutes using the data acquisition system. The core was flooded with fluid suspension for 10 hours. Permeability reductions were calculated and formation damage mechanisms were analyzed using the Wojtanowicz et al. (1987) diagnostic equations presented in the next section.

5.2.1.1.2 Data Analysis

The core plugging tests were performed to investigate the effect of particle concentration and drilling mud properties on formation damage.

Effect of particle concentration on permeability impairment:

The permeability reduction for Fluid-1 is shown in Figure 5.5. The permeability of the core sample reduction was about 96% (K/Ko = 0.04) after 5 hours injection; there was not much further reduction in permeability in the next 5 hours. It is worth mentioning that no mud cake formed at the inlet core face. It was observed that only few bentonite particles were produced from the core. This indicates that significant quantities of bentonite particles were retained within the core.

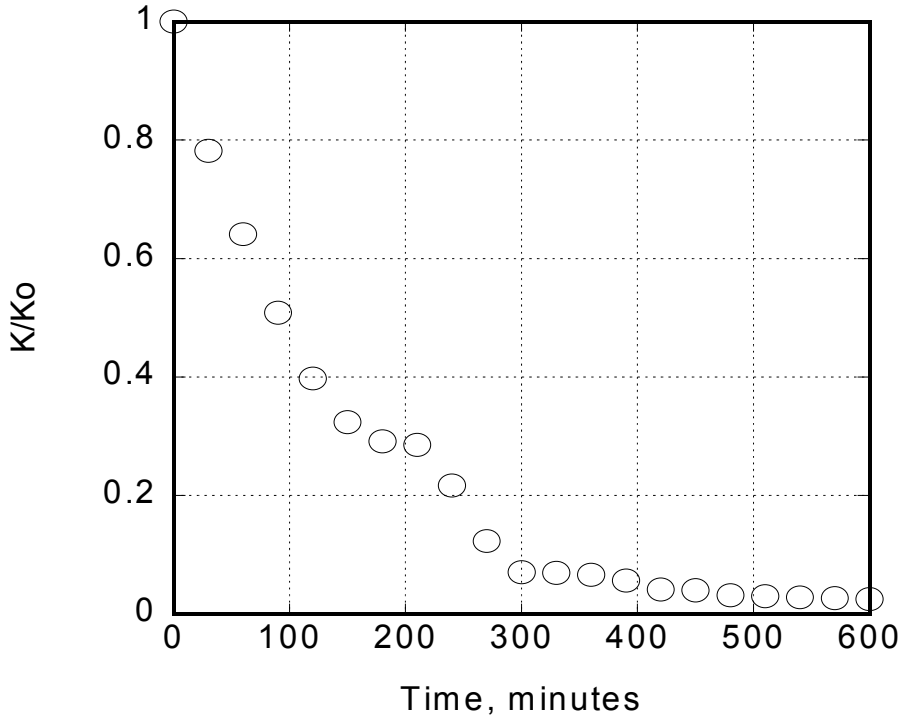

Figure 5.5: Permeability alteration of the core during the injection of Fluid-1

Permeability reduction was observed to be less for the Fluid-2 injection. Permeability was reduced to 40% of its original value after 5 hours and to 20% of its original value after 10 hours. A stable mud cake at the inlet was formed in this case. It appeared that the depth of particle penetration was less for higher bentonite concentration mud because stable particle bridges were formed to prevent further particle invasion. Therefore, higher bentonite concentration results in less damage as observed from the experimental data. Figure 5.6 shows the K/Ko versus time to indicate the permeability alteration over 10 hours of Fluid-2 injection. Further analysis of the damage mechanisms will be investigated in the later section.

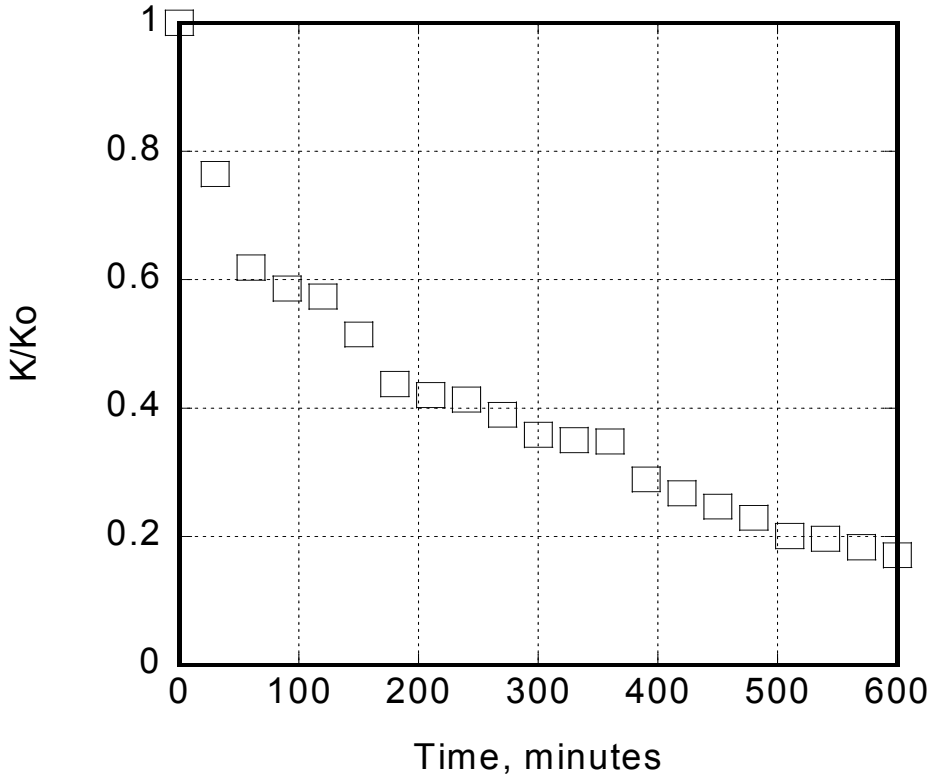

Figure 5.6: Permeability alteration of the core during the injection of Fluid-2

Effect of additives on permeability impairment:

Geovis XT polymer was added to the bentonite drilling mud, Fluid-3, to evaluate its effect on permeability impairment. The result is plotted in Figure 5.7. The permeability reduction was small compared to Fluid-1 and Fluid-2. Addition of polymer to the fluid increased its viscosity and led to a more stable filter cake. The mud cake reduced particle invasion into the core. The permeability in this case was 40% of its original value after the first 5 hours. For the next 5 hours, only an additional 4% permeability reduction occurred because the mud cake was formed and prevented particles invading the core.

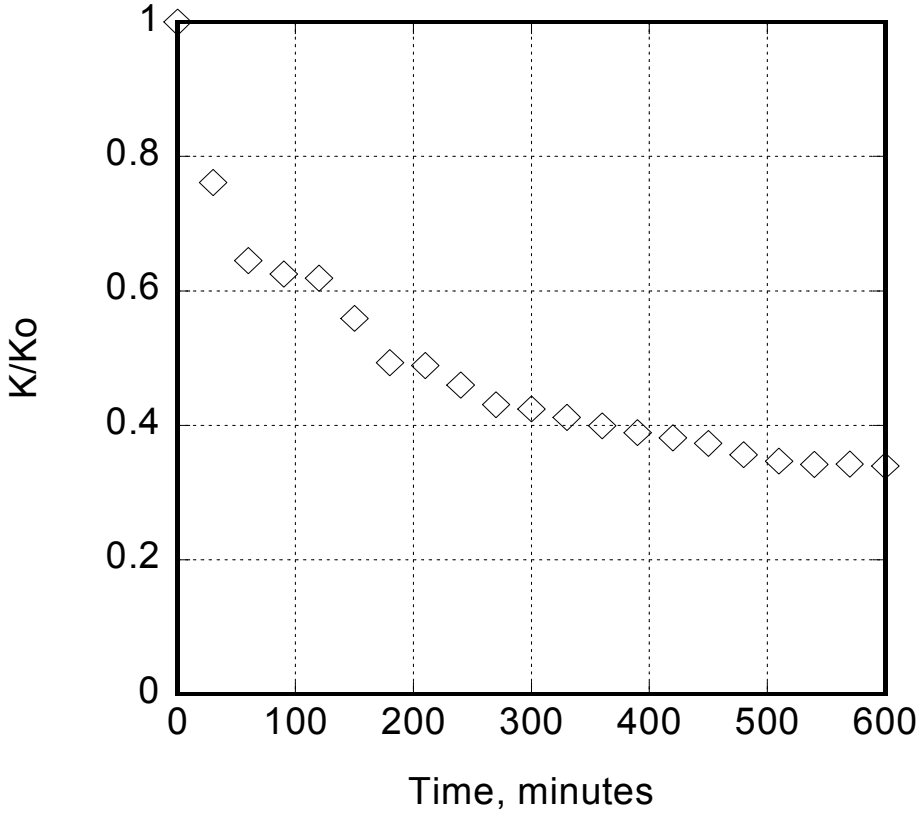

Figure 5.7: Permeability alteration of the core during the injection of Fluid-3

Investigation of the quality of mud cake using standard filter press test:

The quality of the mud cake at the injection point is the key to the depth of particle penetration. Mud particle invasion occurred only during mud spurt loss. Once the mud cake was formed few particles could invade the formation. Because good quality mud cake controlled the quantity of formation invasion particles, standard filter press tests were performed to investigate the mud cake quality. Figure 5.8 shows the comparision of static filtrate loss for the three water based drilling fluids used in the previous sections. It can be seen from this figure that fluid loss was least for the polymer treated drilling mud (Fluid-3). The total filtrate loss for the 3% bentonite fluid was double comparing to the treated one (12.5 cm^3 after 7.5 minute).

Mud cake thickness was measured after the tests. In case#1 (3% bentonite), the thickness was about 0.2 mm, the thicknesses for case#2 (6% bentonite) and case#3 (6% bentonite + 0.2% XT polymer) were 0.6 mm. The mud cake from the treated drilling fluid was found to be more rigid than the untreated ones.

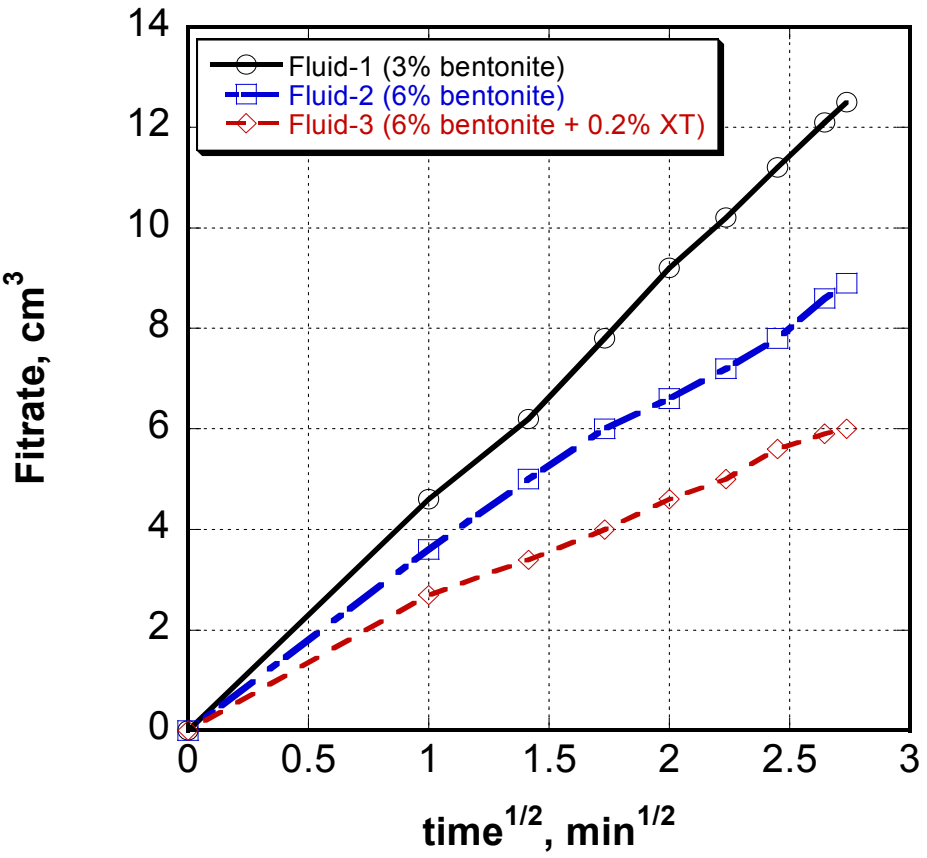

Figure 5.8: Filtrate measurements for three different fluids against square root of time

Wojtanowicz el al. (1987) diagnostic equations:

Wojtanowicz el al. (1987) proposed a method to for analyze single-phase formation damage induced by fine particles migration and deposition. The method was used to analyze the experimental data obtained in this section.

Table 5-2 is a summary of the diagnostic equations and straight-line plotting schemes derived for three different mechanisms for particulate suspension injection. The Wojtanowicz et al. method was based on the fundamental assumption that the pressure

drop occurred at the pore throat, therefore permeability was recorded at the throat location rather than the pore surface. Other assumptions were constant flow rate, low solid concentration (the pore volume reduction due to particles captured was insignificant), no gravity effect, homogeneous formation, and cake incompressibility.

Table 5-2: Wojtanowicz et al. Diagnostic Equations (after Civan 2000)

Permeability Damage Mechanisms	Diagnostic Equation	Straight Line Plotting Scheme	Equation#
Pore surface deposition	$(K/K_o)^{1/2} = 1 - C_1 t$	$(K/K_o)^{1/2}$ *vs. t*	(5.1)
Pore throat plugging	$K/K_o = 1 - C_2 t$	K/K_o *vs. t*	(5.2)
Pore filling	$K_o/K = 1 + C_3 t$	K_o/K *vs. t*	(5.3)

Three different damage mechanisms were recognized as being predominant during the test performed by injecting Fluid-1 into the Berea core sample. During the first 150 minutes small particles were gradually deposited on the pore surface. Equation (5.1) represented the permeability response and plotting scheme. Figure 5.9 illustrates the straight-line plotting of $(K/Ko)^{1/2}$ *vs. t* to characterize the pore surface deposition mechanism. The regression coefficient obtained was $R^2 = 0.97$ implied that this theory was appropriate for the early time less than 2 hours data.

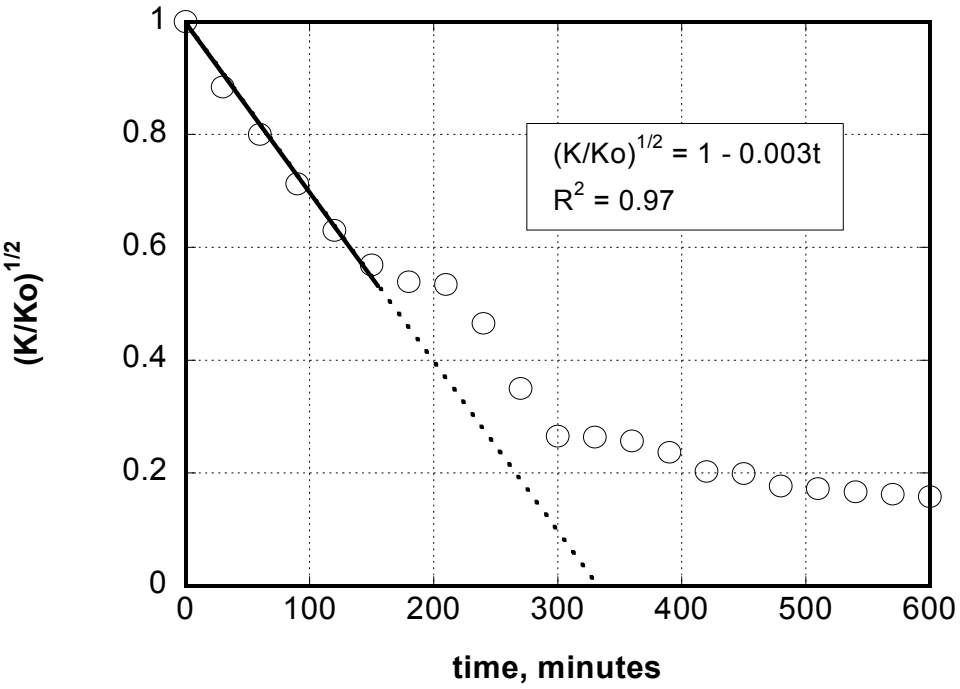

Figure 5.9: Early time pore surface deposition for injection of Fluid-1

The later time of the test were pore throat plugging and pore filling as described by equations (5.2) and (5.3). Figure 5.10 presents the straight-line plot of *K/Ko vs. t* from minute 210th to minute 300th and Figure 5.11 is a plot of *Ko/K vs. t* from minute 480th to minute 600th. The coefficients for the least square linear regression obtained were 0.94 and 0.99, respectively. The regression results were not as good as the early time data because the Wojtanowicz el al. method assumed that only a single mechanism occurred at a time. In fact, a combination of two or all three mechanisms might occur at the same time during the later injection period. The method showed that pore surface deposition was the dominant mechanism in this interval.

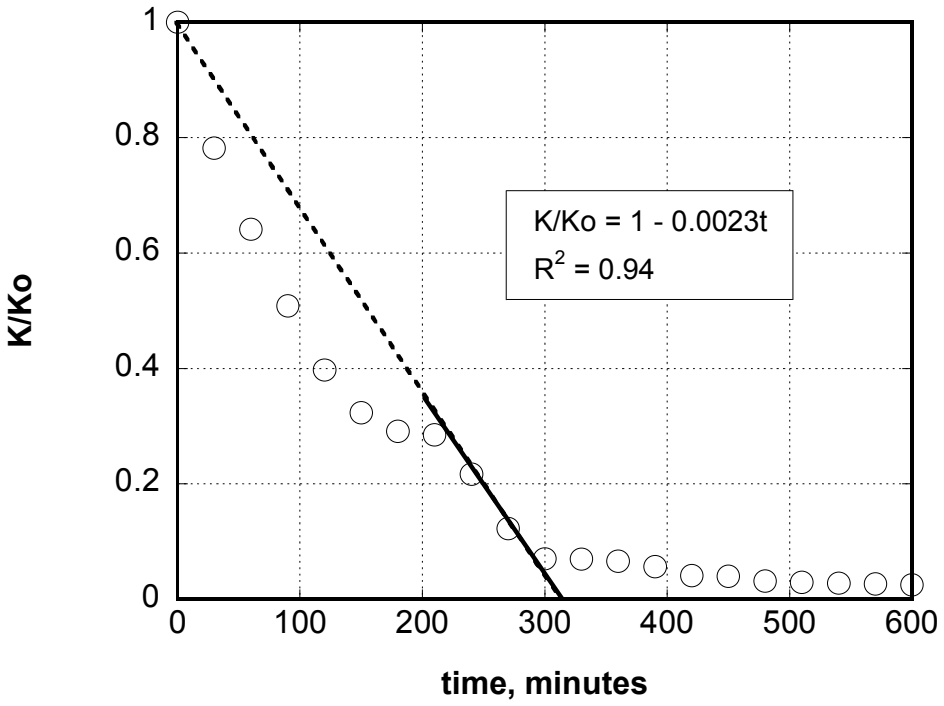

Figure 5.10: Late time pore plugging for injection of Fluid-1

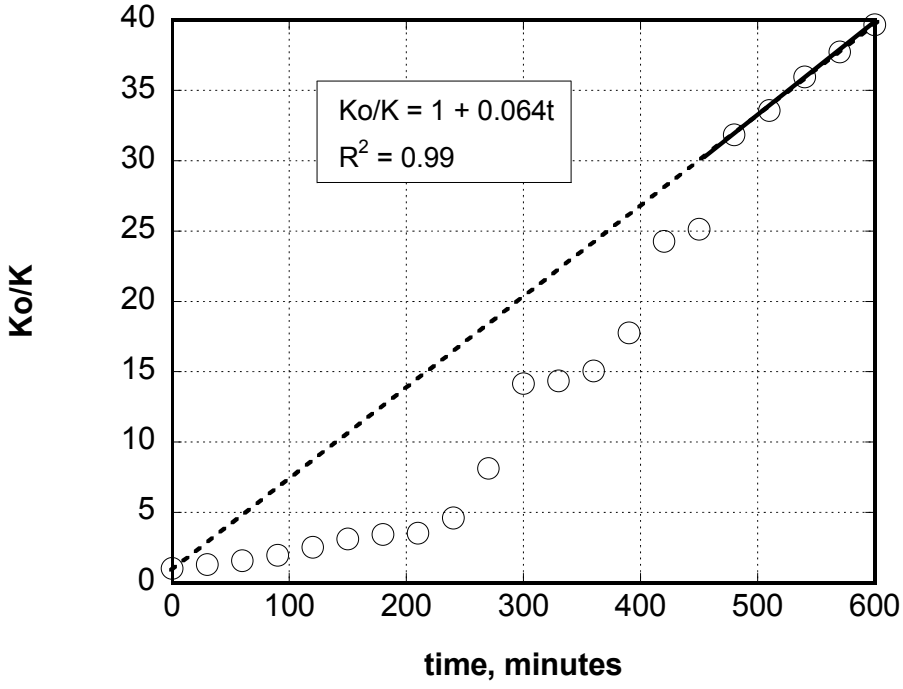

Figure 5.11: Late time pore filling for injection of Fluid-1

Similarly the data obtained for tests with Fluid-2 and Fluid-3 were analyzed to determine the damage mechanisms. Figures 5.12-14 demonstrate three different damage mechanisms for injection of Fluid-2. The pore surface deposition period was shorter than the Fluid-1 injection case. A substantial mud cake prevented particles from invading the core sample. The elapsed time until pores were plugged was also shorter than Fluid-1 case. Higher particle concentration resulted a shorter time to plug pores. Pore plugging was observed after 120 minutes of injection using the Wojtanowicz el al. (1987) diagnostic method. The pore filling mechanism started after 240 minutes of injection. The regression coefficients for the late time damage mechanisms were 0.81, and 0.95 respectively. Lower regression coefficient would be expected because the model assumed a homogeneous rock formation. The rock cores were heterogeneous and the later time mechanisms might include all three processes. Figures 5.15-17 shows the straight-line plotting for the three damage mechanisms for the Fluid-3 data. The pore surface deposition and pore plugging mechanisms occurred about the same time as in case Fluid-2. However the overall permeability damage was less compared to the other two cases. This indicates that the additive polymer helped to create a better quality mud cake near the injection point and avoided further particles invasion.

Figure 5.18 shows the three mechanisms pore surface deposition, pore plugging, and pore filling as in regions 1, 2, and 3 respectively.

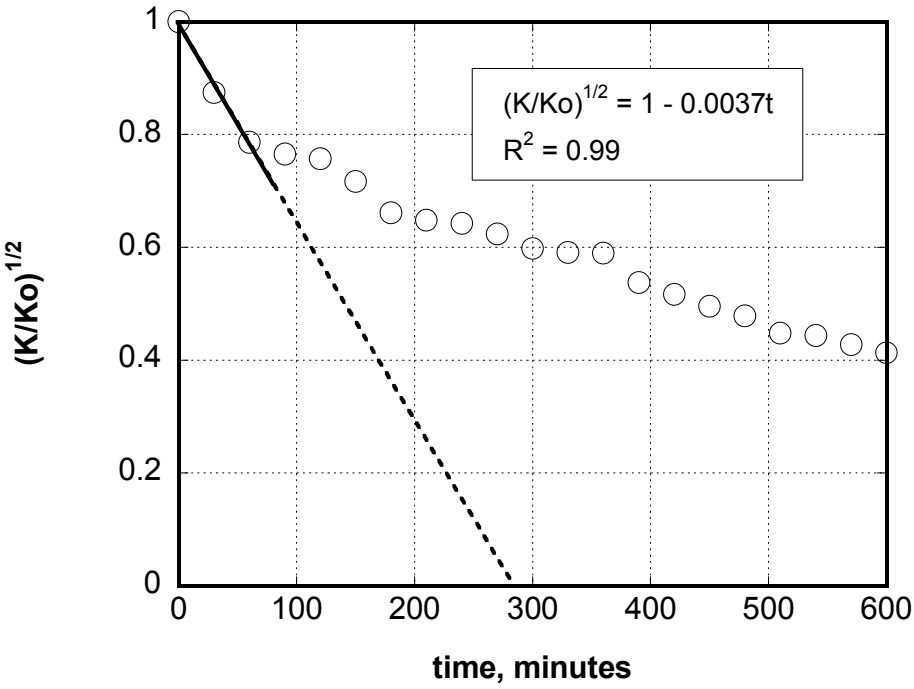

Figure 5.12: Early time pore surface deposition for injection of Fluid-2

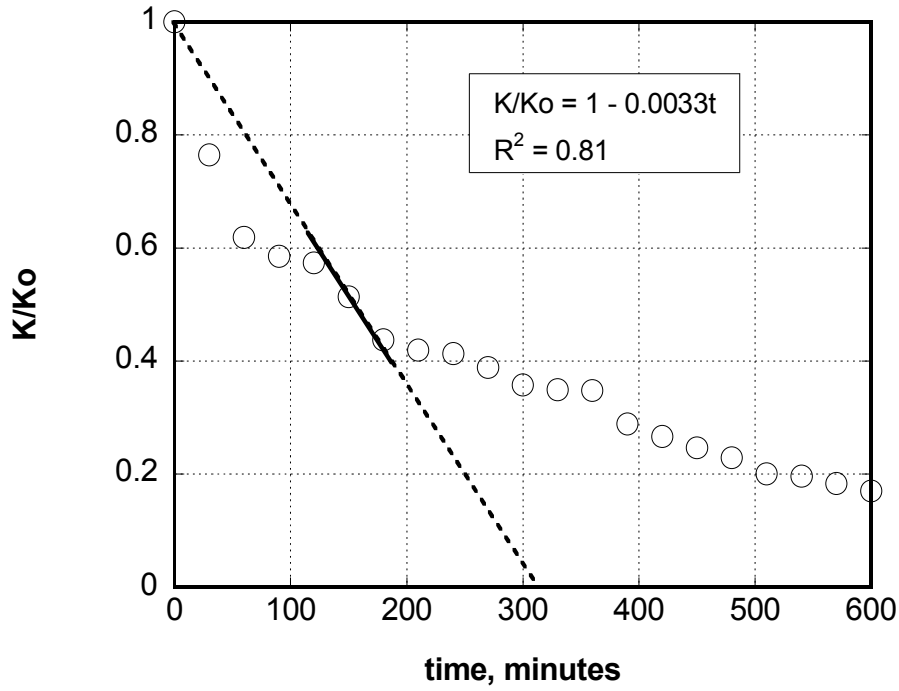

Figure 5.13: Late time pore plugging for injection of Fluid-2

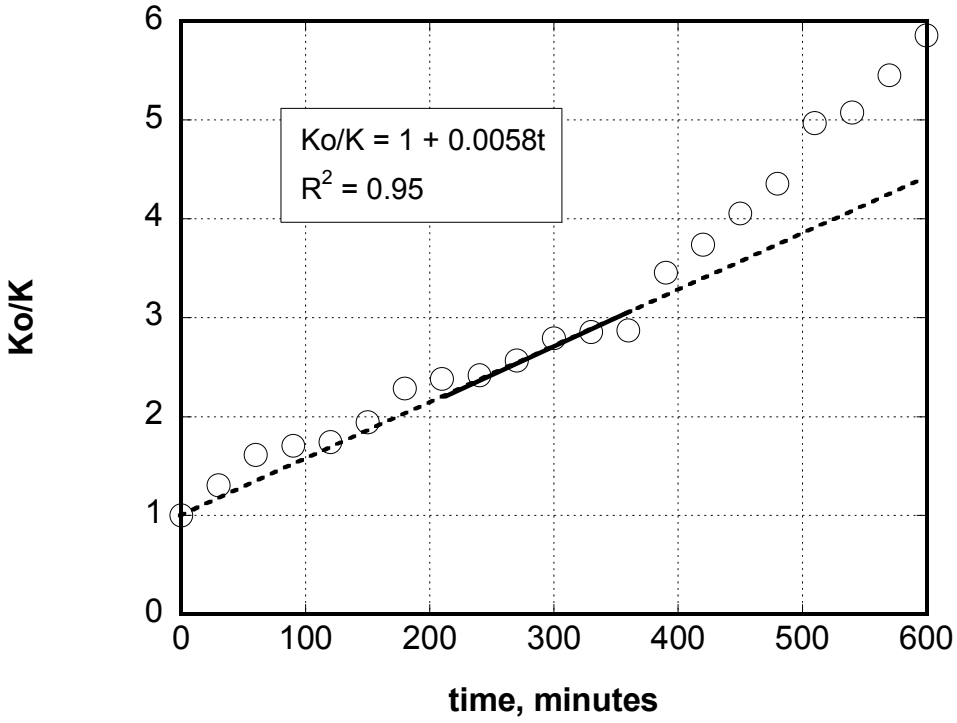

Figure 5.14: Late time pore filling for injection of Fluid-2

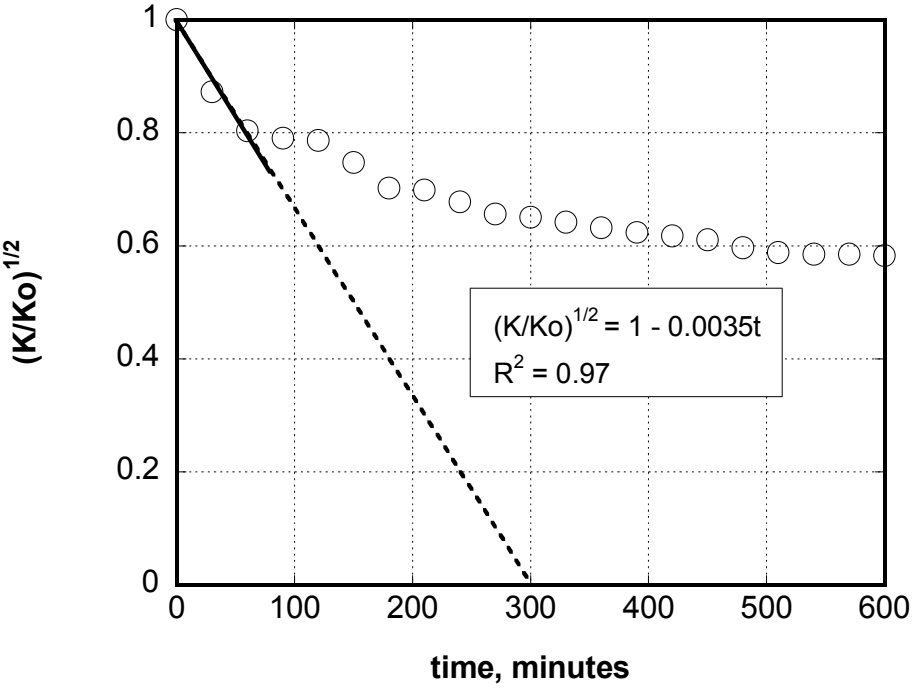

Figure 5.15: Early time pore surface deposition for injection of Fluid-3

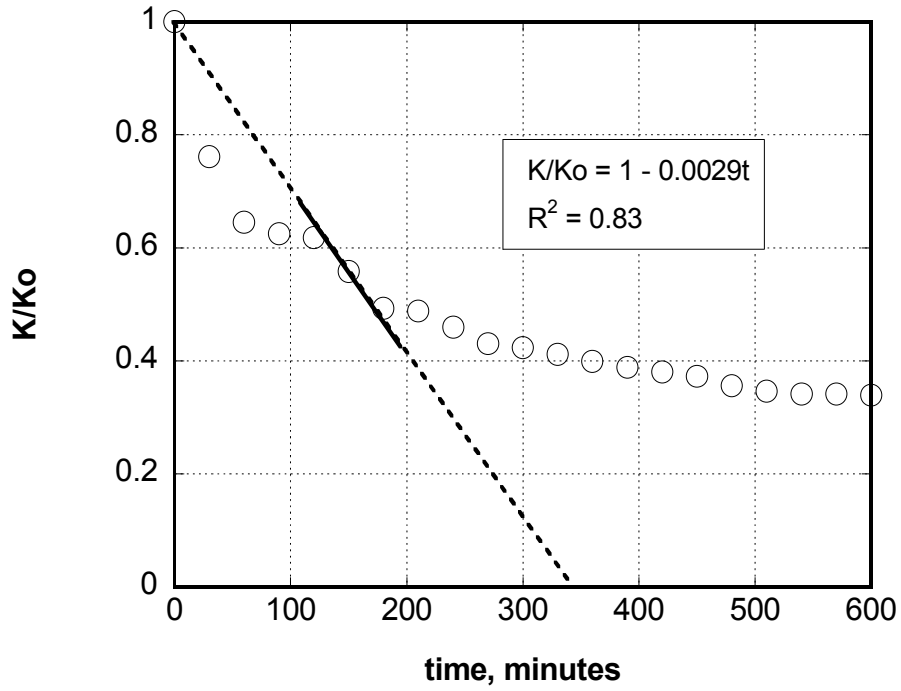

Figure 5.16: Late time pore plugging for injection of Fluid-3

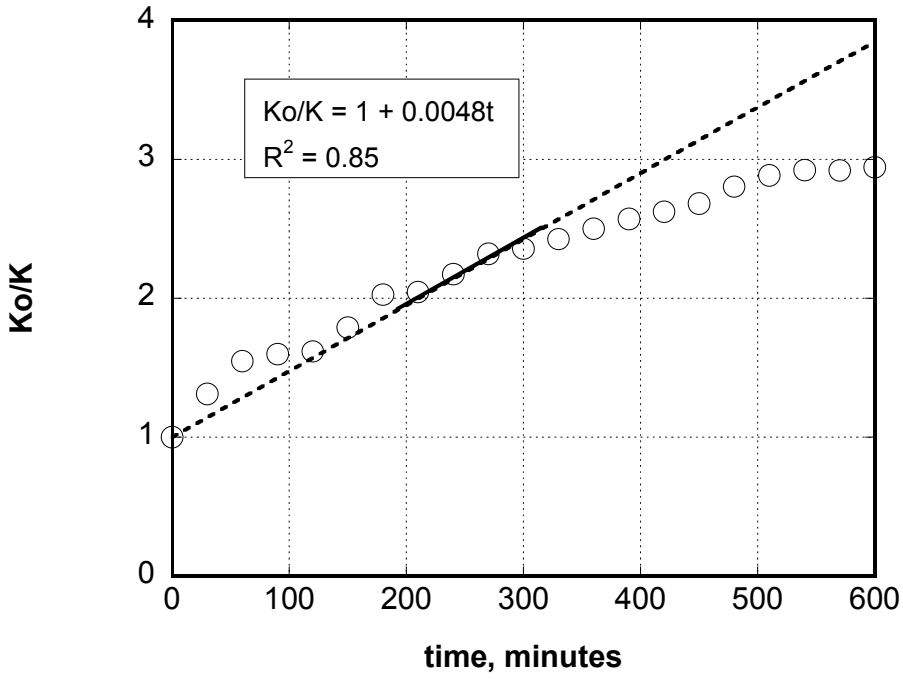

Figure 5.17: Late time pore filling for injection of Fluid-3

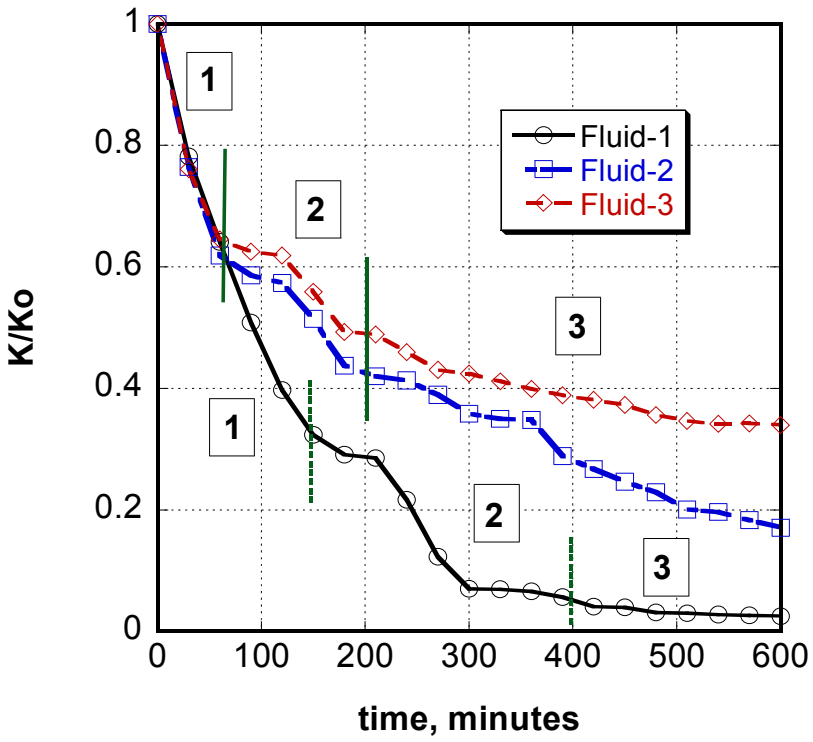

Figure 5.18: Permeability damage mechanisms by particle invasion. Region 1 = Pore surface deposition; Region 2 = Pore throat plugging; Region 3 = Pore filling

5.2.1.2 Nuclear Magnetic Resonance (NMR) Test

One key factor in the economics of drilling and completion projects is the performance of wells during their lifetime. Productivity maintenance requires minimum formation damage. The basic feature that causes formation damage is particle capture by the porous medium and the consequent permeability reduction (Nabzar et al. 1997; Roque et al. 1995).

The trend toward single well completion places additional emphasis on avoiding formation damage. During drilling and completion, near-well bore permeability

impairment can cause a significant reduction of well productivity; however, the damage may be avoided if drilling/completion fluid conditions are properly selected.

Formation evaluation has been improved using well logging to provide accurate information on porosity and formation fluid saturation. However, well logging can not provide a systematic estimation of permeability. Nuclear Magnetic Resonance (NMR) can be used to determine porosity and permeability impairment during the core flood tests.

5.2.1.2.1 Experimental System and Procedures

Experimental System:

Figure 5.19 is a picture of the Oxford-Maran Ultra NMR spectrometer. The unit was housed in a temperature regulated compartment. The system operated at 2.0 Mhz frequency which was the same as the spectrometers used in logging tools. The machine had a series of calibration procedures that had to be carried out before making any measurements. The CPMG pulse sequence was used to measure the traverse relaxation time, T_2. The inter echo spacing (TE) and the wait time (TW) were adjusted to estimate the porosity within $\pm$ 0.5% of the independently measured saturated porosity.

The Ultra NMR spectrometer was used to collect large data sets, useful for accurate T_2 determination. Sets of measurements that used different parameters could be sequenced through Visual Basic scripting using ActiveX software. The Oxford Instruments WinDXP software package was used to fit relaxation data into multiple or distributed exponentials, respectively.

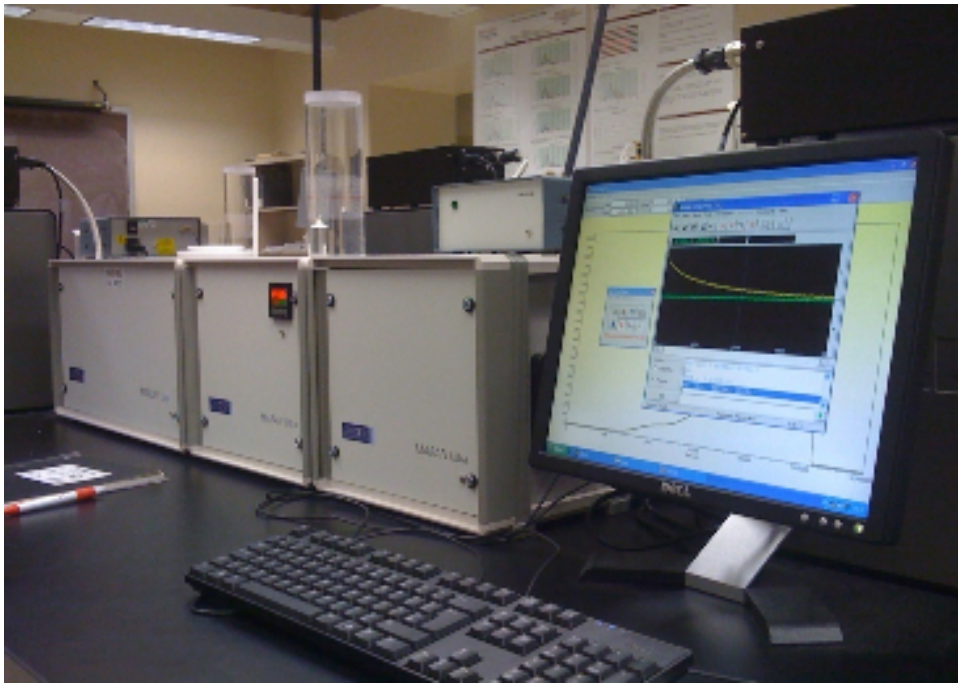

Figure 5.19: The Oxford-Maran Ultra NMR spectrometer system available in the IC^3 laboratory, Sarkeys Energy Center

A separate data file was supplied with the measured areas under the T_2 relaxation spectra for a known volume of water. Porosity of the core sample was computed as the following:

$$\phi = \frac{Total\ Area}{N_{scans} C_f V_b} \text{ ----------(5.4)}$$

where *Total Area* is the total area under the T_2 curve from the data file, N_{scans} is the number of scans applied (typically, N_{scans} = 100 for Berea sandstone), C_f is the calibration factor of the machine, and V_b is the sample bulk volume.

A Beckman Coulter laser diffraction particle size distribution analysis system (LDPSDA) was used to measure the particle size distribution of the particles in the core flood experiments (Figure 5.20). The LDPSDA is a system of multifunctional particle characterization tools. Its laser-based technology permits analysis of particles without risk of missing either the largest or the smallest particles in a sample. The laser diffraction technology is based on both Fraunhofer and Mie theories of light scattering. All the samples had to be dried carefully prior to analysis since the system works only with dry samples.

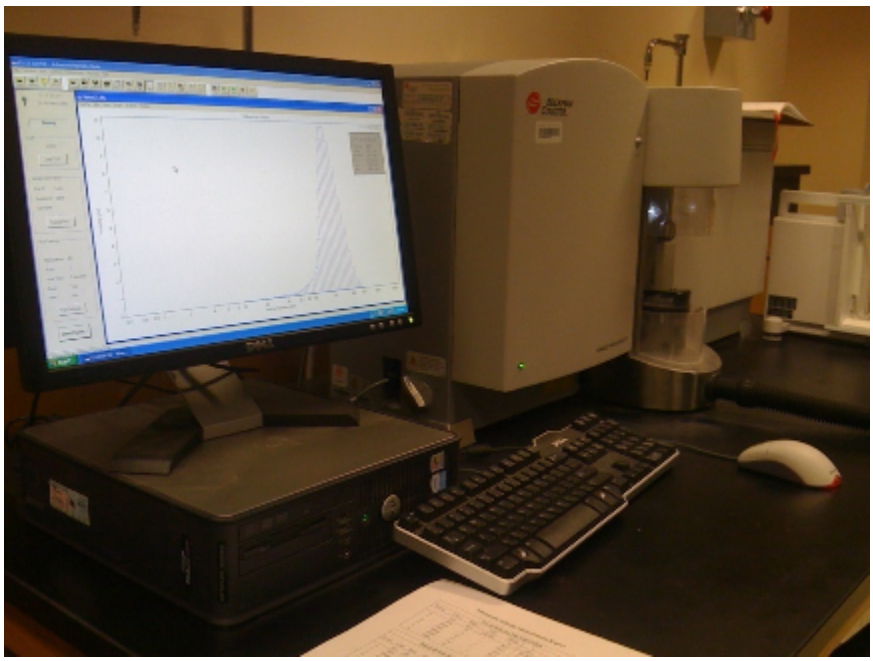

Figure 5.20: Beckman Coulter Laser Diffraction Particle Distribution Analysis System available at IC^3 laboratory, Sarkeys Energy Center

Procedures:

The NMR data used to derive porosity in this study were in the form of T_2 distributions.

Full-core flow experimental procedures were identical to those of section 5.2.1.1.1. Table 5-3 summarizes the core sample properties.

Table 5-3: Summary of core samples properties

Sample No	Permeability	Porosity	Lithology
1	1,240 mD	20.6%	Sandstone
2	265 mD	17.5%	Sandstone
3	28 mD	18.9%	Carbonate

Before beginning the NMR measurements, system calibration steps were required. For these measurements, the number of scans for each measurement was set to be 100 and the Relaxation Delay was sent to be 8,000,000 μs. The full parameter setup and calibration procedure for the Oxford-Maran Ultra system are presented in Appendix E.

5.2.1.2.2 Data Analysis

NMR and LDPSDA techniques were used to provide particle and pore size distribution of the formation before and after being damaged.

Particle and Pore Size Distributions:

The volume-average mean particle diameter of barite suspensions used in this study ranged from 2 to 6 μm, while the minimum particle diameter was 0.5 μm and maximum was 15 μm. Figure 5.21 shows particle size distributions expressed in volume frequency using LDPSDA system.

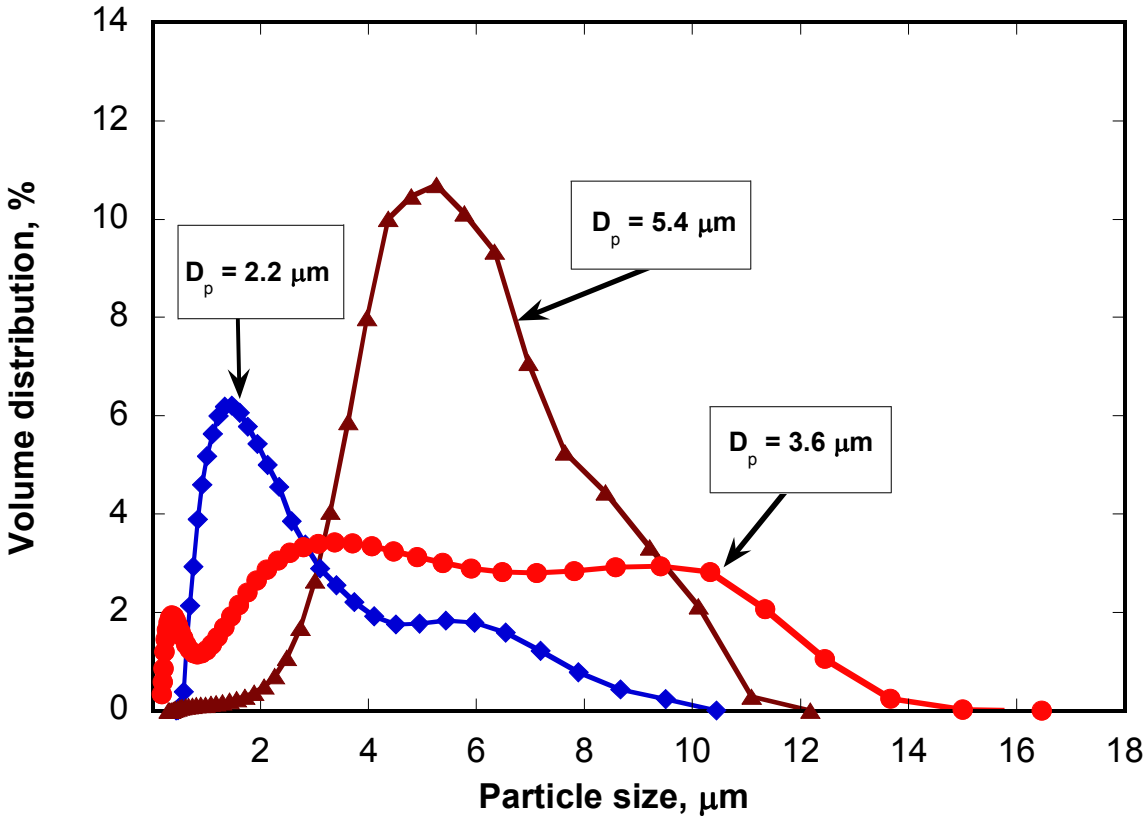

Figure 5.21: Particle size distribution of three different barite samples using LDPSDA system

When a water-wet rock is fully saturated with water, the T_2 value of a single pore is proportional to the surface-to-volume ratio of the pore, which is measured of the size of

the pore. Therefore, the observed T_2 distribution for all the pores in the rock represents the pore size distribution of the rock.

The T_2 NMR relaxation parameter is related to the pore surface, S, to volume, V, ratio by the following equation:

$$\frac{1}{T_2} = \rho_r \frac{S}{V} + \frac{1}{T_{2b}} \text{----------(5.5)}$$

Assuming a cylindrical geometry and ignoring the bulk term in the equation (5.5), the relationship reduces to:

$$\frac{1}{T_2} = \rho_r \frac{2}{r} \text{----------(5.6)}$$

where ρ_r is the rock surface relaxivity, r is the diameter of the pore body of the formation.

The T_2 relaxation spectrum is a reflection of the variation of pore sizes. Hence, T_2 NMR data was scaled to provide pore size distributions using a relaxivity value of 25.5 μm/s and 16.9 μm/s for sample#1 and sample#2, respectively.

Figure 5.22 shows the pore size distribution for the two samples#1(Ko =1,240 mD) and #2 (Ko = 265 mD) using the T_2 relaxation data. The mean pore diameter of the 1,240 mD core was 26.1 μm while that of the 265 mD core was 15.7 μm. Figure 5.23 is the SEM pictures of the two core samples at magnification of 100 times. The T_2 distribution from NMR data offered a reasonable estimate pore size distribution when the zone was 100% water-saturated. This information is very helpful for reservoir quality and depositional environment evaluation.

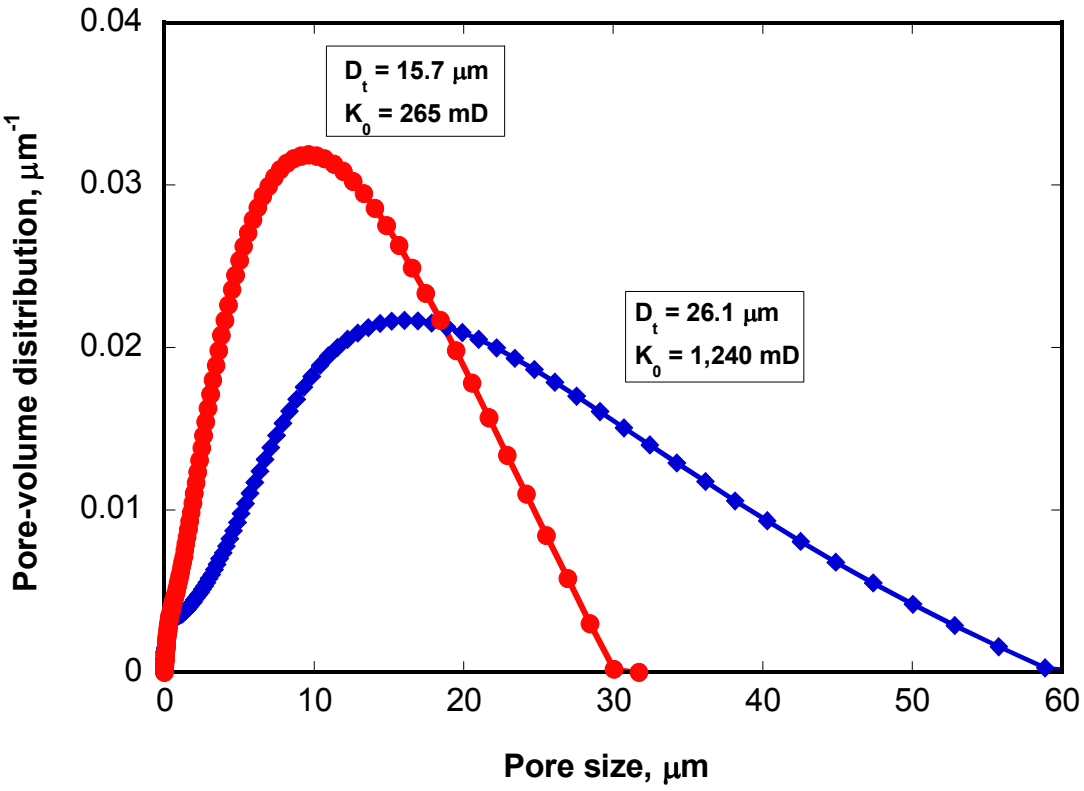

Figure 5.22: Pore size distribution of the 265 mD and 1,240 mD core samples

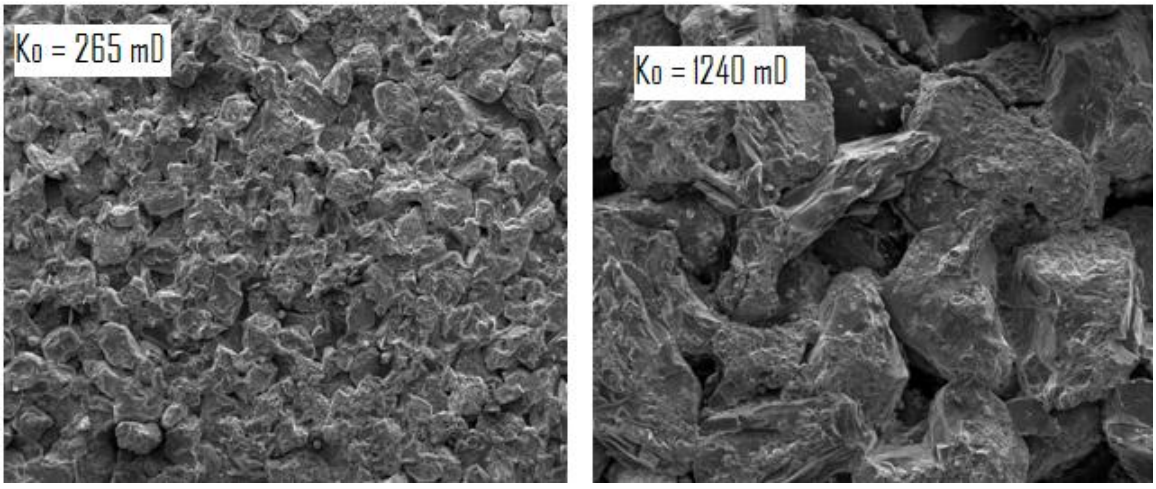

Figure 5.23: SEM of the 265 mD and 1,240 mD rock samples (Mag 100x)

Transverse Relaxation Time T_2 Distributions:

Figure 5.24 represents the T_2 distribution for the sample#1 at time t = 0, 5, and 18 hours of the core flood experiment. The injection rate was a constant 36 cm^3/hour. Barite (5.4 μm mean diameter) concentration was 5% by weight. Porosity was estimated using equation (5.4). It was shown that the overall porosity reduced from 20.6% to 17.6% after 5 hours of flooding. The porosity did not reduce further as fluid injection was continued. The porosity dropped only 0.1% after another 13 hours. The cumulative porosity corresponding to relaxation time T_2 are also shown as Figure 5.25 to illustrate the total porosity of the core sample at different times during the core flood test.

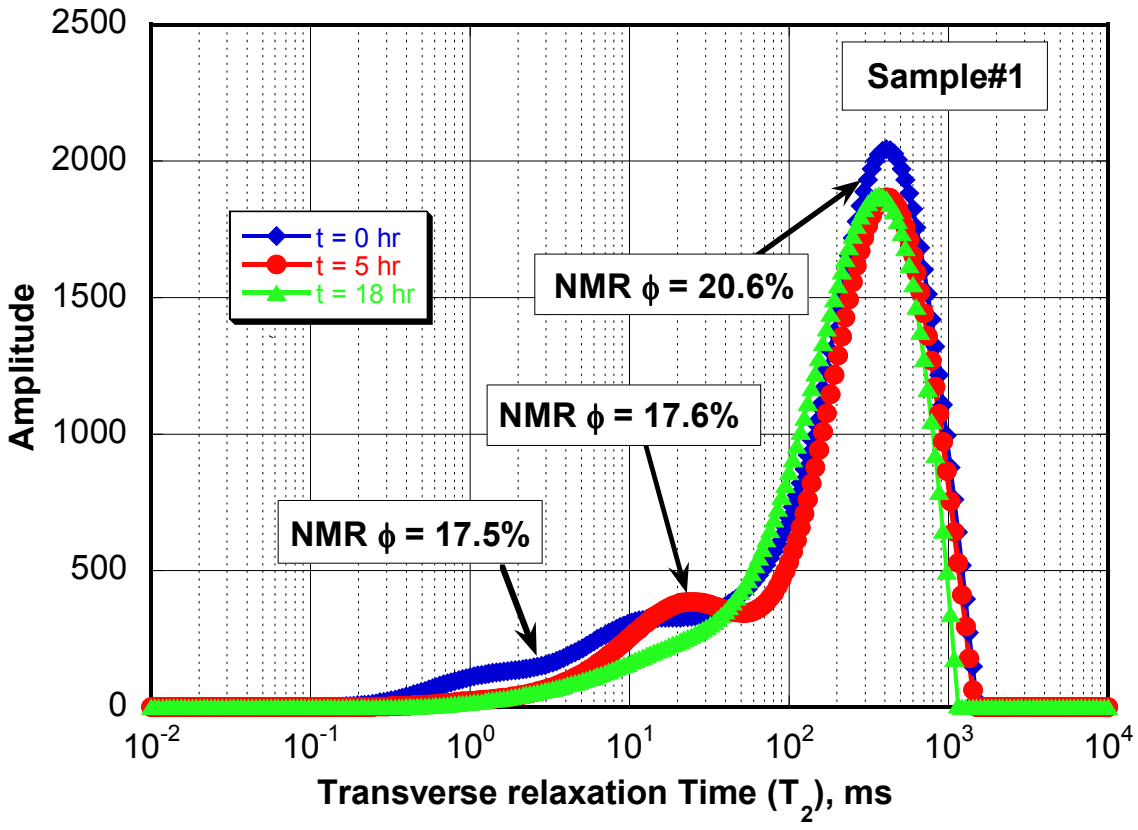

Figure 5.24: T_2 distribution plot for sample#1 at time t = 0, 5, and 18 hours of the injection of 5.4 μm barite suspensions

Several observations can be made from Figures 5.24 and 5.25. The porosity was reduced due to particle capture and deposition over five hours and then remained constant. The probability of particle being captured inside the core sample increased as the pore diameter-to-particle size diameter decreased. In another word, the smaller pores would be blocked and filled with particles before the larger pores. As particles were injected into the core sample, more small pores were blocked. The flow was diverted to larger size pores and the capture probability rate decreased.

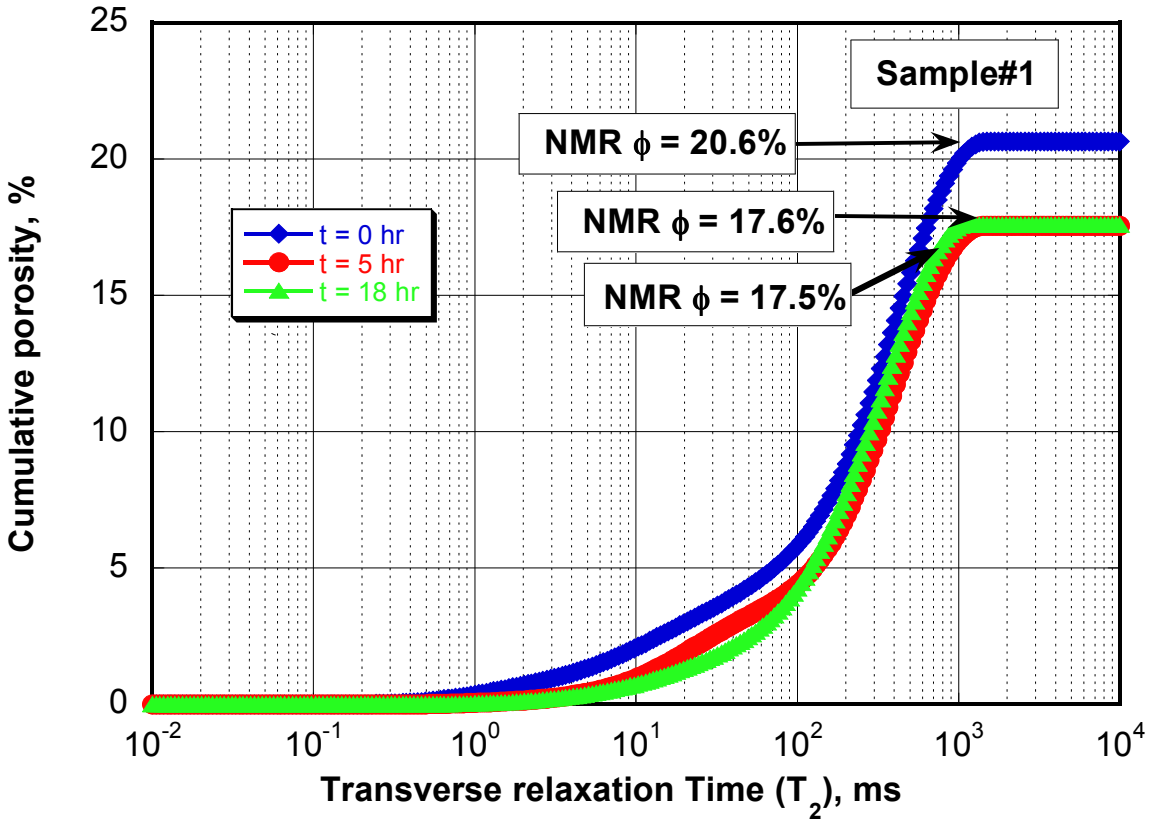

Figure 5.25: Cumulative porosity plot for sample#1 at time t = 0, 5, and 18 hours of injection of 5.4 μm barite suspensions

When all the capture sites were filled, no-more particles could be captured. They would be flushed through the large pore paths. This explains the steady state in porosity established after 18 hours. Additional proof of establishing a steady state during the particle injection test is examined in Figure 5.26.

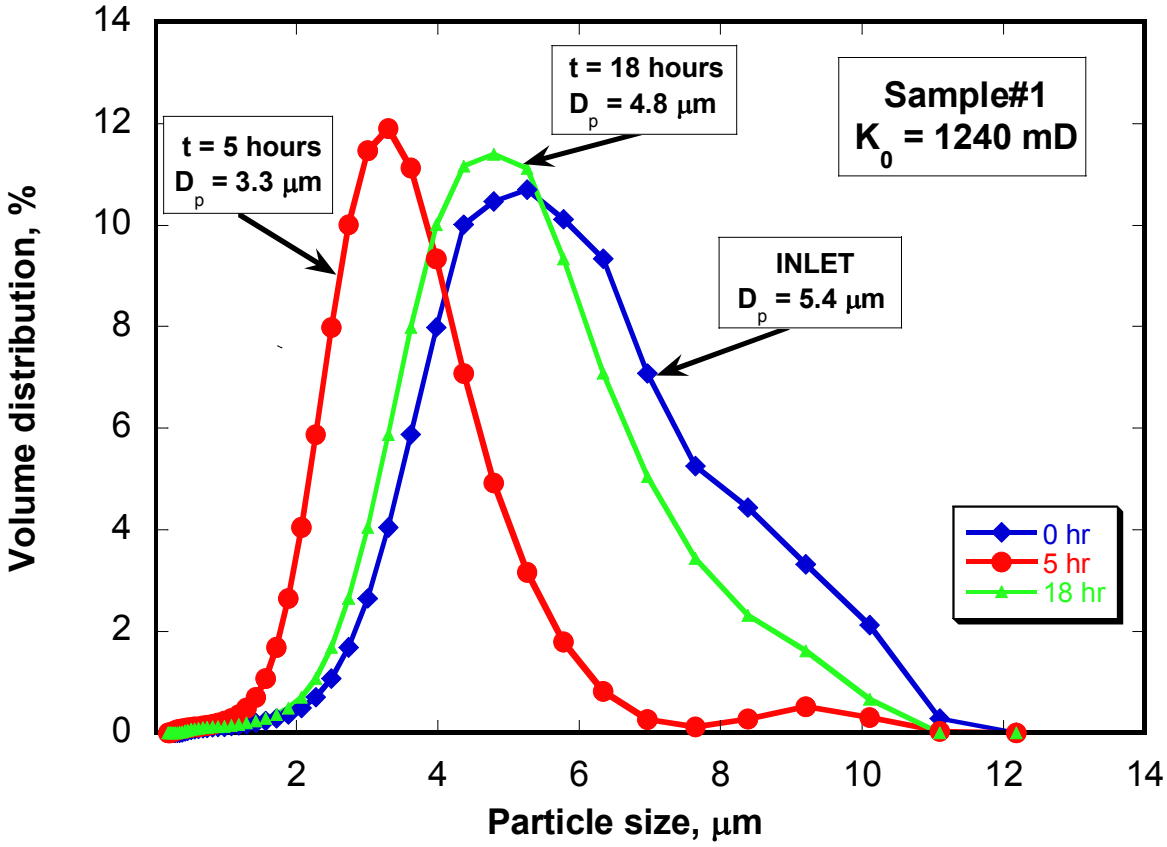

Figure 5.26: Particle size distribution of the effluent at time t = 0, 5 and 18 hours of injection of 5.4 μm barite suspensions

The effluent particle size distribution was analyzed using the LDPSDA method. The particle size of 5.4 μm mean diameter was injected at the inlet. The particle size distribution in the effluent was smaller than in the inlet. This shows that larger particles were captured, while smaller particles were flushed out. As injection proceeded, the outlet particle size distribution shifted to larger diameter until the inlet particle distribution was almost matched. Hence, the steady state flow was attained as the effluent particle size distribution and concentration become constant and identical to the inlet suspension.

Because the pore size-to-particle size ratio is one of the key factors for the capture probability, it is essential to identify different capture mechanisms during suspension injection. Figure 5.27 shows the T_2 distribution for the core flooding experiment in core sample#2 (K_0 = 265 mD). The same barium sulfite suspension was used (mean diameter D_p = 5.4 μm). It was observed that porosity change was small after 5 hours of injection.

From the NMR T_2 distribution data, it is also noticed that the peak at longer T_2 is an indication of big pore dominance. As the core was flooded with suspension for 5 hours, the particles filled in the larger pores to create many other smaller pores inside. Hence, the T_2 distribution response gave another peak at a shorter T_2. The overall porosity drop was from 17.5% to 16.9%. As time proceeded, no further change in porosity was observed. This indicates that no more particles were deposited or captured inside the core. An external filter cake was observed after several hours of injection which implied that the pore-throat blocking/bridging mechanism was the dominance.

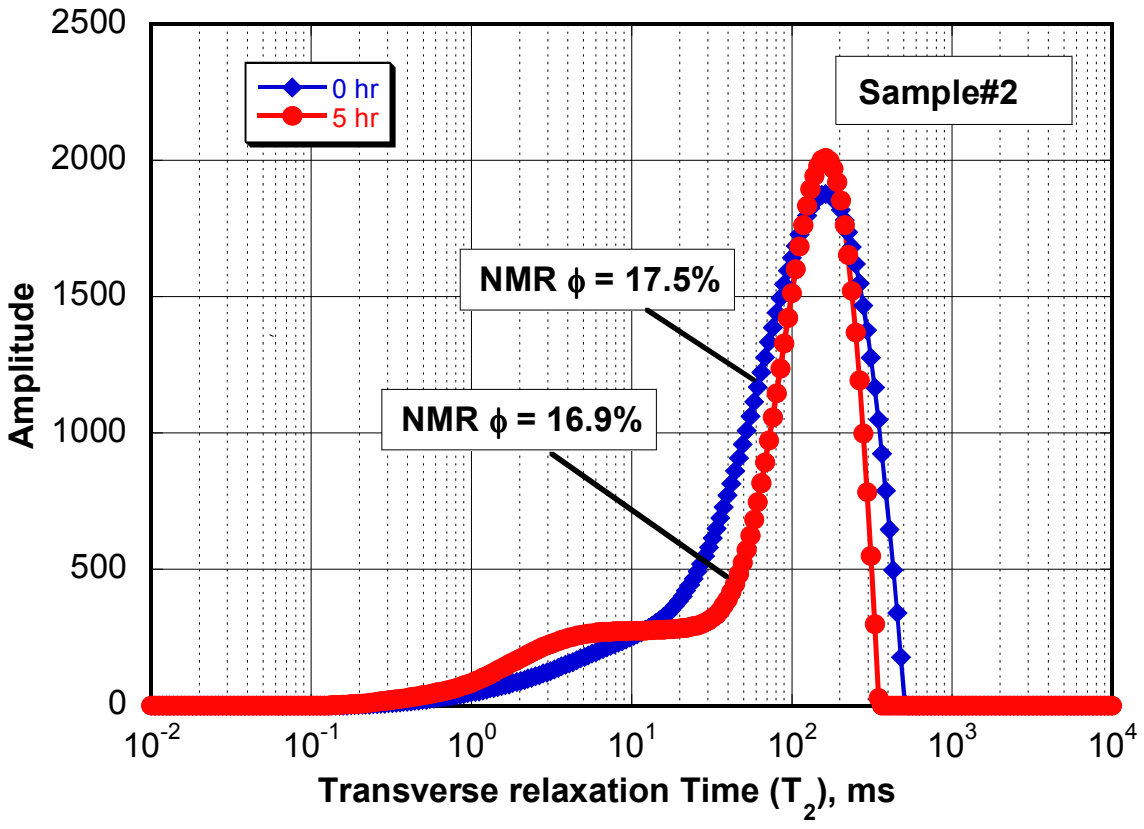

Figure 5.27: T_2 distribution for sample#2 at time t = 0 and 5 hours of injection of 5.4 μm barite suspensions

Figure 5.28 shows the T_2 distribution for the sample#2 experiment at 0, 5, and 18 hours injection of barite suspension (2.2 μm-mean diameter). The peak T_2 shifted to the left indicates that the pore sizes got smaller. The larger pores were substantially filled as time proceeded and the porosity decreased from 17.6% to 14.2% and 13.1% after 5 hours and 18 hours of the experiment, respectively. The distribution changes shown on Figure 5.28 suggest that pore deposition and pore filling mechanisms were the dominant processes.

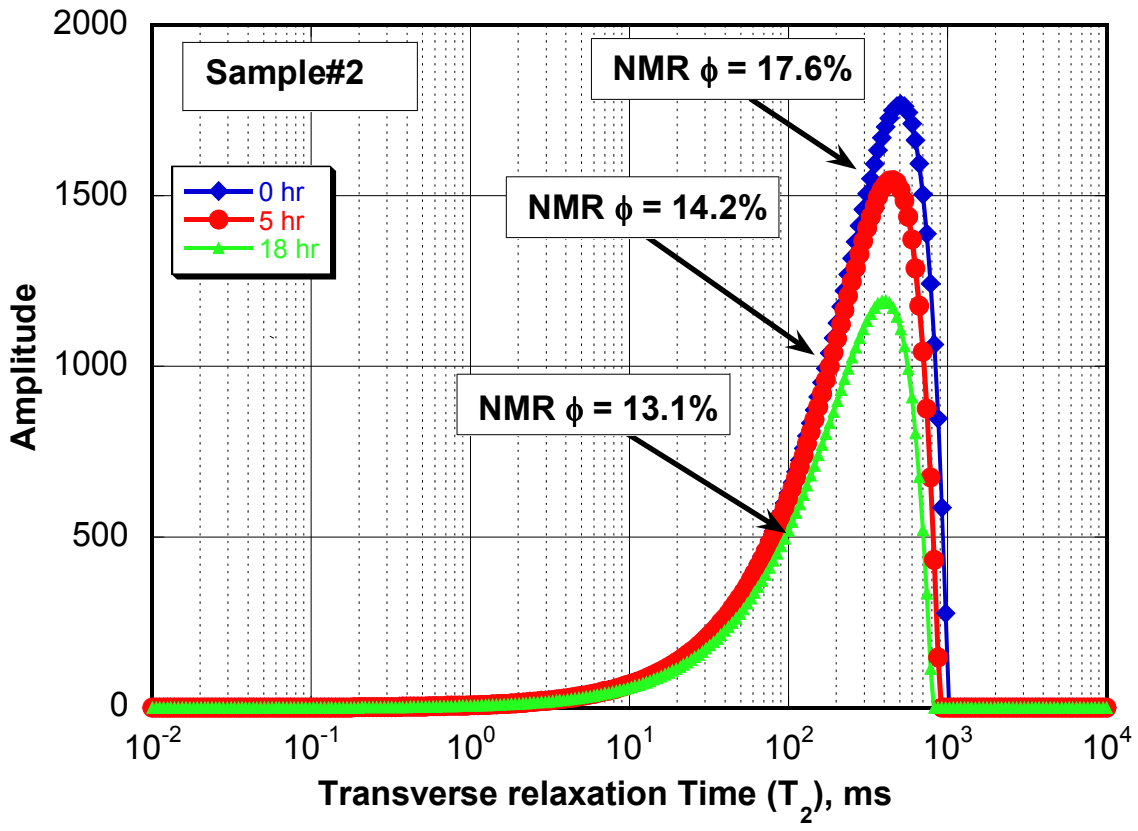

Figure 5.28: T_2 distribution of sample#2 at time t = 0, 5, and 18 hours of injection of 2.2 μm barite suspensions

The effects of particle size distribution on plugging mechanisms were also examined by injecting a wide range of particle sizes (barite with mean-diameter of 3.6 μm) into a carbonate core sample#3 (high porosity but low permeability). The results show that larger particles blocked pore-throats near the injection point and an external filter cake was built to prevent further particle invasion. The porosity change was insignificant after 18 hours of injection. Figure 5.29 represents the T_2 distribution of the

carbonate sample at 0, 5 and 18 hours of injection. The short and long traverse relaxation times, T_2, of the sample before flooding indicates a wide pore size distribution for this rock (range from 1.2 μm to 12 μm). The small reduction in porosity is also explained by the presence of a thick external filter cake after the run. The filter cake acted to prevent further invasion of larger particles into the core.

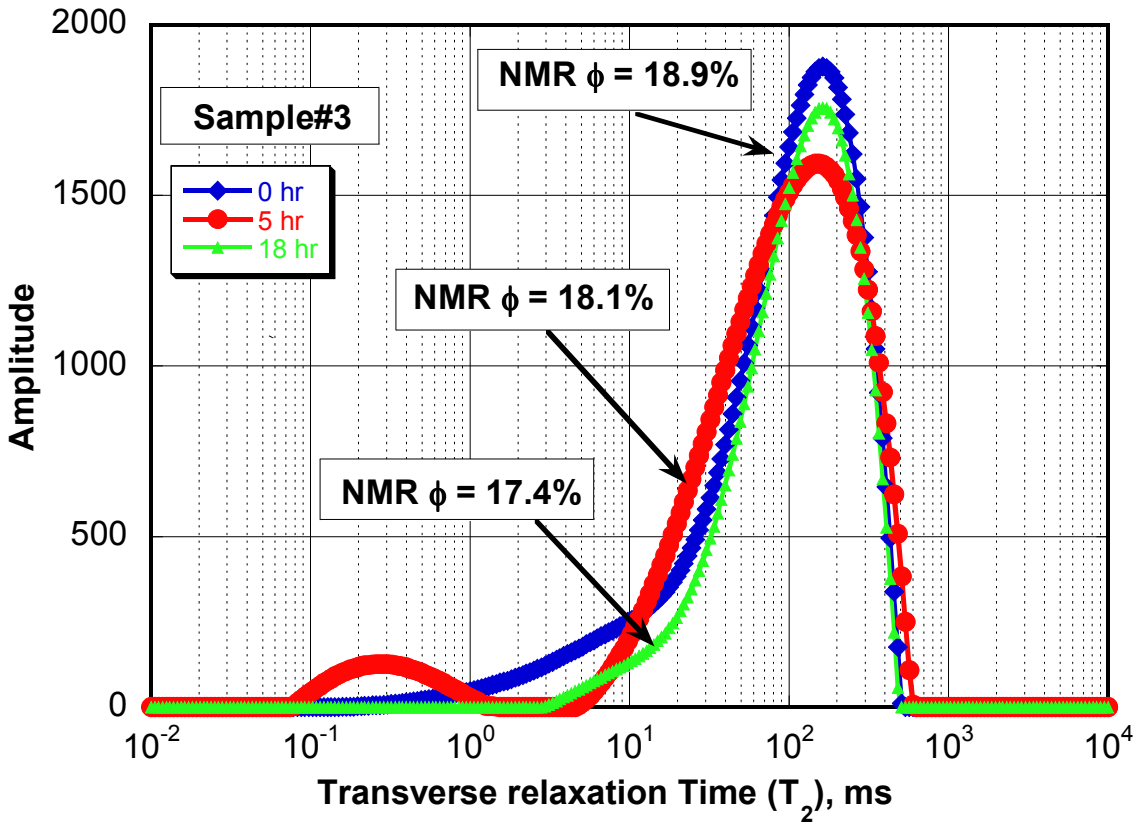

Figure 5.29: T_2 distribution of sample#3 at time t = 0, 5, and 18 hours of injection of 3.6 μm barite suspensions

5.2.2 Sectional-core Measurements

The objective of these experiments was to investigate sectional permeability impairment during the core flood test. The experimental setup was similar to that of section 5.2.1.1.1. The core holder was modified to obtain pressure drops at different sections of the core samples.

5.2.2.1 Experimental System and Procedures

Experimental System:

Figure 5.30 represents the experimental apparatus for this study. The major components of the flow apparatus were a positive displacement pump that provided a constant injection rate. The particulate fluid was stored in the stainless steel accumulator with a Teflon floating piston. The data collected were the overall pressure drop across the core, ΔP, sectional gauge pressure PT1, PT2, and PT3. The nitrogen loaded back-pressure regulator was 500 psi and the confining pressure was 1,000 psi by means of a hydraulic pump.

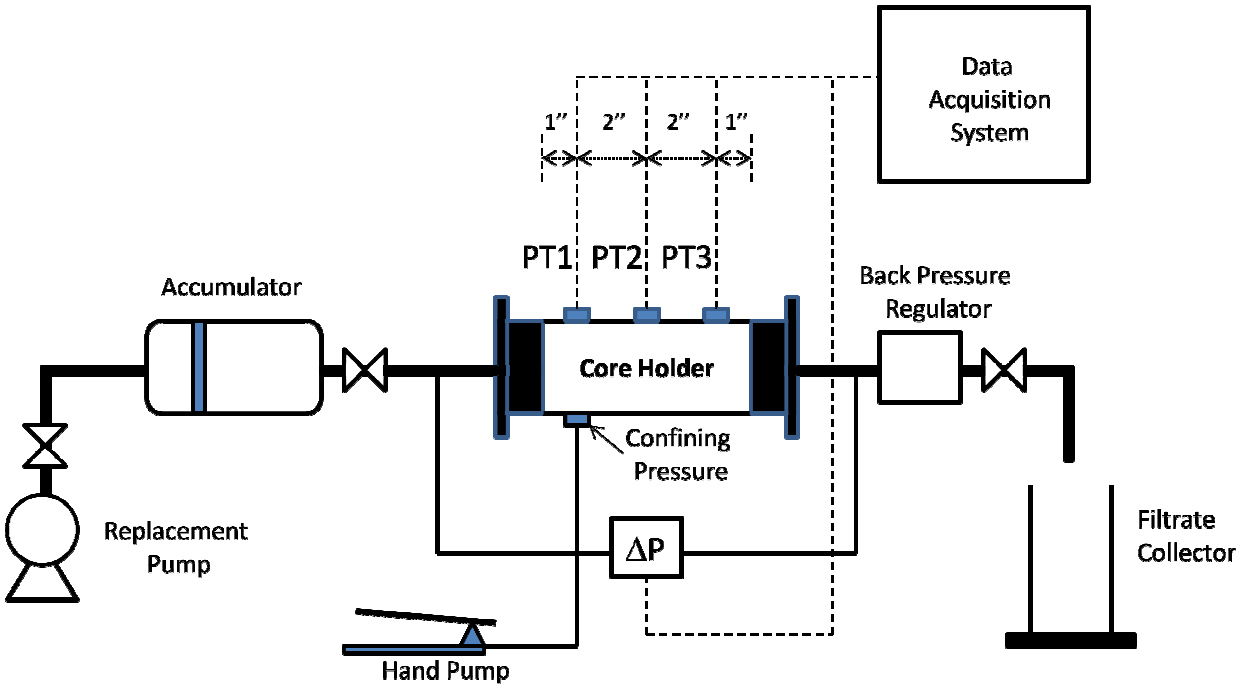

Figure 5.30: Sectional core plugging experimental apparatus

Figure 5.31 shows the picture of the TEMCO multi-pressure tap core holder from TEMCO. The core holder was made from stainless steel and had a pressure limit of 5,000 psi. The core holder was 1.5 feet long and could accommodate 1 inch diameter consolidated cores from 3 inches to 12 inches in length. Cores with 1-in diameter and 6-in length were used in this experiment. There were three pressure taps (2 inches apart) along the length of the core and two confining pressure ports.

The core holder was designed for core flood experiments. Permeability impairment during the test was monitored by section from the pressure drops. The rubber sleeve could be subjected to pressure of 1,500 psi to avoid any bypass.

Figure 5.31: TEMCO multi-pressure tab core holder

Procedures:

Several solid particle size distributions were used in the experiments. The core was first saturated and initial porosity and permeability were determined. Sectional permeability damages were measured during the suspension injection process. The injection rate was constant at 144.0 cm^3/hour.

The procedures followed to conduct the flow test were:

1. Apply 1,000 psi confining pressure to prevent fluid by-pass.
2. Apply backpressure of 500 psi using nitrogen from the tank.
3. Saturate core samples with 3% KCl water for 15 hours and measure the initial permeability and porosity.
4. Shut in the core for an hour to equilibrate the pore water with rock minerals.

5. Pour the particulate fluid into the accumulator. Turn on the displacement pump, set the pump speed to 144.0 cm^3/hour and begin flow.
6. Turn on the Labview 8.0 monitor program to monitor pressure drops and compute permeability for each core segment as a function of flowing time.

5.2.2.2 Data Analysis

The first set of experiments was conducted to determine potential damage during particulate flow of 2.2 μm mean-diameter barite through a sandstone core sample of initial permeability and porosity of 895 mD and 0.21, respectively. The second set of experiments used a core sample from the same block with initial permeability and porosity of 868 mD and 0.20, respectively. Larger barite particles were used (mean diameter ~ 5.6 μm). The flow rate and fluid viscosity were the same for both sets of experiments (q = 144 cm^3/hour, μ = 24 cP). The particle concentration of the injection fluid was 0.2 g/cm^3. The experimental rock and fluid properties are listed in Table 5-4.

Table 5-4: Rock and particulate fluid properties for two experiment sets

Sequence	Permeability	Porosity	Fluid viscosity	Particle diameter
Experiment Set 1	895 mD	0.21	24 cP	2.2 μm
Experiment Set 2	868 mD	0.20	24 cP	5.6 μm

During experiment set 1, the core with the 2.2 μm suspensions exhibited damage throughout the entire length. The overall permeability reduction was about 40% and no external filter cake was visible after 2.5 hours of injection. The filtration and degree of particle invasion was expected to be high in this case. The percentage reduction in all three sections of the core decreased with depth into the core. Two main mechanisms caused permeability impairment in the experiment: i) fines release and migration, and ii) particle invasion.

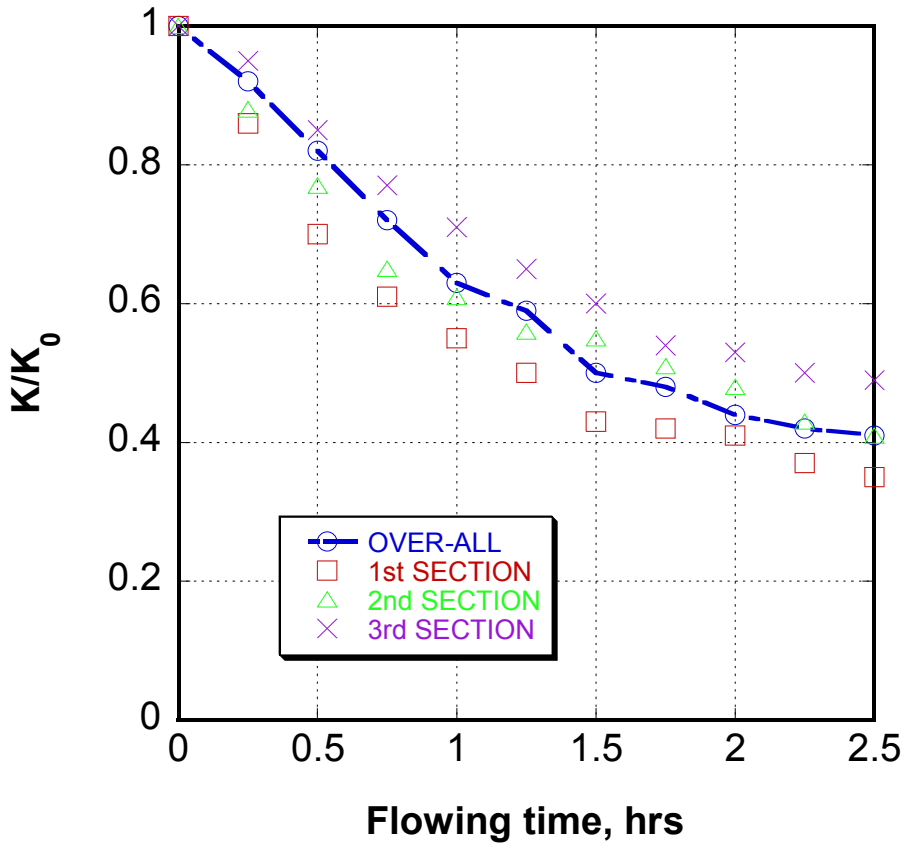

Figure 5.32: Permeability damage obtained by 2.2 μm solid suspended injection (0.2 g/cm^3 in concentration) at flow rate of 144 cm^3/hr into a sandstone core (initial permeability of 895 mD)

Figure 5.32 shows a typical result obtained from the particle suspension injection into a sandstone core sample. It should be pointed out that the permeability in the 1st section includes permeability of section 1 and external filter cake. The damage degree was observed to be higher in the first section (about 65%). Less damage was observed in the second and third sections; however, the damage range did not vary significantly from one to another (range from 50-65% in permeability reduction).

Experiment set 2 yielded similar results. Again the damage decreased with depth and the overall impairment was about 82%. However, there were differences observed from the sectional damages in this experiment. The first section of the core was damaged by about 85% while third section was only reduced 30%. Sturdy external cake was visible after 2.5 hours injection. Figure 5.33 shows a typical result of external cake formation.

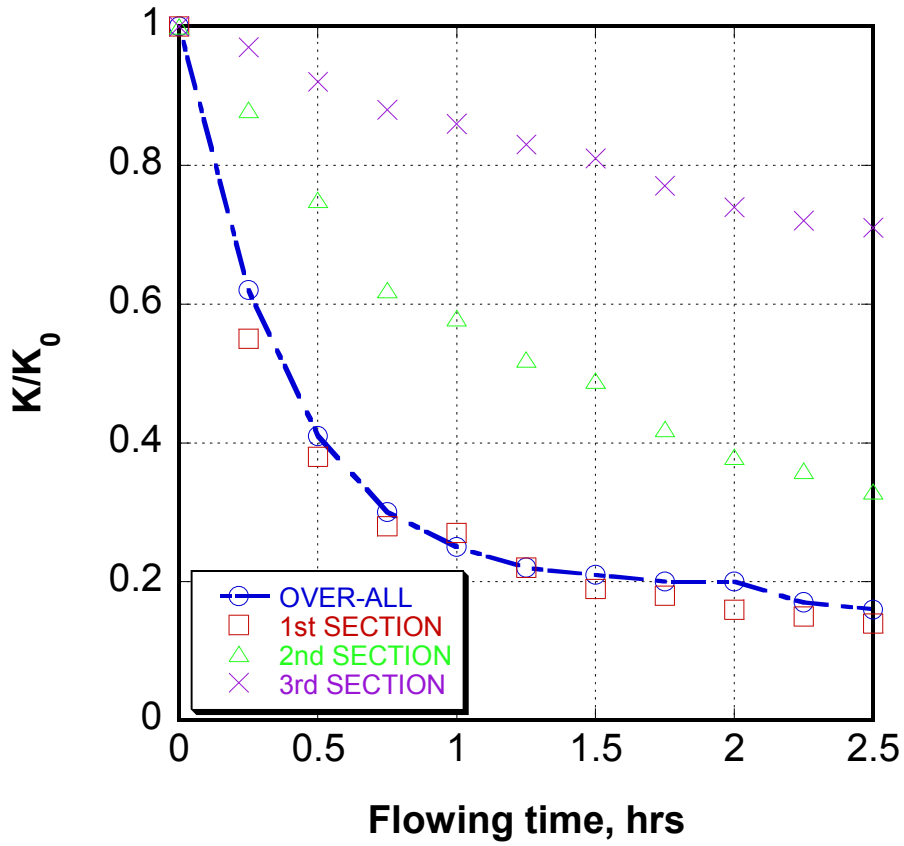

Figure 5.33: Permeability damage obtained by 5.6 µm solid suspended injection (0.2 g/cm^3 in concentration) at flow rate of 144 cm^3/hr into a sandstone core (initial permeability of 868 mD)

5.2.2.2.1 Bedrikovesky et al. (2002) Deep-bed Filtration Model:

Equations of the model presented by Bekrikovesky et al. (2002) were used to model formation plugging by particles in core plugs. The model approach was an extension of the pioneering work of Iwasaki (1937) and Herzig et al. (1970). Their model used a number of simplifying assumptions:

1. Single phase flow (only liquid phase),

2. Incompressible fluid and rock, and
3. Gravity effects are ignored.

The Bedrikovesky et al. (2002) equations for particle balance, kinetics of particle capture, and modified Darcy's law are summarized as follows:

$$\frac{\partial}{\partial T}c(X,T)+\frac{\partial}{\partial X}c(X,T)=-\frac{1}{\phi}\frac{\partial}{\partial T}\sigma(X,T) \quad \text{----------(5.7)}$$

$$\frac{\partial}{\partial T}\sigma(X,T)=\lambda(\sigma)\phi c(X,T) \quad \text{----------(5.8)}$$

$$U=-\frac{K_0K(\sigma)}{\mu L}\frac{\partial P}{\partial X} \quad \text{----------(5.9)}$$

The dimensionless length and time are given by the flowing:

$$X=\frac{x}{L};\quad T=\frac{1}{L\phi}\int_0^t U(t)dt \quad \text{----------(5.10)}$$

The initial and boundary conditions for the above equations are:

$$T=0: c=0,\sigma=0;\quad X=0: c=c_{inj} \quad \text{----------(5.11)}$$

where c is the suspended particle concentration, σ is the deposited particle concentration, ϕ is the porosity, L is the length of the core, λ is the filtration coefficient, $K(\sigma)$ is the damage function which shows how permeability decreases due to particle retention, and U is the total flow velocity.

The relative change in permeability due to deposition is given as:

$$K(\sigma) = \frac{1}{1+\beta\sigma} \text{ ----------(5.12)}$$

where β is the formation damage coefficient.

Knowledge of the two parameters λ and β is essential to predict the injectivity loss. These parameters are empirical and they can be determined from laboratory core flood tests.

For constant filtration coefficient and flow rate, and neglecting the change in porosity, the analytical solution of equation (5.7, 5.8, 5.9) with their initial-boundary value condition (5.12) for T>X (Herzig et al. 1970; Pang and Sharma,1997) is:

$$c(X,T) = c_{inj}\exp(-\lambda X) \text{ ----------(5.13)}$$

$$\sigma(X,T) = \lambda\phi(T-X)c_{inj}\exp(-\lambda X) \text{ ----------(5.14)}$$

Ahead of the concentration front T<X, both concentrations are zero.

The harmonic average permeability of the damage section of the core is calculated by Payatakes et al. (1974):

$$\overline{K(t)} = \frac{x}{\int_0^x \frac{dx}{K(x,t)}} \text{ ----------(5.15)}$$

Substituting equations (5.10) and (5.14) into equation (5.15), and integrating yields the following expression (Bedrikovestky et al. 2001):

$$\frac{K_0}{\overline{K(t)}} = 1 + \frac{\beta c_{inj} U}{x}\left(1-\exp(-\lambda x)\right)t + \beta c_{inj}\phi\exp(-\lambda x) + \frac{\beta c_{inj}\phi}{\lambda x}\left(1-\exp(-\lambda x)\right) \text{ ----------(5.16)}$$

Equations (5.13), (5.14), and (5.16) were used to calculate the deposited particle concentration and permeability reduction at each section of the core sample.

The analytical model for deep-bed filtration with the single particle-capture mechanism proposed by Bedrikovesky et al. (2002) was used to fit the laboratory data of barite suspension injection into sandstone core samples. The classic filtration analytical solution depended on two fitting parameters, the filtration coefficient, λ, and the blocking parameter, β. In general, the filtration coefficient and permeability are arbitrary functions of deposited concentration, and they can be found from pressure drop.

The initial permeability of the core sample was determined from pressure drop at the beginning of the injection, when the rock was not yet impaired. The length of the core (6 inches) and the sectional pressure points were known at distances 1, 3, and 5 inches measured from the injection point of the core. The degree of sectional damage along the core was determined by pressure measurements at three pressure taps. Values for λ and β are shown in Table 5-5 to match the damage measured in three sections of the core.

Figure 5.34 shows permeability reduction profiles computed for each section and the whole length of the core for experimental data set 1. The computed permeability reduction curves provided a good match with the experimental data. In this experiment, the particles were small relative to the pore size distribution. In addition, the concentration of injected particles was low and the particles easily penetrated deep inside the core. The degrees of damage in all three sections of the cores were the same order of magnitude (ranging from 50-62% in permeability reduction).

Table 5-5: Adjustable parameters to match the two experimental data sets

Test	K_0 (mD)	ϕ	D_p (μm)	λ_1	λ_2	λ_3	λ	β_1	β_2	β_3	β
Set 1	895	0.21	2.2	2.14	1.71	1.82	1.89	0.75	0.94	0.81	0.83
Set 2	868	0.20	5.6	6.14	1.23	0.54	2.64	0.12	0.37	0.39	0.29

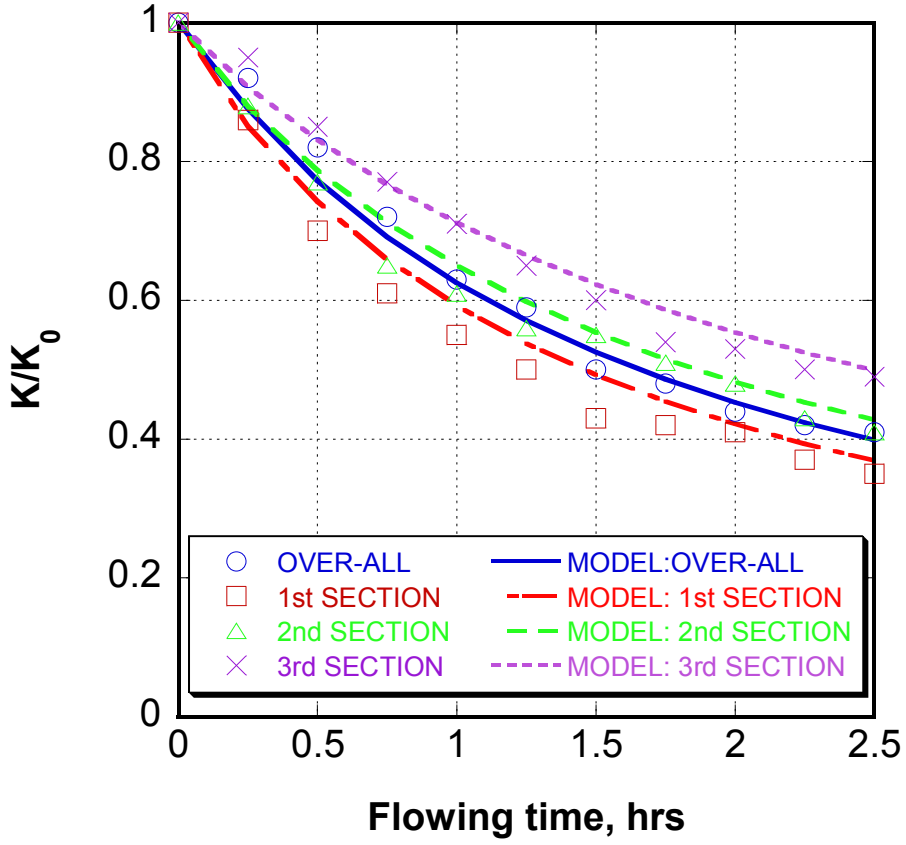

Figure 5.34: Comparison between experimental and computed results using Bedrikovesky et al. (2002) model (particle average diameter = 2.2 μm)

After solving for retained concentration $\sigma(X,T)$ from equation (5.14), the permeability reduction along the core can be predicted using equation (5.16). Figure 5.35 shows the simulated permeability reduction versus the distance from the injection port for

various times during the core flood test of 2.2 μm diameter suspensions. The plot shows that the damage is most severe at the injection port, and it is less further from the injection point.

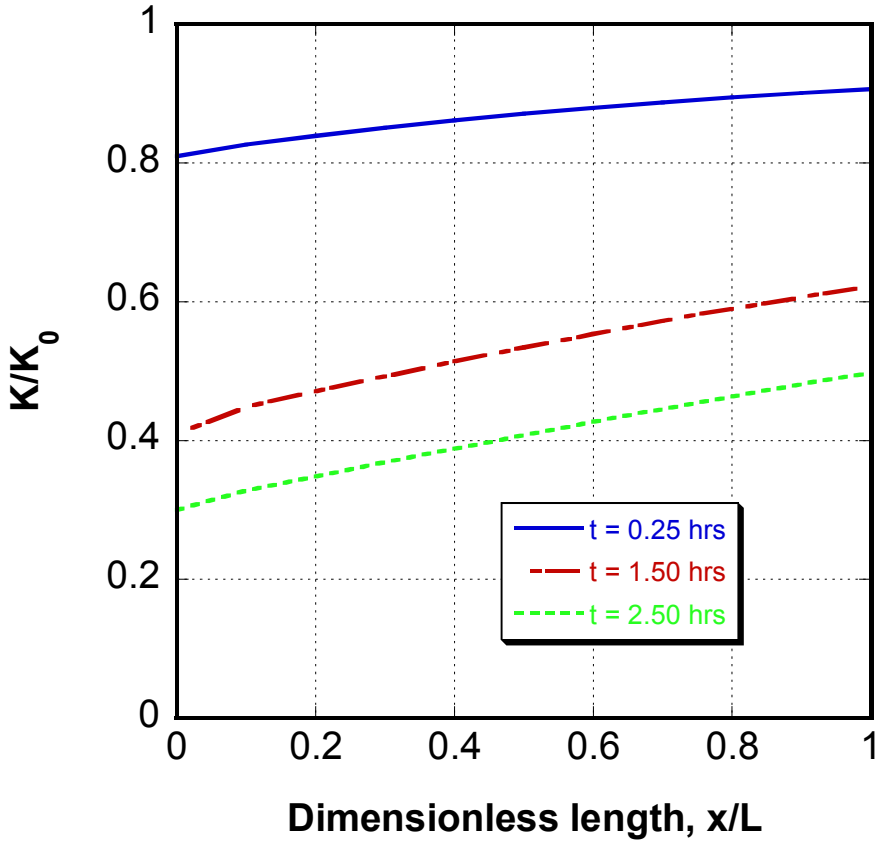

Figure 5.35: Permeability reduction versus distance from the injection port for time 0.25, 1.50, and 2.50 hour core flood test of 2.2 μm diameter suspension

Figure 5.36 shows the computed overall and the three sectional permeability reductions for the core in experiment set 2. The average particle size was 5.6 μm and its concentration was also 0.2 g/cm^3.

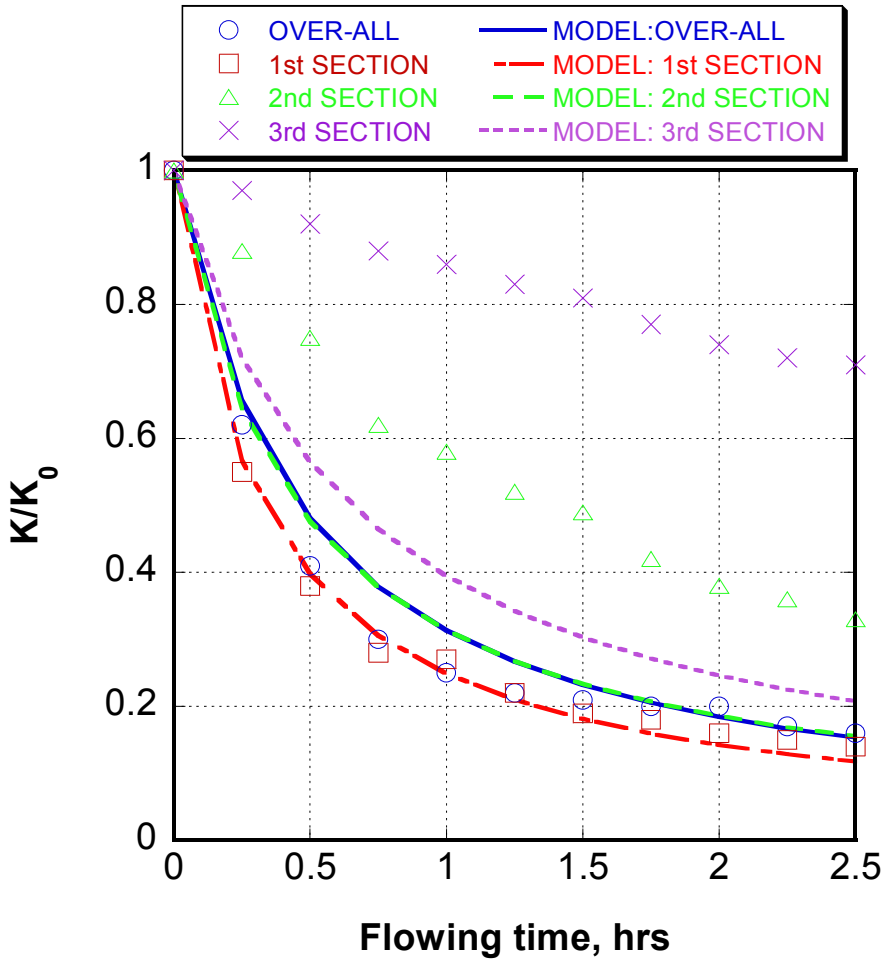

Figure 5.36: Comparison between experimental and computed results using Bedrikovesky et al. (2002) model (particle average diameter = 5.6 μm)

The model predicted the first sectional permeability damage and overall permeability reduction quite well but it did not match the experimental data for the second and third sections. This can be explained by the assumption that the linear damage function had a single capture mechanism. In this case, major particle invasion occurred only in the first section of the core and particle invasion was much less in the second and third sections. And it might be that the primary permeability impairment was due to fines release and migration.

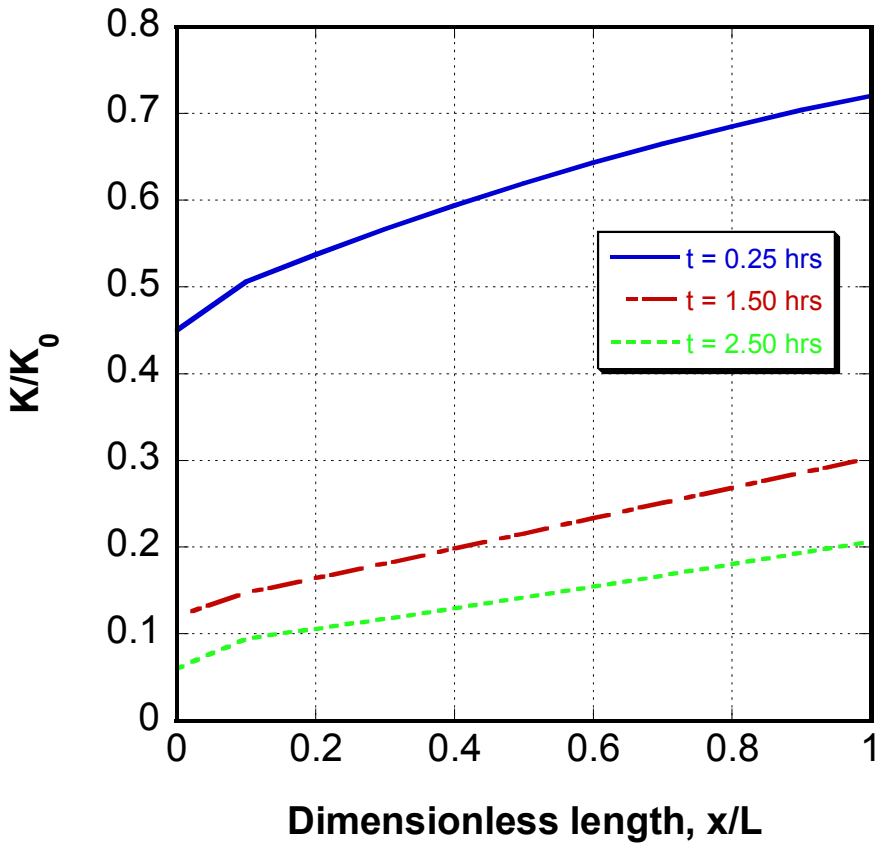

Figure 5.37: Permeability reduction versus distance from the injection port for time 0.25, 1.50, and 2.50 hour core flood test of 5.6 μm diameter suspension

Figure 5.37 represents the computed permeability reduction along the length of the core based on the single capture mechanism assumption in this classical model. A trend was observed that was similar to experiment set 1. The degree of damage was most severe at the injection port and indicates the formation of external filter cake.

5.2.2.2.2 Civan and Nguyen (2005) Improved Plugging-Nonplugging Parallel Pathways Model:

The plugging and non-plugging model first proposed by Gruesbeck and Collins (1982) describes the hydronamically induced fine migration. The fines migration model developed by Nguyen and Civan (2005) was used to correlate the particle concentration and fraction of depositing particle to permeability. The model assumed that the porous medium was incompressible, homogenous, and isotropic. The fluid was considered incompressible. The simulation was for Darcy flow, single phase, one-dimensional linear flow. The porous medium consisted of plugging and non-plugging pathways. Permeability changes in the plugging sections were negligible compared to permeability changes in the non-plugging sections.

The governing equations of the modified plugging-nonplugging parallel pathways model are summarized in the following (Civan and Nguyen, 20005):

The plugging and non-plugging porosities are given by subtracting the fraction of depositing particles from the initial values of the plugging and non-plugging porosities:

$$\phi_p = \phi_{p0} - \varepsilon_p \text{ ----------(5.17)}$$

$$\phi_{np} = \phi_{np0} - \varepsilon_{np} \text{ ----------(5.18)}$$

The bulk volume fraction f_p and f_{np} of porous media that contain the plugging and non-plugging pathways, respectively, vary due to the net deposition of particles. The fractions of plugging and non-plugging porosities are given by:

$$f_p = \frac{\phi_p}{\phi} \text{ ----------(5.19)}$$

$$f_{np} = \frac{\phi_{np}}{\phi} \text{ ----------(5.20)}$$

The instantaneous total porosity and fraction of depositing particles are the sum of the plugging and non-plugging porosities:

$$\phi = \phi_p + \phi_{np} \text{ ----------(5.21)}$$

$$\varepsilon = \varepsilon_p + \varepsilon_{np} \text{ ----------(5.22)}$$

From equations (5.19) to (5.21):

$$f_p + f_{np} = 1 \text{ ----------(5.23)}$$

The partial derivative of the fraction of depositing particles with respect to time are given as the product of the surface deposition constant, velocity, particle concentration, and the plugging porosity:

$$\frac{\partial \varepsilon_p}{\partial t} = k_p u_p \sigma_p \phi_p \text{ ----------(5.24)}$$

$$\frac{\partial \varepsilon_{np}}{\partial t} = k_p u_{np} \sigma_{np} \phi_{np}^{2/3} - k_e \varepsilon_{np} \phi_{np}^{2/3} \eta_e \left(\tau_{np} - \tau_{cr}\right) \text{ ----------(5.25)}$$

The initial conditions for equation (5.19) and (5.20) are given by:

$$\varepsilon_p = \varepsilon_{p0}, \quad t = 0 \text{ ----------(5.26)}$$

$$\varepsilon_{np} = \varepsilon_{np0}, \quad t = 0 \text{ ----------(5.27)}$$

The pore filling rate constant k_p in equation (5.22) is given by:

$$\begin{array}{l} k_p \neq 0, \ for \ t > t_{cr} \ when \ \beta < \beta_{cr} \\ k_p = 0, \ otherwise \end{array} \text{ ----------(5.28)}$$

where t_{cr} is a critical time when the pore throats are first obstructed by particles. The parameter $\beta = D_T/D_p$ is the ratio of pore-throat-to-particle diameter ratio.

The critical value β_{cr} required for pore throat blocking is determined by the exponential expression proposed in chapter 3 and 4:

$$\beta_{cr} = A \exp\left(-B \, \mathrm{Re}_p\right) + C \text{ ----------(5.29)}$$

where A, B, and C are empirical parameters.

The fraction of uncovered deposits is represented exponentially as a function of non-plugging depositing particles:

$$\eta_e = \exp\left(-k \varepsilon_{np}\right) \text{ ----------(5.30)}$$

The flow rate is calculated using Darcy's flow equation:

$$q = -\frac{KA\Delta P}{\mu L} \text{ ----------(5.31)}$$

The fluid fluxes through the plugging and non-plugging pathways expressed are modified after Gruesbeck and Collins (1987):

$$u_p = f_p \frac{K_p}{K} u \text{ ----------(5.32)}$$

$$u_{np} = f_{np} \frac{K_{np}}{K} u \text{ ----------(5.33)}$$

The total volumetric flux through porous media is given by:

$$u = u_p + u_{np} \text{ ----------(5.34)}$$

The permeabilities in the plugging and non-plugging pathways are represented with exponential expression as follows:

$$K_p = K_{p0} \exp\left(-\alpha\left(\phi_{p0} - \phi_p\right)^{n_1}\right) = K_{p0} \exp\left(-\alpha \varepsilon_p{}^{n_1}\right) \text{ ----------(5.35)}$$

$$K_{np} = K_{np0} \exp\left(\phi_{np}/\phi_{np0}\right)^{n_2} = K_{np0} \exp\left(1 - \varepsilon_{np}/\phi_{np0}\right)^{n_2} \text{ ----------(5.36)}$$

The average particle volume deposited along the core is given by:

$$\varepsilon(t) = \varepsilon_p(t) + \varepsilon_{np}(t) = \frac{1}{L}\int_0^L \left[\varepsilon_p(t) + \varepsilon_{np}(t)\right] dx \text{ ----------(5.37)}$$

The pressure drop across the core plug can be calculated from Darcy's law given by:

$$u = \frac{q}{A} = -\frac{K(x,t)}{\mu}\frac{\partial P(x,t)}{\partial x} \text{----------(5.38)}$$

Civan and Nguyen (2005) developed a numerical solution of particle migration and deposition in core flood tests using the plugging-nonplugging pathways model over a uniform linear grid system, as shown in Figure 5.38.

The method of lines was applied to reduce the partial differential equations (PDEs) to a convenient set of first-order ordinary differential equations (ODEs). The ODEs were solved using conventional 4th order Runge-Kutta method. The number of grid blocks was chosen to be 20 for simulation purpose. The relative deviation between the numerical solutions at consecutive iteration steps, denoted by the superscripts of s and (s+1), is defined as:

$$E_r^{(s+1)} = \frac{F^{(s+1)} - F^{(s)}}{F^{(s+1)}} \text{----------(5.39)}$$

where $F \in (\varepsilon_p, \sigma_p)$ represents the solution array. The solution of nonlinear system of ODEs was carried out iteratively until the convergence criteria was less than 1.0×10^{-6}.

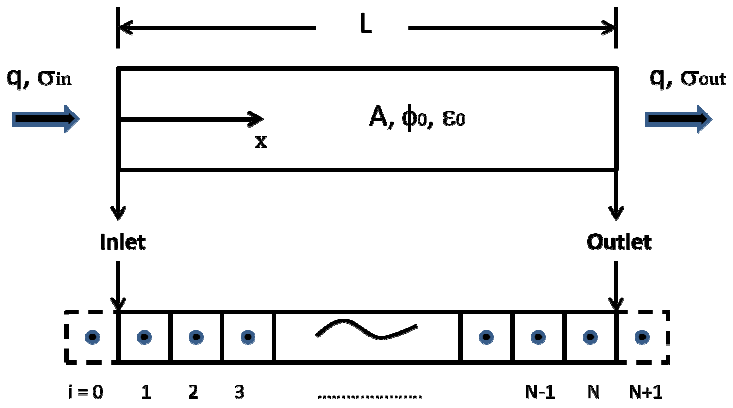

Figure 5.38: Uniform linear grid system of core plug for numerical solution (after Civan and Nguyen, 2005)

Civan and Nguyen's numerical approach was applied here to simulate deep-bed filtration. The parameter values were adjusted to fit the two experimental data sets. The most sensitive parameters were the deposition and entrainment (mobilization or sweeping) rate constants, such as σ, k_p, k_d, and k_e. These parameters depended on particle concentration and injection rate. The parameters *A, B,* and *C* were adapted from the pore bridging/plugging correlation in chapter 3. Tables 5-6 and 5-7 show the input parameters and the adjustable parameter values that yielded a successful match to the experimental set 1 data.

Table 5-6: Fixed Parameter Values for experiment set 1

Parameter	Value	Units
L_{core}	6	cm
d_{core}	2.54	cm
D_p	2.2	μm
c_p	0.2	g/cm^3
ϕ_0	0.21	Fraction
τ	1.41	cm/cm
$\varepsilon_{p,i}$	0	Fraction
$\varepsilon_{np,i}$	0	Fraction
ρ_p	2.72	g/cm^3
q	144	cm^3/hr
σ_{in}	0.2	g/cm^3
μ	24	cP
$K_{p,i}$	0.898	Darcy
K_{npi}	0.0898	Darcy

Table 5-7: Adjustable Parameter Values for experiment set 1

Parameter	Value	Units
α	10	Dimensionless
n_1	0.24	Dimensionless
n_2	0.68	Dimensionless
δ	0.004	cm^{-1}
k_p	1.89	cm^{-1}
k_d	1.56	cm^{-1}
k_e	0.005	Pa^{-1}
τ_{cr}	0.000042	hr^{-1}
A	3.98	Dimensionless
B	0.46	Dimensionless
C	1.32	Dimensionless

The permeability impairment simulation results are shown in Figure 5.39. The satisfactory prediction of the experimental observations indicates that the model based on plugging and nonplugging pathways is valid for this experimental system. Figure 5.40 indicates that more particle deposition occurred at the injection point. Equilibrium is

reached after a certain time when the permeability reduction no longer changed with time, not shown in Figure 5.39.

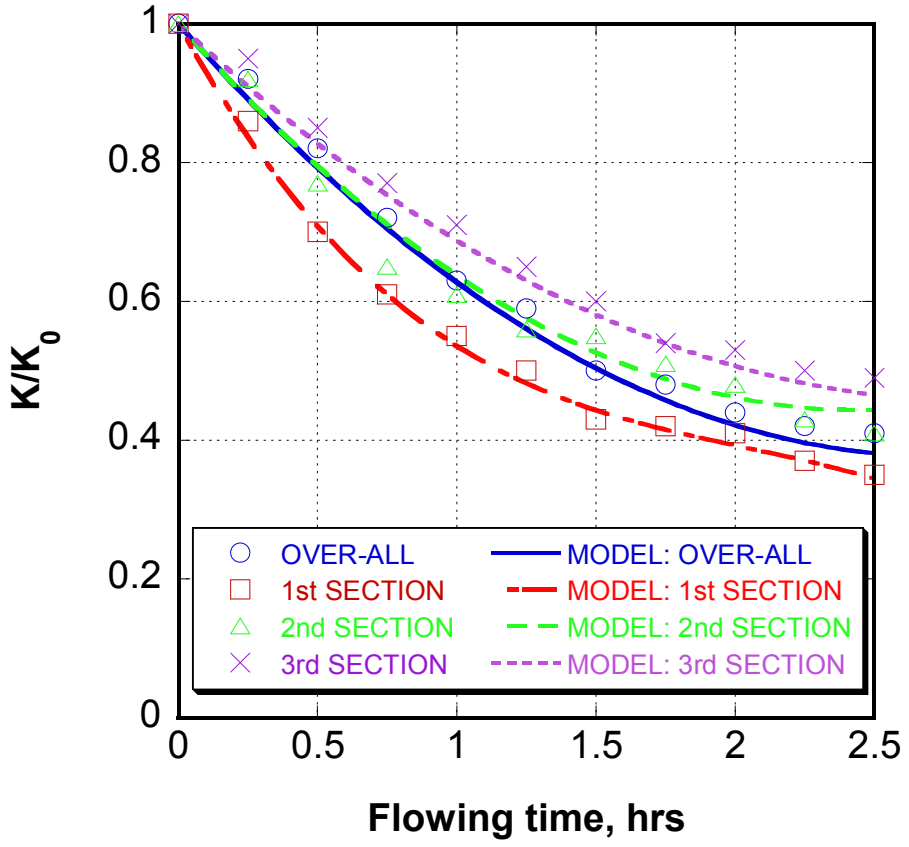

Figure 5.39: Comparison between experimental and computed results using plugging-nonplugging pathways model (particle average diameter = 2.2 μm)

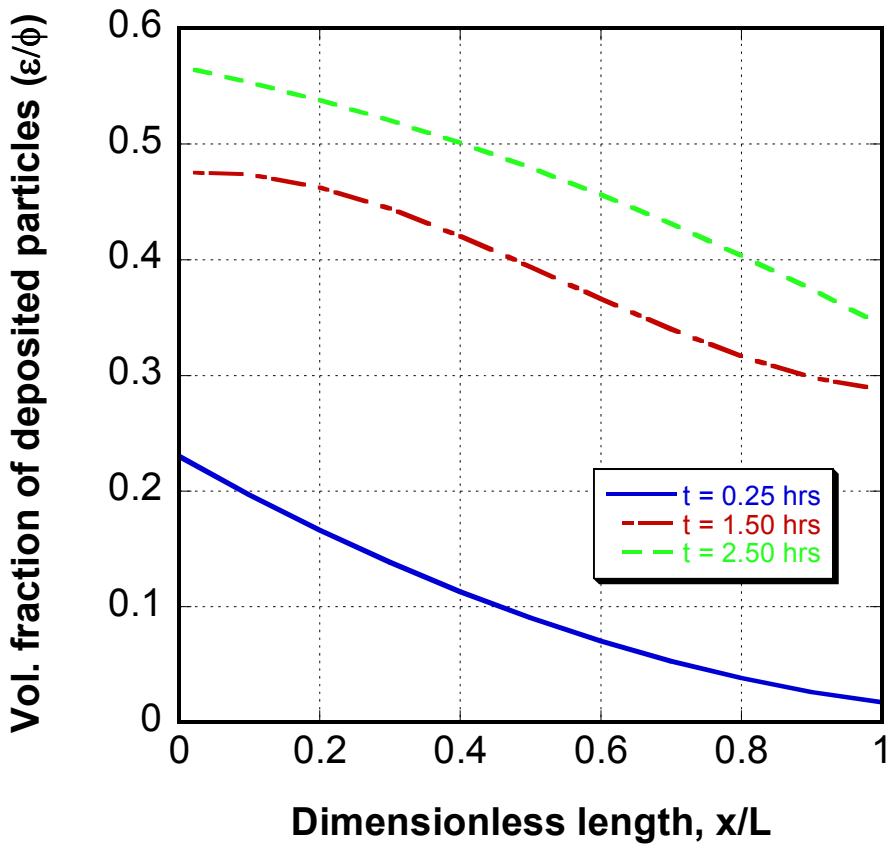

Figure 5.40: Volume fraction of particles retained along the length of the core during deposition and entrainment of 2.2 μm diameter particle

As particles plugged the plugging pathways, flow was diverted to the nonplugging pathways. These had much higher permeability and hydraulic diameter. For small particles and low concentration, the retainment can still happen but in reduced magnitude because of the high pore-throat-to-particle diameter ratio.

Similar simulation results were obtained for experiment set 2. The input and adjusted parameter values are presented in Table 5-8 and 5-9.

Table 5-8: Fixed Parameter Values for experiment set 2

Parameters	Values	Units
L_{core}	6	cm
d_{core}	2.54	cm
D_p	2.2	μm
c_p	0.2	g/cm^3
ϕ_0	0.20	Fraction
τ	1.41	cm/cm
$\varepsilon_{p,i}$	0	Fraction
$\varepsilon_{np,i}$	0	Fraction
ρ_p	2.72	g/cm^3
q	144	cm^3/hr
σ_{in}	0.2	g/cm^3
μ	24	cP
$K_{p,i}$	0.869	Darcy
K_{npi}	0.0869	Darcy

Table 5-9: Adjustable Parameter Values for experiment set 2

Parameters	Values	Units
α	10	Dimensionless
n_1	0.27	Dimensionless
n_2	0.86	Dimensionless
δ	0.004	cm^{-1}
k_p	13.8	cm^{-1}
k_d	0.93	cm^{-1}
k_e	0.0001	Pa^{-1}
τ_{cr}	0.000042	hr^{-1}
A	2.57	Dimensionless
B	0.13	Dimensionless
C	1.18	Dimensionless

The simulation results for permeability reduction in three sections (Figure 5.41) were much better compared to ones predicted using the Bedrikovesky et al. (2002) classical model in section 5.2.2.1.1. The reason is that the plugging and nonplugging pathways model included multiple plugging mechanisms by adjusting values of parameters k_p, k_d, k_e and also the exponents n_1, n_2 for permeability estimations.

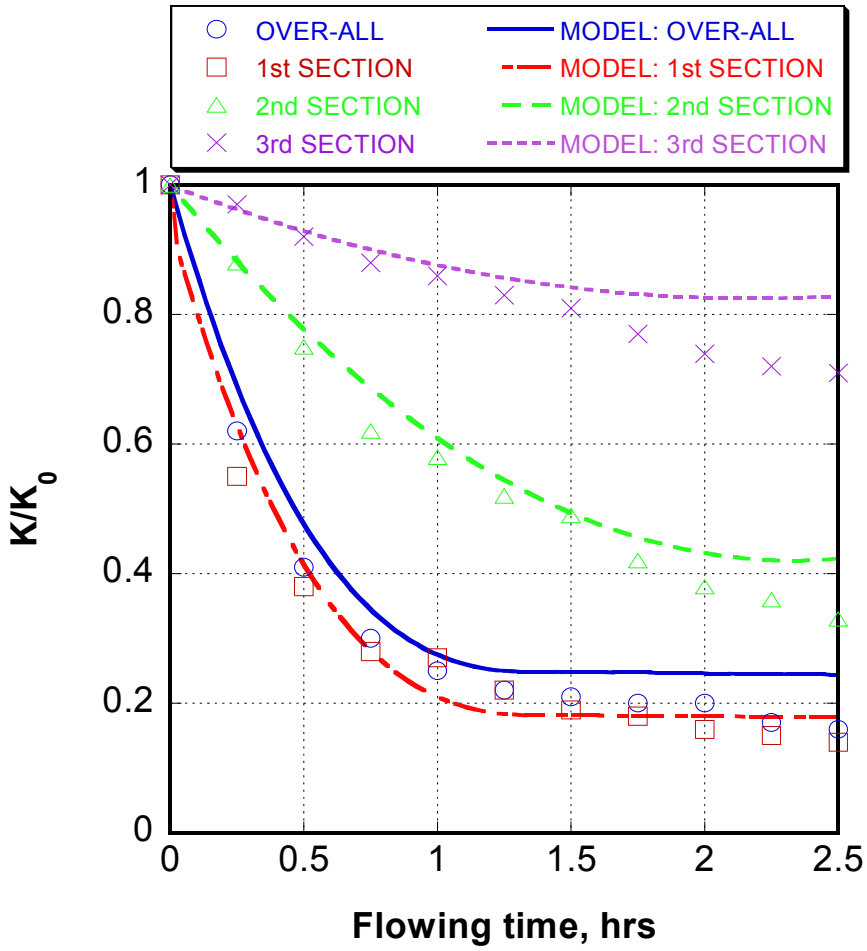

Figure 5.41: Comparison between experimental and computed results using plugging-nonplugging pathways model (particle average diameter = 5.6 μm)

In this case of larger particles, the nonplugging pathways eventually could be transformed into plugging pathways, which could be clogged by particles under favorable conditions (small pore-throat-to-particle size ratio, high particle concentration, and etc.). Plugging conditions were determined using the *A*, *B*, and *C* presented in the table of parameter values. Figure 5.42 shows the particle deposition along the length of the core for the 5.6 μm particle injection experiment. The results have an expected trend since the

particle deposition rate was much higher at the injection point and indicate external filter cake formation.

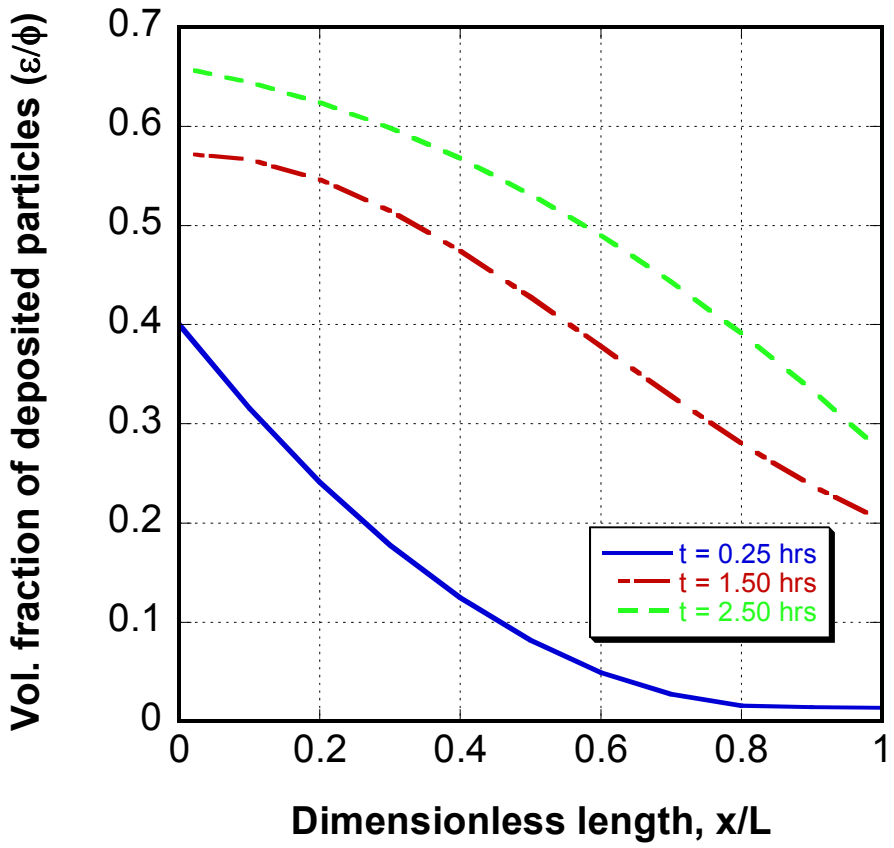

Figure 5.42: Volume fraction of particles retained along the length of the core during deposition and entrainment of 5.6 μm diameter particle

5.3 Thin-slice Studies

In this particular test, the permeability and porosity alteration relationships during the injection of fine particles through a thin-slice core sample was investigated. A numerical model was developed to match data obtained from the experiments.

5.3.1 Experimental System and Procedures

Experimental System:

The setup used was described in section 5.2.1.1.1. The only differences were the suspension properties and the core samples.

Tables 5-10 and 5-11 summarize the experimental conditions for the tests. The sandstone core used in the test was 1 inch diameter and 0.25 inch long.

Table 5-10: Properties of the rock

Names	Quantities	Values	Units
Core Permeability	K_0	1.25	Darcy
Core Porosity	ϕ	0.23	Fraction
Core Diameter	D	1.0	inch
Core Length	L	0.25	inch

Table 5-11: Properties of suspension

Names	Quantities	Values	Units
Fluid density	ρ	1.18	g/cm^3
Fluid viscosity	μ	14	cP
Initial particle concentration	$(c_p)_{in}$	0.5	g/cm^3
Injection rate	q	10.4	cm^3/hour

Procedures:

The core was saturated with clear injection fluid (DI water with 0.3% Xanthan by weight) prior to the injection of a barium sulfate ($BaSO_4$) suspension. The rheological measurements of the fluid are presented in Table 5-12. Initial permeability and porosity of the core were measured. The suspension fluid was prepared by mixing 0.3% by weight of Xanthan with DI water to create a viscous fluid to suspend the fine particles. Barium sulfate particles, with a density of 4.5 g/cm^3 and average diameter of 5.0 μm, were added to the solution at the designed concentration. Tests were at a constant flow rate. The back pressure regulator was set to be 500 psig. Effluent samples were collected to measure the particle concentration every hour. The differential pressure was monitored and recorded every 15 minutes.

A Labglass Filtration Assembly was used to determine the concentration of particles in the effluent. The assembly includes a 300-ml funnel on the top to catch the fluid sample, a sintered glass disk in the middle to provide even, flat support structure for membrane filter, and an outlet tube for vacuuming. The parts were held together with an anodized aluminum clamp. A nylon membrane of 0.4 μm pore size and 47 mm diameter was used to capture barium sulfate particles from the effluent. The nylon membrane was strong, inherently hydrophilic, and compatible with a broad range of aqueous solutions that included alcohols and solvents. Vacuum was applied at the bottom of the assembly to withdraw the fluid from the funnel through the membrane. The particles captured at the membrane were carefully dried and weighed to determine the particle concentration in the effluent. The experimental data were used to adjust relevant parameters of the thin section formation plugging model described in the data analysis section.

Table 5-12: Shear rate reading of the injection fluid

Shear Rate (RPM)	Shear Stress (Dynes/cm^2)
3	15.3
6	20.4
20	30.6
60	40.8
100	51.1
200	56.2
300	71.5
600	91.9

5.3.2 Data Analysis

The objectives of the experimental work were to generate experimental data to compare with the theoretical plugging predicted by the numerical model, and to produce data which might be applied to predict variation of porosity and permeability of the formation.

The core damage test was carried out for 5 hours under constant flow rate. The differential pressure across the core increased as a function of time (Figure 5.43) which indicated permeability reduction during the test. The overall percentage damage to

permeability was about 40% and no external filter cake was visible. The instantaneous permeability of the core plug was determined using Darcy's equation for linear, incompressible, and steady-state single phase fluid flow:

$$K = \frac{q\mu}{A}\frac{L}{\Delta P} \quad \text{.....(5.40)}$$

where q is the constant flow rate; A and L are the surface area and core length, respectively; μ is the fluid viscosity; and ΔP is the measured differential pressure.

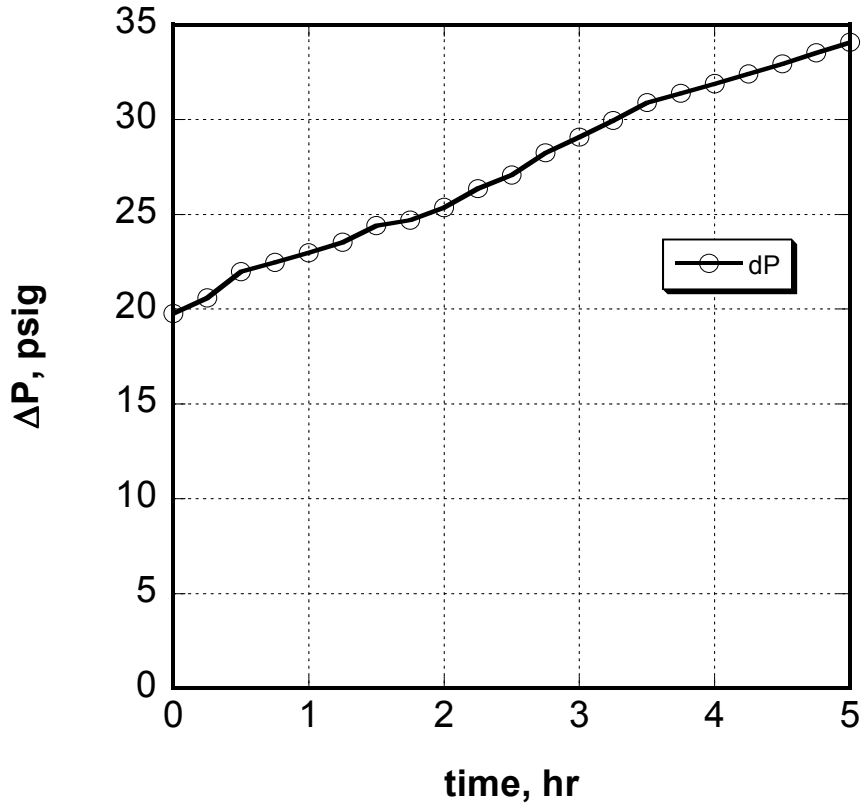

Figure 5.43: Differential pressure across the thin-slice core during the core flow test

The effluent particle concentration was measured once every hour using the labglass filtration assembly. The particle concentration from the core was found to be less than the initial particle concentration injected into the core. The difference was the amount of particles captured inside the core to cause porosity reduction. The instant permeability and porosity alteration were measured and plotted in Figure 5.44.

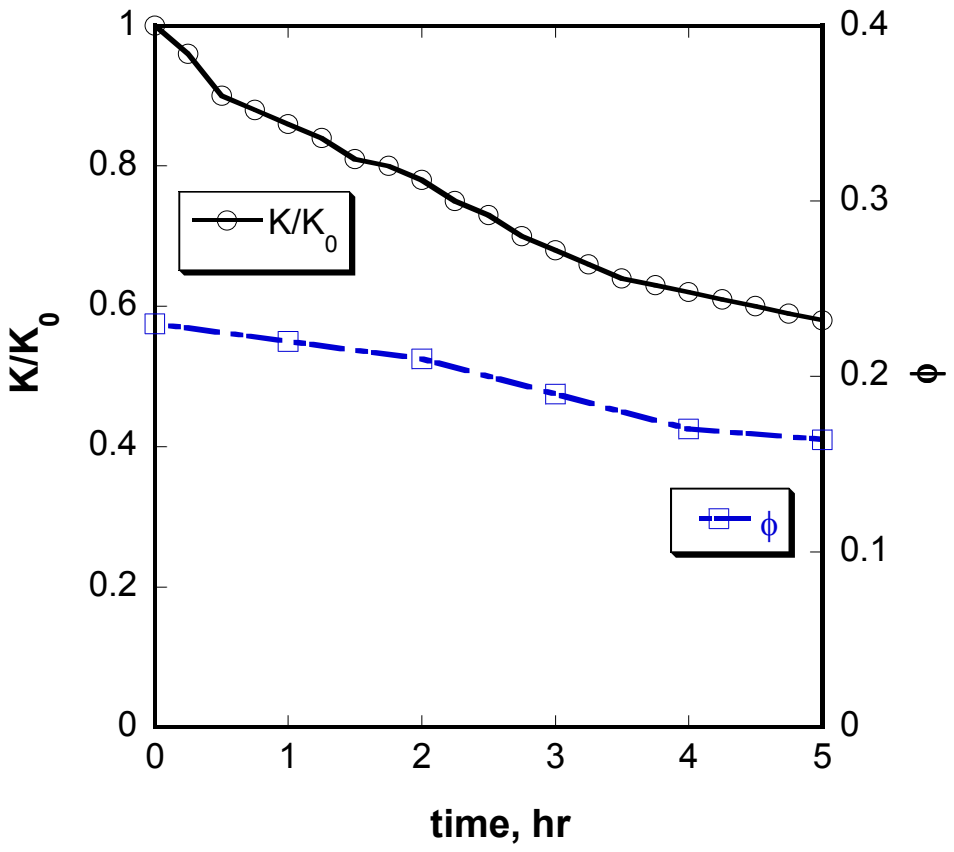

Figure 5.44: Permeability and Porosity alteration during the core flow test

The overall porosity reduction was about 30% (reduced from 0.23 to 0.16) after 5 hours of injection.

Wojtanowicz et al. (1987) Diagnostic Method:

The Wojtanowicz et al. (1987) diagnostic method was used to determine the damage mechanisms for the thin section formation plugging experiment (section 5.3.2).

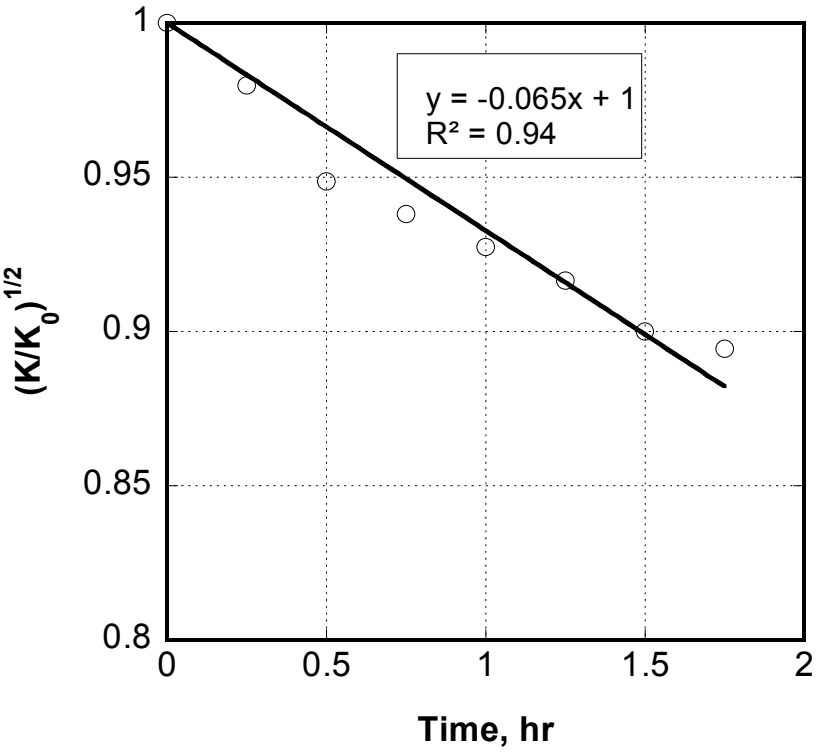

Figure 5.45: Pore surface deposition mechanism using Wojtanowicz et al. (1987) diagnostic method

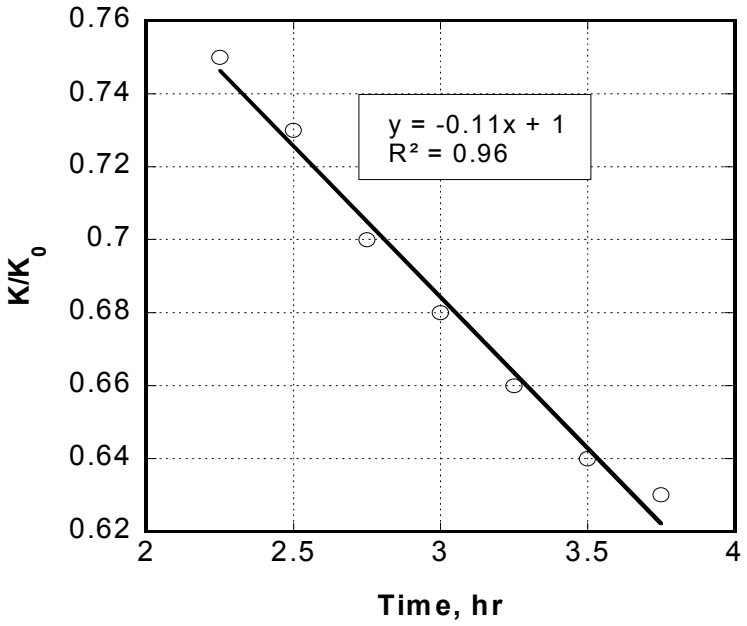

Figure 5.46: Pore-throat plugging mechanism using Wojtanowicz et al. (1987) diagnostic method

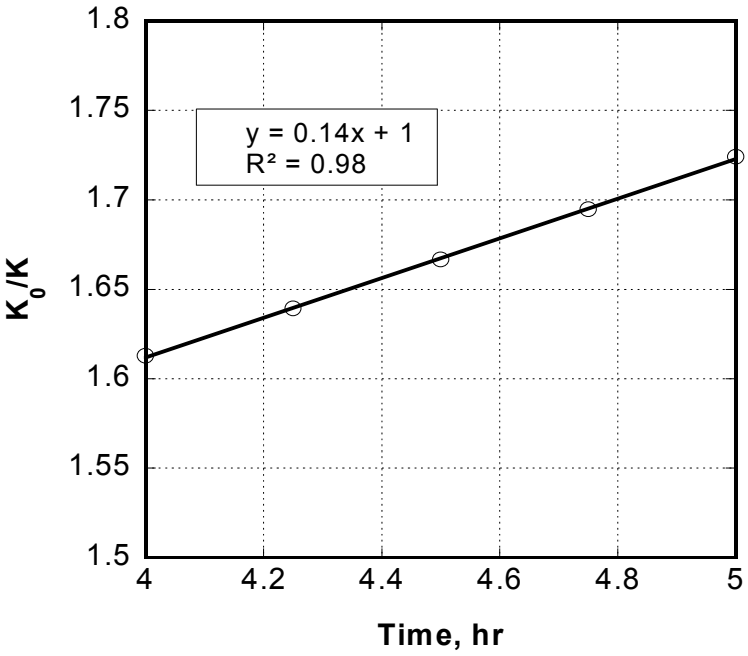

Figure 5.47: Pore filling mechanism using Wojtanowicz et al. (1987) diagnostic method

It was found that the pore surface deposition occurred during the first 2 hours of the test (Figure 5.45). In the next 1.75 hours, the pore throat plugging mechanism was observed (Figure 5.46). Finally, the pore filling mechanism was observed in the last 1.25 hours of the experiment run (Figure 5.47). All three mechanisms may have operated during this period.

Civan (2007) Thin Section Formation Plugging Model:

The thin slice core is depicted in Figure 5.48. The suspension fluid was injected into the core at constant flow rate. Because the particles have sizes suitable for bridging to occur, the particle concentration of the fluid leaving the core will be less than the concentration of the fluid entering the core. Civan (2007) presented the equations from which the Wojtanowicz et al. (1987) diagnostic equations can be derived and used to determine the plugging conditions for the thin section.

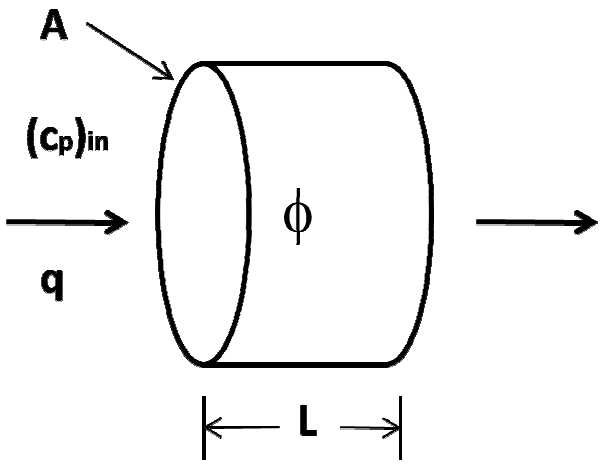

Figure 5.48: Schematic of a thin slice core sample

The thin-slice plugging modeling equations presented by Civan (2007) are summarized below.

Assuming that the particles were captured at pore throats, the mass balance over a thin core slice is:

$$\frac{\mathrm{d}}{\mathrm{dt}}\left[AL\left(\phi c_p + \sigma_p\right)\right] + q\left(c_p\right) - q\left(c_p\right)_{in} = 0 \text{ ----------(5.41)}$$

where A and L are the areal surface and length of the core respectively, ϕ is the instant porosity of the core, c_p is the concentration of particles inside the core and σ_p is the particle concentration captured at the pore throats.

The particle rate of capture at pore throat is:

$$\frac{\mathrm{d}\sigma_\mathrm{p}}{\mathrm{dt}} = k_d c_p - k_e \sigma_p \text{ ----------(5.42)}$$

Here k_d and k_e denote the surface deposition and mobilization rate constants, respectively.

The instant porosity of the core is computed from the following equation:

$$\phi = \phi_0 - \frac{\sigma_p}{\rho} \text{ ----------(5.43)}$$

where ρ is the density of the suspension fluid.

The initial conditions for equation (5.41) through (5.43) are:

$$c_p = 0, \quad \sigma_p = 0, \quad \phi = \phi_0, \quad when\ t = 0 \text{ ----------(5.44)}$$

Expanding equation (5.41) and substituting equation (5.42) and (5.43), Civan (2007) obtained:

$$\frac{dc_p}{dt} = \frac{\frac{q}{AL}\left[\left(c_p\right)_{in} - c_p\right] + \left(\frac{c_p}{\rho} - 1\right)\left(k_d c_p - d_e \sigma_p\right)}{\phi_0 - \frac{\sigma_p}{\rho}} \text{----------(5.45)}$$

Simultaneous solutions of equations (5.45) and (5.42) can be found using a Runge-Kutta method. The variation of the core porosity is calculated by equation (5.43). An Excel VBA^{TM} code was written to solve the system of ODEs using the Runge-Kutta method.

The concentration of particles in the effluent was calculated from initial concentration less particle concentration captured inside the core:

$$c_{effluent} = \left(c_p\right)_{in} - \sigma_p \text{----------(5.46)}$$

The permeability and porosity relationship was determined using the modified Kozeny-Carman equation by Civan (2001, 2002, 2003, 2005):

$$\sqrt{\frac{K}{\phi}} = \Gamma\left(\frac{\phi}{\alpha - \phi}\right)^n \text{----------(5.47)}$$

where K and ϕ is the measured permeability and porosity of the core, respectively; Γ is the interconnectivity parameter, α is a cement exclusion parameter in fraction, and n is an exponent. The value of α = 1 represents porous media containing no pore filling materials, and no grain embedment and fusing effects. In a heterogeneous core with pore filling material effects for this experiment, α should be in the range $0 < \alpha < 1$.

To fit the experimental data obtained from the thin section formation plugging test in section 5.3.1, the governing equations were solved numerically assuming trial values for the two coefficients k_d and k_e until a match was achieved.

Table 5-13 shows the values of the input parameters that were measured for the experiment. Table 5-14 is a list of the adjustable parameters that gave a successful match to the thin-core flow experimental data. The concentration of particles in the effluent, and the pressure drop across the core versus time were matched simultaneously.

Table 5-13: Experimental input parameters

Names	Quantities	Values	Units
Core Permeability	K_0	1.25	Darcy
Core Porosity	ϕ	0.23	Fraction
Core Diameter	D	2.54	cm
Core Length	L	1.27	cm
Fluid density	ρ	1.18	g/cm^3
Fluid viscosity	μ	24	cP
Initial particle concentration	$(c_p)_{in}$	0.5	g/cm^3
Injection rate	q	10.4	cm^3/hour

Table 5-14: Model adjustable parameters

Names	Quantities	Values	Units
Deposition coefficient	k_d	0.04	$hour^{-1}$
Erosion coefficient	k_e	0.001	$hour^{-1}$
Interconnectivity parameter	Γ	2.06	Dimensionless
Cement exclusion parameter	α	0.231	Fraction
Exponent	n	0.02	Dimensionless

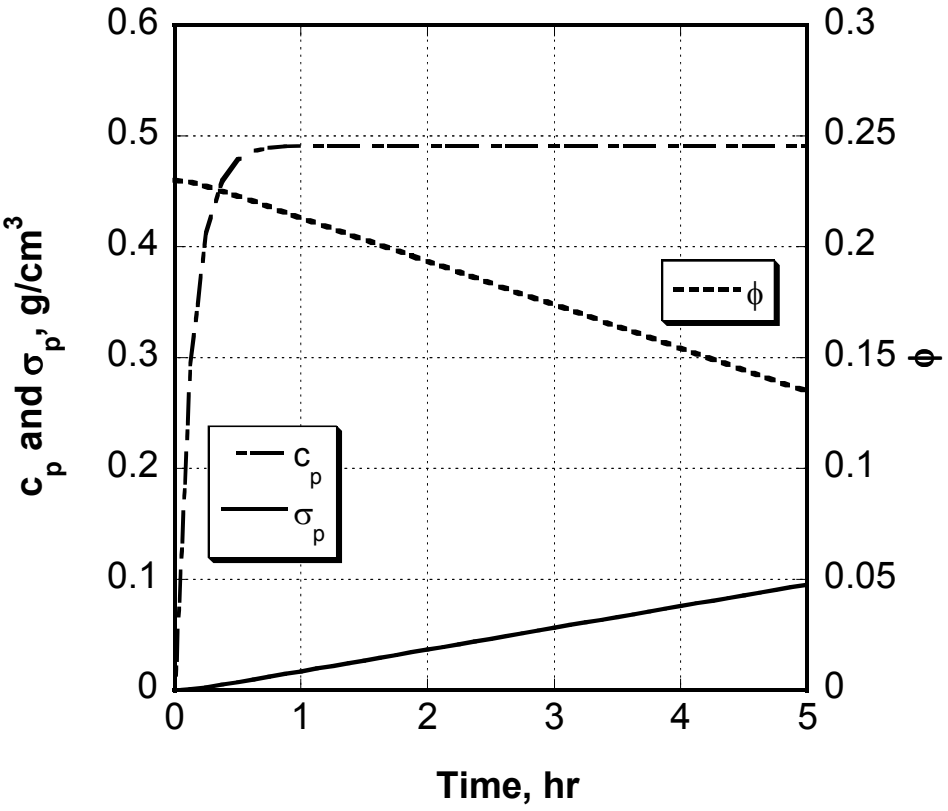

Figure 5.49: Simulation results for porosity variation using the property input in Table 5-13 and 5-14

The simulation results are plotted in Figure 5.49 providing the particle concentration in the core, c_p, the capture particle concentration, σ_p, and the instant porosity, ϕ, as a function of time.

The suspension particle concentration in the effluent versus time was plotted in Figure 5.50. The particle concentration at the outlet decreased as more particles were captured inside the core and therefore narrowed the pore throats.

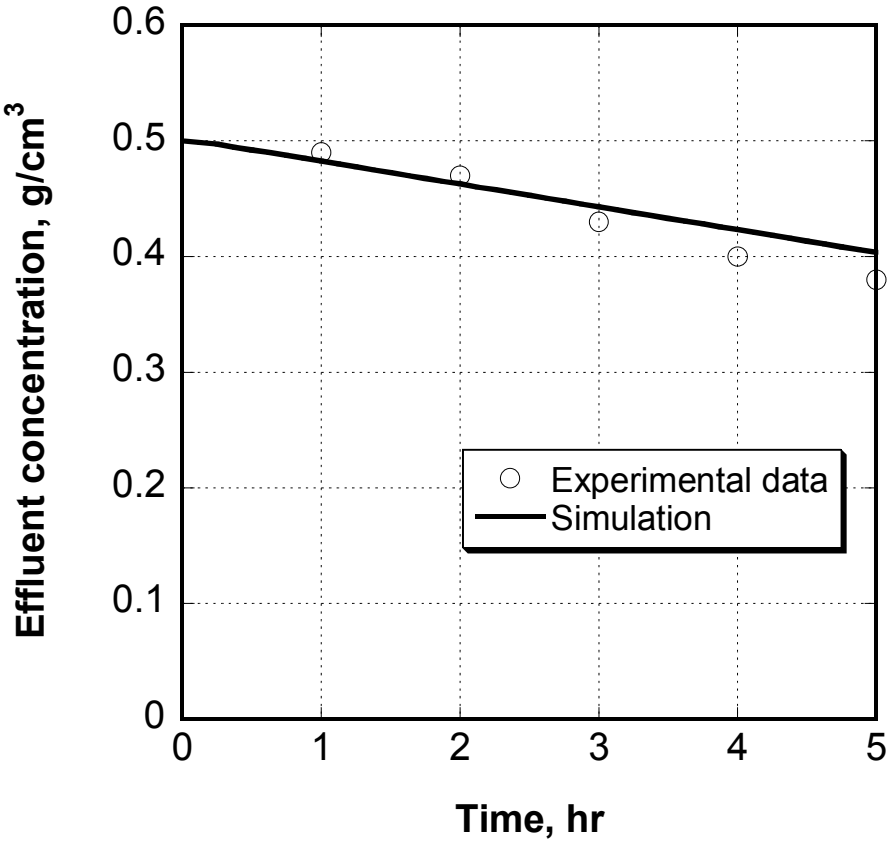

Figure 5.50: Suspension of particle concentration in the effluent versus time

Figure 5.51 shows the permeability impairment with respect to injection time. The model did not really handle the multi-damage mechanisms properly; however it qualitatively matched the overall experimental data in the thin section core sample.

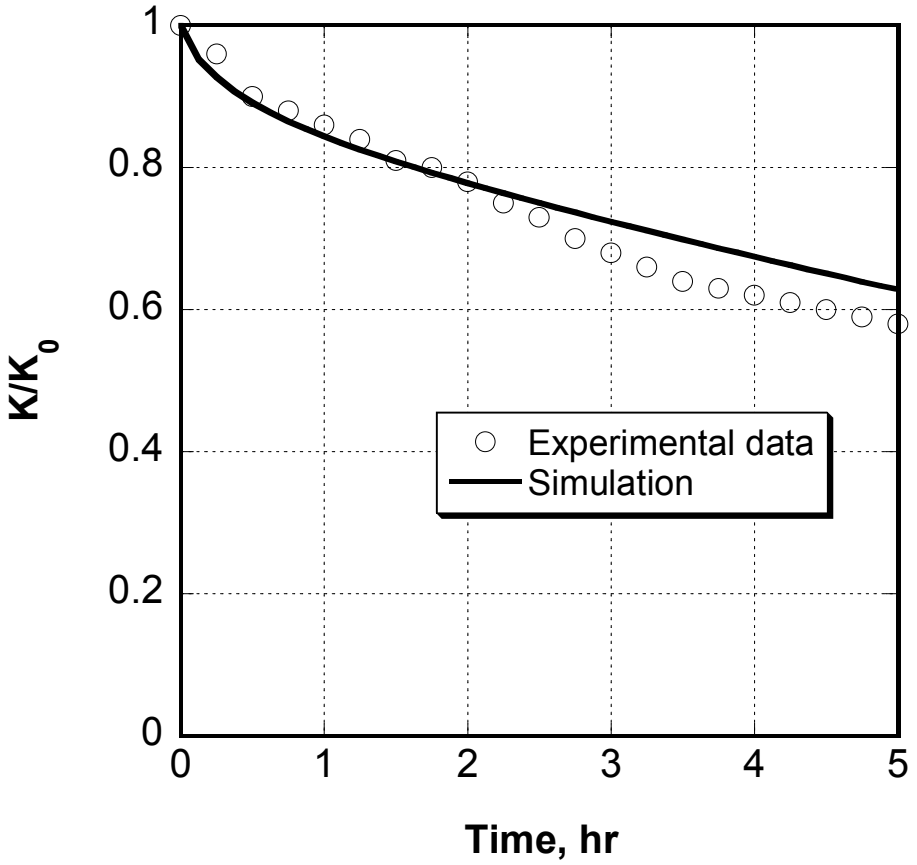

Figure 5.51: Permeability damage obtained by suspended solid injection

Permeability impairment was simulated through reduction in pore throat diameters caused by particle capture in the pore. The porosity and permeability alteration are strongly dependent on particle concentration in the injection fluid. The simulation results of fluid injection with different particle concentrations are presented in Figure 5.52 and 5.53. The injection rate was kept constant (q = 10.4 cm^3/hr). The fluid properties

were those listed in Table 5-13. Simulation results were for particle concentrations, c_{in}, of 0.50, 0.75, and 1.00 g/cm^3.

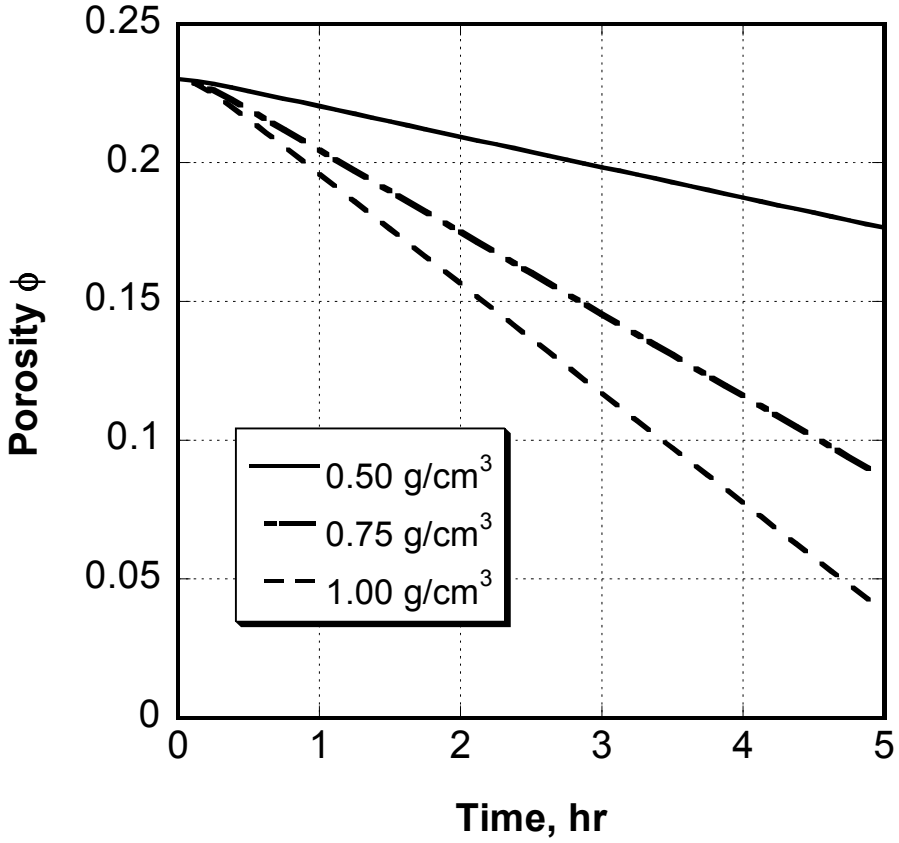

Figure 5.52: Simulation of porosity variation due to injection of different solid concentration

As shown in Figures 5.52 and 5.53, the overall porosity and permeability impairment became severe as the particle concentration increased. The results of injection

of c_{in} = 1.00 g/cm^3 particle concentration predicted that the thin core was totally plugged after 5 hours as porosity and permeability reduced to zero.

The satisfactory prediction of the experimental data indicates that the model based on the pore throat-to-particle size ratio and the particle concentration that caused bridging at the pore throat that led to reduced permeability is valid when fluid is continuously injected into the core. As particle concentration increased, bridging at the pore throat occurred more readily. Hence, porosity and permeability of the thin core samples decreased faster at higher particle concentration.

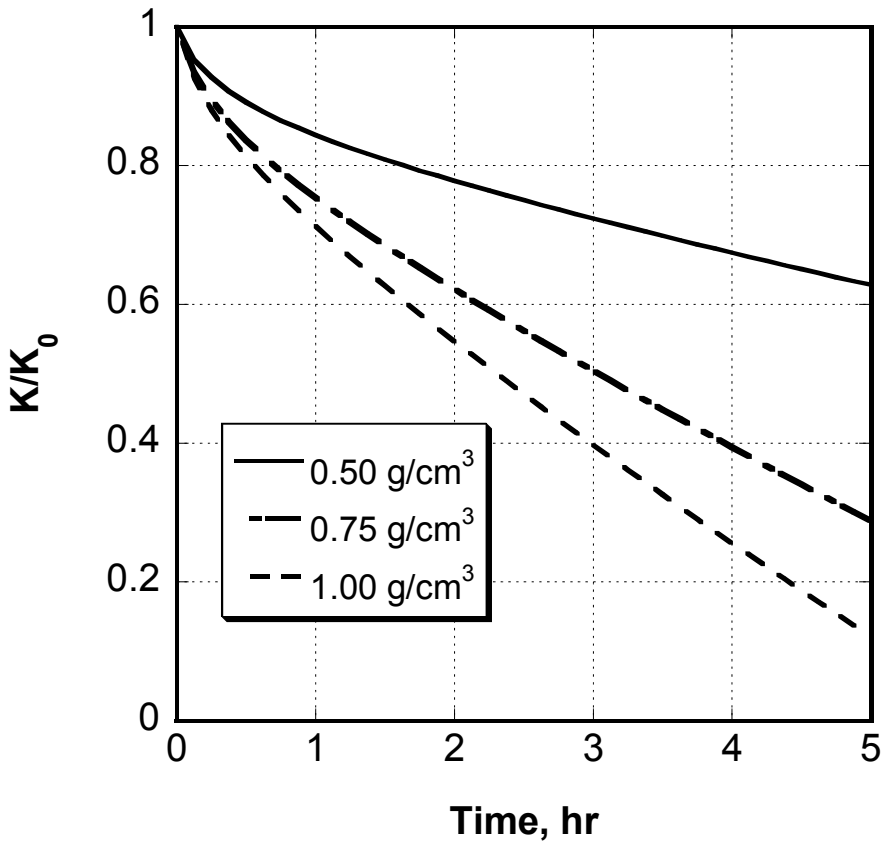

Figure 5.53: Simulation of permeability damage due to injection of different solid concentration

Figures 5.54 and 5.55 illustrate the simulation results to compare the porosity and permeability reductions for two different injection rates. Particle concentration was constant (c_{in} = 0.5 g/cm^3). Two different flow rates were investigated (q = 10.4 cm^3/hr and $q' = 4q$ = 41.6 cm^3/hr). The lower injection rate of 10.4 cm^3/hr created more damage to the core than the higher flow rate. This is expected because particles are less mobile at a lower flow rate due to insufficient shear stress. Hence more particles tend to deposit on the surface of the matrix formation under lower injection rate.

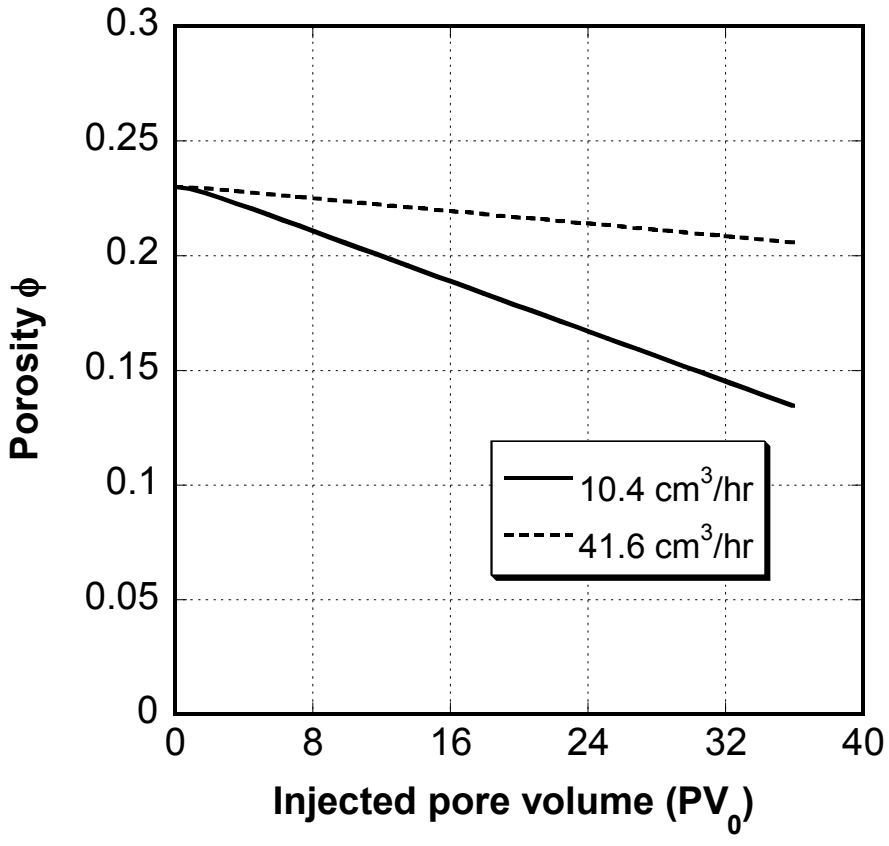

Figure 5.54: Simulation of porosity reduction versus injected pore volume of suspension

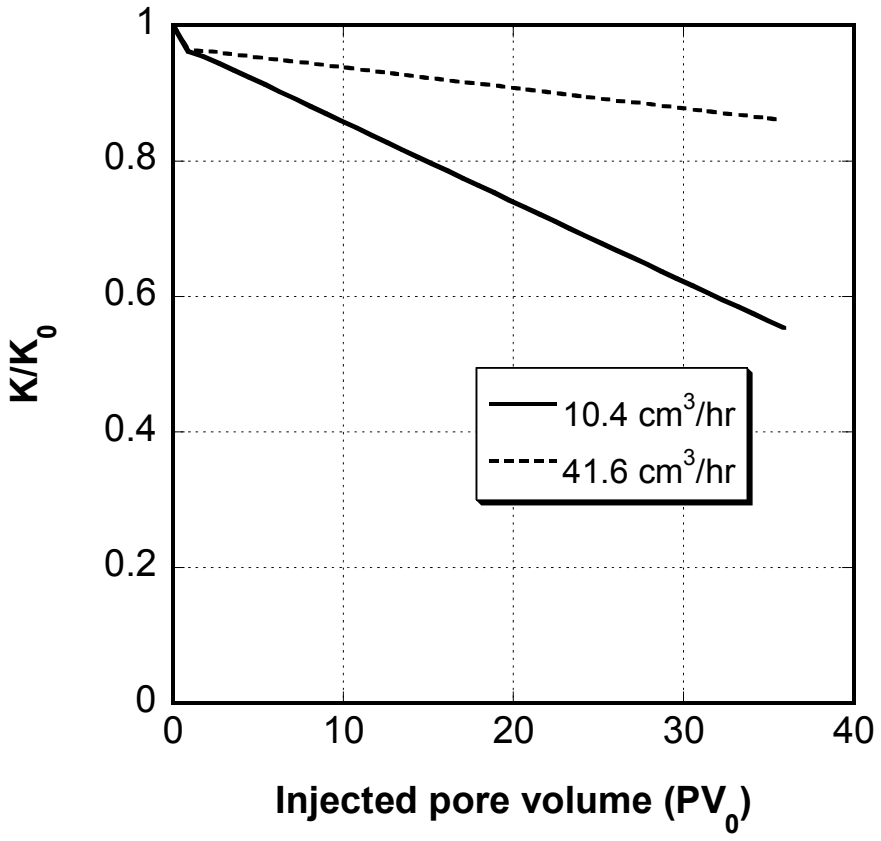

Figure 5.55: Simulation of permeability reduction versus injected pore volume of suspension

5.4 Conclusions

1. The experimental core plugging approach taken to investigate the governing damage mechanisms was straight-forward and led to a fairly prediction of permeability loss. This approach can help avoid overdesign in drilling and completion operations.
2. When fines are injected into porous media, the particles are retained in the pores and permeability decreases. As particle concentration increases, the

capture probability increases and leads to external filter cake formation and restriction of particle invasion into the core sample. Depth of particle invasion also strongly depends on mud properties such as polymer additives. As polymer is added into the drilling mud, better filter cakes are formed that are sturdy and less permeable.

3. Nuclear Magnetic Resonance ability to measure of porosity, pore size distribution, and permeability of the formation can provide determination of the formation properties during drilling/completion operations. Procedures have been developed whereby porosity distribution in porous media can be determined accurately from NMR.
4. The Bedrikovesky et al. (2002) classical deep bed filtration and Civan and Nguyen (2005) plugging-nonplugging pathways models for particulate fluid flow in porous media used in this work contributed some understanding of the influence of such factors as particle size, pore size distributions, fluid properties on formation damage evaluations.
    - The classical deep-bed filtration model works well under condition of small particle size and low particle concentration in the injection fluid. The model overestimated the permeability reduction in the downstream sections of the cores for larger particle size injection. The model assumed that porosity remained constant during the core flood test. This assumption was not valid for a thin slide core injection and will not be valid for formation damage during long production.

- The plugging and nonplugging model proposed by Civan and Nguyen (2005) fits the experimental data very well for the two cases. As stated by Civan and Nguyen (2005), the model provided valuable macroscopic details concerning particle capture and entrainment mechanisms during flow through a porous media. However, this model had 17 empirical parameters, which were adjusted to match the experimental data. Since the model is nonlinear, the uniqueness of the parameter values to match the data is not guaranteed.

5. The tests conducted in thin section formation plugging allowed better assessment and selection of proper drilling fluid to optimize the productivity of oil and gas. To minimize formation damage, a good quality mud cake is desirable. The particles not only block the small pore throats, but they are also captured on pore walls and in crevices. The principle damage mechanisms appeared to be the plugging and deposition of particle at pore throats and within pore space that restrict allowable flow areas inside the formation.
6. It was also observed that the injection rate affected porosity and permeability alteration. If suspensions are injected at a low flow rate, particle settling and retardation will take place. This results in an increased particle deposition rate. If the flow rate is high enough to overcome the settling forces, particles will flow through the porous channels without being trapped and result in less formation damage.

7. Modeling particle capture and predicting permeability reduction are clearly more complicated than the simple geometrical application of the pore size to particle size ratio presented in this chapter. Nevertheless, the modeling of thin section formation plugging and prediction of permeability loss was valuable for drilling/completion fluid selection to avoid formation damage.

6. Chapter 6: Conclusions and Recommendation for Further Work

6.1. Conclusions

The main findings obtained from this work are:

1. Conditions for plugging in orifices, slots, and porous formations, and the time required for plugging to occur can be quantified in terms of relevant parameters such as pore throat-to-particle size ratio, particle concentration in the flowing fluid, width-to-length ratio of the slot, and properties of the flowing fluid.
2. When plugging conditions exist, the higher the particle volume fraction, the shorter the plugging time.
3. Laboratory core tests were done with different particle concentrations and fluid viscosities to investigate various formation damage mechanisms developed for a single-phase fluid system. The Wojtanowicz et al. (1987) diagnostics method indentified relevant mechanisms during the core damage test. The Civan (2007) thin section formation plugging model provided valuable information for drilling/completion fluid selection to avoid damaging of formation.
4. The Bedrikovesky et al. (2002) and Civan and Nguyen (2005) models were both applicable for deep bed filtration and provided information about particle invasion along the core plugs. However, results indicated that the Civan and Nguyen (2005) model described experimental data more accurately, although it was more complex to apply. Parameters obtained from matching cannot be proven to be unique.

5. Experimental techniques and procedures for Nuclear Magnetic Resonance were developed to determine porosity distributions of porous medium during core flood tests.
6. Injection rates affected porosity and permeability alteration. If suspensions were injected at a low flow rate, particle settling and retardation took place and caused an increased particle deposition rate. If the flow rate was high enough to overcome the settling forces, particles flowed through the porous channels without being trapped and resulted in less formation damage.

6.2. Recommendations

1. Application of commercial numerical simulation software such as FLUENT^{TM} and 3D FLOW^{TM} are recommended for simulation of the flow of particles through orifices, slots, or pore-throats of porous formations. They may provide valuable and detailed insight to the plugging mechanisms caused by particles. They will provide quick results for data analysis and avoid lengthy, tedious physical experiments.
2. The results in section 5.3 indicate that the particle mobilization affects the rate of particle deposition on the pore. When water is the pore fluid, the drag forces on particles may be attained in turbulent condition. Therefore, a study of the effects of turbulent flow on mobilization, transport, and entrapment of particles in porous media is needed.

3. NMR technique only provided the pore distribution of the overall formation. Studies to integrate NMR and SEM imaging may provide more insight into the damage mechanisms caused by suspension injections.

References

Ali, A., Kallo, C.L., and Singh, U.B. 1994. *Preventing Lost Circulation in Severely Depleted Unconsolidated Sandstones Reservoirs. SPEDC*: 32-38.

Argiller, J.F., Audibert, A., Longeron, D.G. 1999. *Performance evaluation and formation damage potential of new water-based drilling formulas*. SPE Drilling and Completion, **14:** 266-273.

Baghdikian, S.Y., Sharma, M.M., and Handy, L.L. 1987. *Flow of Clay Suspensions through Porous Media*. Journal of the Society of Petroleum Engineers, SPE 16257.

Bailey, L., Boek E., Boassen, T., Selle, O., Longeron, D. 1999. *Particulate invasion from drilling fluids*. Journal of Petroleum Engineers, SPE 54762.

Barkman, J.H. and Davidson, D.H. 1972. *Measuring water quality and predicting well impairment*. J. Pet. Tech.: 865-873.

Bedrikovetsky, P., Marchesin, D., Shecaira, F., Souza, A.L., Milanez, P.V., and Rezende, E. 2001. *Characterization of Deep Bed Filtration System From Laboratory Pressure Drop Measurements*. Journal of Petroleum Science and Engineering, **32**: 167-177.

Bedrikovetsky, P., Tran, P. Broek, V., Marchesin, D., Rezende, E., Siqueira, A., Serra, A. and Shecaira, F. 2002. *Damage characterization of deep bed filtration from pressure measurements*. Paper presented at the SPE International Symposium and Exhibition on Formation Damage Control, Lafayette, Louisiana. SPE 73788.

Bertness, T.A. 1953. *Observations of water damage to oil productivity*. Drilling and Production Practive, API.

Bleier, R. 1990. *Selecting A Drilling Fluid*. J. Pet. Tech, **July**: 832.

Bouhroum, A. and Civan, F. 1995. *A Critical Review of Existing Gravel-Pack Design Criteria*, J. Canadian Petroleum Technology, **34** (1), pp. 35-40.

Burton, R.M. and Hodge, R.M. 1999. *Drilling and Completion of Horizontal Wells Requiring Sand Control.* Paper SPE 52812 presented at SPE/IADC Drilling Conference, 9-11 March, 1999, Amsterdam, Netherlands.

Cerda, C.M. 1988. *Mobilization of Quartz Fines in Porous Media*. Clays and Clay Minerals, **36**: 491-497.

Chang, F. and Civan, F. 1991. *Modeling of Formation Damage Due to Physical and Chemical Interactions between Fluids and Reservoir Rocks*. Paper SPE 22856 presented at SPE Annual Technical Conference and Exhibition, 6-9 October 1991, Dallas, Texas.

Civan, F. 2000. *Reservoir Formation Damage- Fundamentals, Modeling, Assessment, and Mitigation,* Gulf Pub. Co., Houston, TX, 742p.

Civan, F. 2007. *Reservoir Formation Damage- Fundamentals, Modeling, Assessment, and Mitigation,* Second Edition, Elsevier, Gulf Professional Pub., Burlington, MA, 1114p.

Coates, G.R, Xiao, L., Prammer, M.G. 1999. *NMR Logging Principles and Applications*, Gulf Publishing Co., Houston, TX, 234p.

Cunningham, W.C. and Smith, D.K. 1968. *Effect of salt cement filtrate on subsurface formations.* Journal of Petroleum Technology. March: 259-264.

Ding, Y., Longeron, D.G., Audibert, A. 2004. *Modeling of near-wellbore damage and natural clean up of horizontal wells drilled with water-based drilling fluids.* Journal of Society of Petroleum Engineers: 252-264.

Douglas, J. Jr., Peaceman, D.W. and Rachfort, H.H. Jr. 1959. *A method for calculating multi-dimensional immiscible displacement*. Trans. AIME: 216-297.

Dunn, K.J., Bergman, D.J., Latorraca, G.A. 2002. *Nuclear Magnetic Resonance: Petrophysical and Logging Applications*, Pergamon Press, New York, 293p.

Gaida, K.H., Kessel, H.V., Zimmerle, W. 1985. *Geological Parameters of Reservoir Sandstones as Applied to Enhance Oil Recovery*. Proceedings of International Symposium on Oilfield Chemistry, SPE 13570, Phoenix, AZ, April 9-11: 219-229.

Gentzis, T, Deisman, N., and Chalaturnyk, R. 2009. *Effect of drilling fluids on coal permeability: Impact on horizontal wellbore stability.* J. Coal Geol. doi: 10.1016/j.coal.2009.01.001.

Gruber, N.G. and Adair, K.L. 1995. *New laboratory procedures for evaluation of drilling induced formation damage and horizontal well performance.* Journal of Canadian Petroleum Technology, **34**: 27-32.

Gruesbeck, C. and Collins, E. 1982a. *Entrapment and Deposition of Fine Particles in Porous Media*. Journal of the Society of Petroleum Engineers: 847-856.

Gruesbeck, C. and Collins, E. 1982b. *Particle Transport through Perforations*. Journal of the Society of Petroleum Engineers: 857-865.

Haynes, C.D. and Gray, K.E. 1974. *Sand particle transport in perforated casing*. Journal of Petroleum Technology, **26** (1): 80-84.

Herzig, J.P., Leclerc, D.M., Goff, P.L. 1970. *Flow of Suspensions through Porous Media-Application to Deep Filtration.* Ind. Eng. & Chem., **62** (5): 8-35. doi 10.1021/ie50725a003.

Iscan, A.G, Civan, F., Kok, M.V. 2007. *Alteration of permeability by drilling fluid invasion and flow reversa.* Journal of Petroleum and Engineering, **58:** 227-244.

Iscan, A.G. and Civan, F. 2006. *Correlation of Criteria for Perforation and Pore Plugging by Particles*. Journal of Porous Media, **9** (6): 541-558.

Iwasaki, T. 1973. *Some notes on sand filtration*. Journal of the American Water Works Association, **29**: 1591-1602.

Jiao, D. and Sharma, M.M. 1996. *Mud-Induced Formation Damage in Fractured Reservoirs. SPEDC*: 11-16.

Jiao, D. and Sharma, M.M. 1996. *Mud-induced formation damage in fracture reservoir*. SPE Drilling and Completion: 11-16.

Khilar, K.C. and Fogler, H.S. 1998. *Migration of Fines in Porous Media*, Kluwer Academic Publishers, 171.

Khilar, K.C., Fogler, H.S., and Ahluwalia, J.S. 1983. *Sandstone water sensitivity: existence of a critical rate of salinity decrease for particle capture*. Chemical Engineering Science, **38** (5): 789-800.

Kia, S.F., Fogler, H.S., and Reed, M.G. 1987. *Effect of pH on Colloidally INduced Fines Migration*. Journal of Colloid and Interface Science, **118** (1)**:** 58-168.

Krueger, R.F. 1986. An Overview of Formation Damage and Well Productivity in Oilfiled Operations. *Journal of Petroleum Technology*, February: 131-152.

Krueger, R.F., Vogel, L.C., and Fischer, P.W. 1967. *Effects of pressure drawdown on clean-up of clay- or silt-blocked sandstone*. Journal of Petroleum Technology, **19**: 397-403.

Leoppke, G.E., Glowka, D.A. and Wright, E.K. 1990. *Design and Evaluation of Lost-Circulation Materials for Severe Environments*. *JPT*: Trans. AIME, **289**: 328–337.

Maroudas, A. and Elsenklam, P. 1965. *Clarification of suspensions: A study of particle deposition in granular media*, part 2: A theory of clarification. Chem. Eng. Sci., **20**: 875-888.

Massei, N., Lacroix, M., Wang, H.Q., and Dupont J. 2002. *Transport of particulate material and dissolved tracer in highly permeability porous medium: comparison of the transfer parameters*. Journal of Contaminant Hydrology, **57**: 21-39.

McDowell-Boyer, L.M. 1992. *Chemical Mobilization of Micron-Sized Particles in Saturated Porous Media under Steady Flow Conditions*. Environmental Science & Technology, **26:** 586-593.

Messenger, J.U. 1981. *Lost Circulation*, Pennwell Publishing Co., Tulsa, 112p.

Monaghan, P.H., Salathiel, R.A., Morgan, B.E. 1959. *Laboratory studies of formation damage in sands containing clays*. Transactions, American Institute of Mechanical Engineers, **216**: 209-225.

Muecke, T.W. 1979. *Formation Fines and Factors Controlling Their Movement in Porous Media.* Journal of Petroleum Technology, **31**: 144-150.

Nabzar, L., Coste, J.P., and Chauveteau, G. 1997. *Water Quality and Well Injectivity*. Paper 044 presented at the 9th European Symposium on Improved Oil Recovery, The Hague, 20-22 October.

Nguyen, V. and Civan, F. 2005. *Modeling particle migration and deposition in porous media by parallel pathways with exchange*. Chapter 11, Handbook of Porous Media, Second Edition, Vafai, K. (Ed), CRC Press, Taylor and Francis Group, Boca Raton, FL: 457-484.

Nowak, T.J. and Krueger, R.F. 1951. *The effect of mud filtrates and mud particles upon the permeabilities of cores.* Drill and Prod. Prac., API.

Ohen, H.A. and Civan, F. 1993. *Simulation of Formation Damage in Petroleum Reservoirs*. SPE Advanced Technology Series, **1** (1): 27-35.

Pandya, V.B, Bhuniya, S., and Khilar, K.C. 1998. *Existence of a critical particle concentration in plugging of a packed bed*. AIChE Journal, **4**: 978-981.

Pang, S. and Sharma, M.M. 1997. *A Model for Predicting Injectivity Decline in Water-Injection Wells*. SPE Form. Eval. **12** (3): 194-201. SPE-28489-PA. doi 10.2118/28489-PA.

Parn-anurak, S. and Engler, W.T. 2005. *Modeling of fluid filtration and near-wellbore damage along a horizontal well*. Journal of Petroleum Science Engineering, **46**: 149-160.

Payatakes, A.C., Rajagopalan, R., and Tien, C. 1974. *Application of Porous Media Models to the Study of Deep Bed Filtration*. The Canadian Journal of Chemical Engineering, **52**: 722-731.

Peaceman, D.W. 1977. *Fundamentals of numerical reservoir simulation.* Elsevier Scientific Publishing Company, New York: 83-95.

Reddi, L.N., Ming, X., Hajra, M.G., and Lee, I.M. 2000. *Permeability reduction of soil filters due to physical clogging*. Journal of Geotechnical and Geoenvironmental Engineering, **126** (3): 236-246.

Roque, C., Chauveteau, G., Renard, M. Thibault, G., Bouteca, M., and Rochon, J. 1995. *Mechanisms of Formation Damage by Retention of Particles Suspended in Injection Water*. Paper SPE 30110, presented at SPE European Formation Damage Conference, The Hague, 15-16 May.

Santos, A. and Bedridkovetsky, P. 2004. *Size exclusion during particle suspension transport in porous media: stochastic and averaged equations*. Computational and Applied Mathematics, **23** (2-3): 259-284.

Shamar, M.M., Chamoun, H., Sharma, D.S.H.S.R, Schechter, R.S. 1992. *Factors Controlling the Hydrodynamic Detachment of Particles from Surfaces*. Journal of Colloid and Interface Science, **149** (1): 121-134.

Sharma, M.M. and Yortsos, Y.C. 1987a. *Transport of particulate suspensions in porous media: Model Formulation*. AICHE Journal, **33**(10): 1636-1643.

Sharma, M.M. and Yortsos, Y.C. 1987b. *Fines migration in porous media*. AICHE Journal, **33** (10): 1654-1662.

Sigal, R. 2002. *Coates and SDR permeability: two variations on the same theme*. Petrophysics, **43**,38-46.

Thomas, G.W. 1982. *Principles of numerical reservoir simulation*, International Human Resources Development Corp., Boston.

Tran, T.V., Civan, F., and Robb, I. 2009. *Correlating Flowing Time and Condition for Perforation Plugging by Suspended Particles*. SPE Drilling & Completion Journal, **24** (3): 398-403.

Vaidya, R.N. and Fogler, H.S. 1990. *Formation Damage due to Colloidally Induced Fines Migration.* Colloids and Surfaces, **50** (12): 215-229.

Valdes, J.R. and Santamarina, C.J. 2006. *Particle Clogging in Radial Flow: Microscale Mechanisms*. Journal of Society of Petroleum Engineers: 193-198.

Wennberg, K.E., Batrouni, G., Hansen, A. 1995. *Modelling Fines Mobilization, Migration and Clogging*. Society of Petroleum Engineers, SPE 30111: 352-364.

Wojtanowicz, A.K, Krilov, Z., Langlinas, J.P. 1987. *Study on the Effect of Pore Blocking Mechanisms on Formation Damage*. Paper SPE 16233, presented at SPE Production Operations Symposiums, Oklahoma City, March 8-10.

Yortsos, Y.C. and Sharma, M. 1986. Application of percolation theory to noncatalytic gas-solid reactions. AIChE Journal, **32** (1): 46-55.

Appendices

Appendix A: Nomenclature

a, b	empirical parameters for equation (3.6)
A, B, C	empirical parameters for equation (3.2) and equation (3.3)
c_p	particle mass concentration, g/cm^3
D_p	average particle diameter, cm
D_T	perforation or pore diameter, cm
K	rock permeability, mD
w	fracture opening width, cm
L	fracture opening length, cm
v	velocity of the suspension, cm/s
Re_p	Particle-Volume-Fraction Reynolds number
t_p	the time elapsed until bridge formation, s

Greek Symbols

μ	viscosity of the fluid, cP
ρ	average fluid density, g/cm^3

ρ_f	fluid mass density, g/cm^3
ρ_p	particle mass density, g/cm^3
σ_p	particle volume fraction, fraction
ϕ	porosity, fraction
α	cement exclusion parameter, dimensionless
β	slot size-to-particle (or pore-to-particle diameter) size ratio, dimensionless
β'	mean slot size-to-particle size ratio, dimentionless
γ	fracture's shape factor, dimensionless
τ	tortuosity
Γ	interconnectivity parameter

Appendix B: Plugging conditions and times for orifice and slot experiments

Table B-1: Re_{pcr} and β_{cr} values for orifice plugging experiments

Uniformed Nylon particles		Mixture of 2 Nylon particles		Carbo proppants	
Re_{pcr}	β_{cr}	Re_{pcr}	β_{cr}	Re_{pcr}	β_{cr}
126.8	2.00	15.7	1.45	3.21	3.63
445.1	2.90	23.0	1.60	1.07	2.67
39.4	1.33	35.2	1.78	4.79	4.46
108.6	1.93	26.1	1.66	1.54	3.21
293.3	2.67	61.3	1.93	3.82	4.12
69.9	2.00	195.2	2.32	0.18	1.51
26.8	1.33	94.5	2.29	0.43	2.11
		342.9	2.67		
		19.2	1.45		
		43.2	1.60		
		81.9	1.78		
		32.7	1.60		
		53.9	2.00		
		240.1	2.67		
		80.3	2.11		
		149.5	2.32		
		335.4	2.58		
		441.7	2.91		
		825.8	2.92		
		19.2	1.45		

Mixture of 3 Nylon particles	
Re_{pcr}	β_{cr}
16.83	1.52
22.73	1.62
30.39	1.67
45.36	1.90

	43.2	1.60	
	81.9	1.78	
	33.1	1.55	
	48.5	1.66	
	64.6	1.78	
	52.1	2.13	
	105.8	2.29	
	193.7	2.46	
	16.8	1.52	
	22.7	1.62	
	30.4	1.67	

Table B-2: Re_{pcr} and β_{cr} values for orifice plugging experiments with angles

θ = 0		θ = 15		θ = 30		θ = 45	
Rep_{cr}	β_{cr}	Rep_{cr}	β_{cr}	Rep_{cr}	β_{cr}	Rep_{cr}	β_{cr}
69.9	2.00	63.1	2.00	61.0	2.00	49.9	2.00
39.4	1.33	33.5	1.33	31.8	1.33	22.9	1.33
192.0	2.50	144.3	2.50	122.0	2.50	98.6	2.50
54.9	1.67	51.3	1.67	45.6	1.67	32.5	1.67
48.4	1.60	42.6	1.60	38.2	1.60	30.1	1.60

Table B-3: Re_{pcr} and β_{cr} values for slot plugging experiments (w = 0.16 cm)

L = 0.64 cm		L = 1.28 cm		L = 2.56 cm	
Rep_{cr}	β_{cr}	Rep_{cr}	β_{cr}	Rep_{cr}	β_{cr}
0.105	1.26	0.139	1.26	0.201	1.26
0.247	1.51	0.414	1.51	0.482	1.51
0.511	1.90	1.109	1.90	1.572	1.90
0.782	2.18	1.642	2.18		
1.355	2.46				

Table B-4: Re_{pcr} and β_{cr} values for slot plugging experiments (w = 0.32 cm)

L = 0.64 cm		L = 1.28 cm		L = 2.56 cm	
Rep_{cr}	β_{cr}	Rep_{cr}	β_{cr}	Rep_{cr}	β_{cr}
0.117	1.32	0.193	1.32	0.215	1.32
0.292	1.60	0.479	1.60	0.587	1.60
0.667	2.10	1.488	2.10	3.483	2.10
1.299	2.67				
2.219	3.02				

Table B-5: Plugging time vs. Particle volume fraction for Carbo proppants at different orifice-to-particle diameter ratios

$\beta = 2$		$\beta = 2.5$		$\beta = 3$	
Particle Vol. Frac.	Plugging time (s)	Particle Vol. Frac.	Plugging time (s)	Particle Vol. Frac.	Plugging time (s)
0.045	18	0.065	16	0.075	19
0.055	16	0.075	14	0.085	17
0.065	13	0.085	14	0.095	15
0.085	10	0.095	13	0.105	14
0.105	8	0.105	11	0.205	11
0.305	5	0.205	8	0.305	9
		0.305	7		

Table B-6: Plugging time vs. Particle volume fraction for Carbo proppants at different slot-to-particle size ratios

$\beta' = 1.83$		$\beta' = 2.03$		$\beta' = 2.15$	
Particle Vol. Frac.	Plugging time (s)	Particle Vol. Frac.	Plugging time (s)	Particle Vol. Frac.	Plugging time (s)
0.1	16	0.1	18	0.1	20
0.15	13	0.15	14	0.15	15
0.25	10	0.25	11	0.25	12
0.35	8	0.35	8	0.35	9

Appendix C: Power law correlations for plugging conditions in orifice experiments

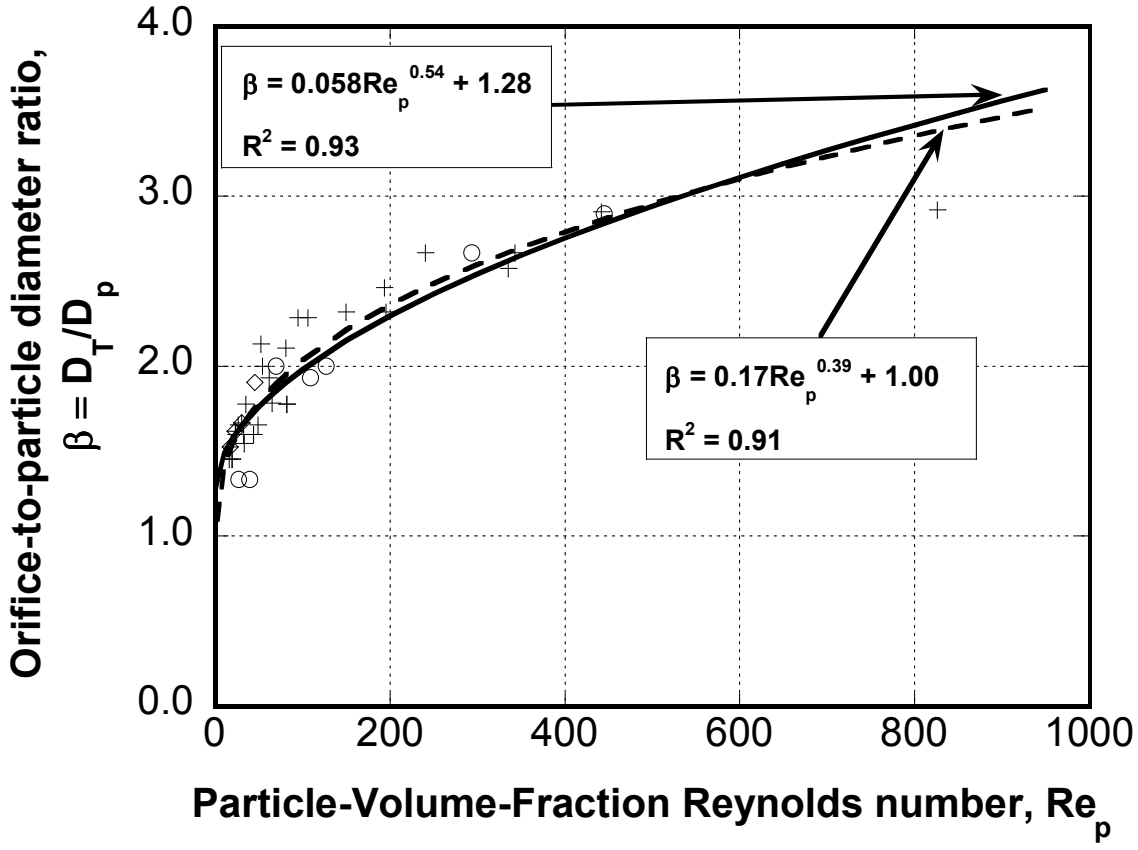

Figure C.1: Power law model for mixture of nylon particles in brine under constant flow rate of 8.00 cm^3/s

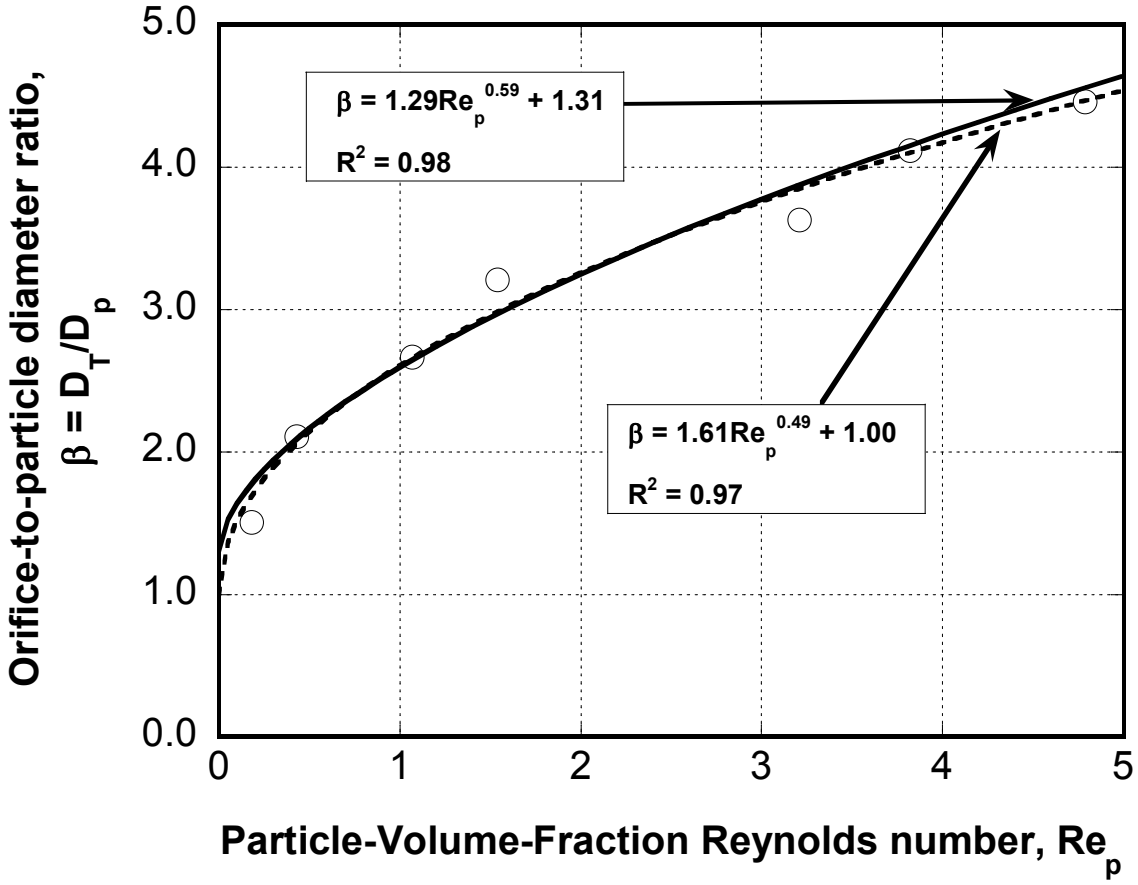

Figure C.2: Power law model for Carbo proppant particles in Geovis XT under constant flow rate of 4.25 cm^3/s

Appendix D: Pressure reading for core flood experiments

Table D-1: Pressure reading for core flood tests

Drilling Fluid-1 (μ = 7 cP)		Drilling Fluid-2 (μ = 12 cP)		Drilling Fluid-3 (μ = 29 cP)	
Time, min	ΔP, psi	Time, min	ΔP, psi	Time, min	ΔP, psi
0	8.2	0	14.0	0	33.9
30	10.5	30	18.3	30	44.5
60	12.8	60	22.7	60	52.5
90	16.1	90	23.9	90	54.2
120	20.6	120	24.5	120	54.8
150	25.3	150	27.3	150	60.7
180	28.1	180	32.1	180	68.7
210	28.7	210	33.4	210	69.4
240	37.7	240	33.9	240	73.7
270	66.6	270	36.0	270	78.7
300	115.9	300	39.2	300	79.9
330	117.4	330	40.1	330	82.3
360	123.4	360	40.3	360	84.9
390	145.4	390	48.5	390	87.2
420	198.7	420	52.5	420	88.9
450	205.6	450	56.9	450	90.9
480	260.7	480	61.1	480	95.1
510	274.7	510	69.7	510	97.8
540	294.4	540	71.3	540	99.1
570	308.9	570	76.5	570	99.1
600	324.8	600	82.2	600	99.8

Table D-2: Pressure reading for thin-slice core flood tests

Time, min	ΔP, psi
0	19.8
15	20.6
30	22.0
45	22.5
60	23.0
75	23.5
90	24.4
105	24.7
120	25.3
135	26.4
150	27.1
165	28.2
180	29.1
195	30.0
210	30.9
225	31.4
240	31.9
255	32.4
270	32.9
285	33.5
300	34.1

Appendix E: Setup procedures for the Oxford-Maran Ultra system

Table E-1: Parameter setup for the Oxford-Maran Ultra system

Description	ID	Value
90 Degree Pulse (μs)	P90	20.3
180 Degree Pulse (μs)	P180	38.4
Probe Dead Time (μs)	DEAD1	80.0
Receiver Dead Time (μs)	DEAD2	20.0
Spectrometer Frequency (MHz)	SF	2.202286
Offset from SF (Hz)	O1	0.82
Filter Width (Hz)	FW	4000.0
Dwell Time (μs)	DW	1.0
Points per Echo (points)	SI	1
Number of Echoes	NECH	2048
Number of Scans	NS	100
Receiver Gain (%)	RG	100.00
Relaxation Delay (μs)	RD	8000000.0
90-180 Degree Pulse Gap (μs)	TAU	300.00
90 Degree Pulse Phase List (rec: 0213)	PH1	0213
Receiver Phase List (rec: 0213)	PH2	0213
180 Degree Pulse Phase List (rec: 1122)	PH3	1122
Dummy Scans	DS	0
RF Amplitude (%)	RFA0	100.0

The following is a stepwise calibration procedure for the NMR MARAN Ultra:

1. Click on RINMR, the acquisition and processing software for MARAN Ultra.
2. Place the calibration standard in the NMR sample holder.
3. Adjust the length of the sample holder to 23.5 cm and put sample holder inside the NMR machine.
4. Click on **"LOAD"** and select the **"Wobble"** option from the **"TOOL"** menu on the menu bar.
5. Click on **"GS1"** option from Command menu to execute the Wobble command.
6. There will be a display of two parabolas one normal and one inverted in the Data Window.
7. From the **"VIEW"** menu select the **"MAGNITUDE"** option. It will toggle the display of the inverted parabola.
8. Adjust the **"RED KNOB"** on the machine to center parabola at the origin.
9. Click on the **"STOP"** option in Command menu.
10. Execute the **"AUTO01"** command in the Command menu. After the command is executed you will see a "pop up" window that will show the value of **"OFFSET"**. Click "OK" and rerun the **"AUTO01"** command. The two parallel bars (green/yellow) one for real and other for the imaginary data are displayed. A window will pop up that will show a value of **"OFFSET"**.
11. Click on the **"Acquisition Parameter"**. If the offset is negative or positive, subtract it or add it from the Spectrometer Frequency (MHz). Make sure you take the unit conversion into consideration. Repeat Steps 10 & 11 until the offset lies between -1 to +1. Note the offset and the Spectrometer Frequency (MHz).

12. From the **"TOOL"** menu on the menu bar click on **"LOAD"** and select the **"Train 90"** option.
13. Click on the **"GS1"** option from Command menu on menu bar to execute the *Train 90* command. Small bars in yellow and green are parallel to each other.
14. The two should overlay on each other near the x-axis and should be lying on the x-axis. If not then type in **"P90"** command and hit "Enter" key in the command line which is just below the command history window.
15. A value next to P90 in the command line is displayed. Use **"PgUp"** or **"PgDn"** key so that the bars lie as close as possible to the x-axis. Repeat this step until a good match is obtained. Note the value that appears next to P90.
16. Click on **"STOP"** option in Command menu and from the **"TOOL"** menu on the menu bar click on **"LOAD"** and select the **"Train 180"** option.
17. Click on **"GS1"** option from Command menu on menu bar to execute the Train 180 command. Small bars in yellow and green parallel to each other lying near to x-axis are displayed.
18. Follow Steps 14 & 15 again but use the **"P180"** command instead of ***"P90"*** command. Note the value that appears next to P180.
19. Click on the **"STOP"** option in the Command menu.
20. Open the **"Acquisition Parameter"**. Adjust the parameter values as presented in Table E-1.
21. The machine is now calibrated and ready for use.